THE CYCLIC STRAINING OF ALUMINUM - 4% COPPER

THE CYCLIC STRAINING OF ALUMINUM - 4% COPPER

By

ANDRAS ABEL, Dipl. Eng., A.I.M.

A Thesis

Submitted to the Faculty of Graduate Studies

in Partial Fulfilment of the Requirements

for the Degree

Master of Science

McMaster University

May 1965

MASTER OF SCIENCE (1965)
(Metallurgy)

McMASTER UNIVERSITY
Hamilton, Ontario.

TITLE: The Cyclic Straining of Aluminum - 4% Copper

AUTHOR: Andras Abel, Dipl. Eng. (Budapest)

A.I.M. (England)

SUPERVISOR: Professor R. K. Ham

NUMBER OF PAGES: v, 160

SCOPE AND CONTENTS:

In this thesis the nature and strengthening effect of the various precipitates in Al-4% Cu are reviewed, followed by a literature survey on the response of this alloy to fatigue. The first experiments described were carried out to measure the Bauschinger effect and the results of these are presented. The experimental study was further extended by cyclic straining corresponding to fatigue conditions and the results obtained are presented graphically and through electron micrographs. The fatigue behaviour was further investigated at liquid air temperatures. Also, the effect of heat treatments carried out during the interruption of fatigue on a specimen containing metastable θ" precipitates is reported. All the experiments were carried out on single crystals and most of them with 112 orientation as indicated later.

Acknowledgements

The author wishes to express his most sincere thanks to Dr. R. K. Ham and is particularly grateful for his instruction, constant advice and encouragement which enabled the completion of this work.

The author is also indebted to Dr. R. H. Hay of Aluminium Laboratories Limited for providing the alloy, to Mr. D. W. Eley of Englehard Industries, Dr. J. Rezek of Canadian Westinghouse Limited, Mr. G. Globe of Greening Industries Limited and the Steel Company of Canada Limited, for assistance in forming the alloy.

Thanks are also due to McMaster University for providing an Instron testing machine, in addition to providing regular facilities and to The Defence Research Board of Canada for providing the necessary funds.

Table of Contents

CHAPTER I

Introduction

It has been estimated that over 90% of mechanical failures in normal engineering service are caused by fatigue, so that there has been increasingly intensive research on the fundamental nature of this process over the past hundred years.

Recent reviews have been given by Thompson and Wadsworth[1] and Thompson[2]. Since 1962 further advances have been made, especially with the use of the transmission electron microscopy of thin films[3,4,5,6,7,8]. It is now apparent that in the first few hundred or thousand cycles of fatigue, the general hardening of pure metals like aluminium or copper occurs by the formation of small prismatic dislocation loops and dipoles, which amount to 80 - 90% of the total dislocation density. In a few local regions slip continues with the formation of intensely concentrated slip "striations", in which the dislocations form a well-developed sub-structure (Laufer and Roberts[9] and McGrath and Waldron[10]). The striations do not penetrate far (about 50 - 100μ) below the surface of the metal, but they lead to the initiation of cracks at the surface within about 10% of the expected life in a specimen lasting 10^6 cycles. The rest of the fatigue process

consists of growing the crack. Thus there is relatively ample knowledge of the fatigue process in pure metals and detailed quantitative explanations are now being attempted with some promise of success.

However, much less is known about the fatigue behaviour of alloys, although work on aluminium alloys of the age hardening type has been particularly intensive, since these are of vital importance to the aircraft industry. It has long been known that the fatigue strength of these alloys is not improved in proportion to their tensile strength by heat treatment. Orowan[11] suggested first that under fatigue conditions, these metallographically unstable alloys may suffer overageing. This possibility was pursued further by Hanstock[12], who obtained metallographic evidence of precipitation induced by fatigue in support of the overageing hypothesis. However, Hanstock's interpretation has been criticized by Broom and his co-workers[13,14], who were unable to corroborate Hanstock's observation of precipitation and found instead that the material beneath fatigue striations could be selectively etched. The effect could be suppressed at very low temperatures (-183°C), and reheat-treatment of the alloys destroyed this effect. The electron microscopy of oxide replicas could not detect the striations, but a further ageing treatment after fatigue led to the observation of what were apparently denuded zones in the region of the striations. Broom also observed similar effects in regions near the fracture surfaces from these alloys pulled in tension. He summarized the possible mechanisms as follows:

i) The creation of vacant lattice sites by moving dislocations with the consequent increase in diffusion rate leading to overageing comparable to that occurring isothermally at a "high" temperature[14].

ii) An increase in the diffusion rate brought about by multiplication of dislocations and the consequent greater possibilities of "short-circuit" diffusion paths (pipe diffusion)[15].

iii) The interaction of mobile dislocations with other dislocations which form the boundaries of coherent precipitates, such that these precipitates become incoherent, thus reducing local elastic strains[16].

iv) The nucleation of stable (as distinct from transitional) precipitates[17].

v) The re-solution of precipitates. This is in distinction to (i) - (iv), which could be embraced by the term "overageing". It is supposed that there must always be a distribution of solute atoms between dislocations (as atmospheres) and precipitates. The multiplication of dislocations may necessitate the transfer of solute atoms from precipitates[18].

vi) According to an estimate of Freudenthal and Weiner[19], sufficiently high temperatures may be generated in slip bands by moving dislocations for normal thermal ageing to take place, leading to softening and cracking. Eshelby and Pratt[20] have shown that the estimate is unacceptable and that the temperature rise in a slip band may be only a few degrees.

The classical work of Forsyth and Stubbington[21,22] and Forsyth[23] should also be mentioned. These workers found that upon fatiguing solution treated Al-4 wt.% Cu alloy, the extrusion of thin ribbons of metal occurred at striations, followed by crack initiation. The extrusion effect was clearly associated with metallurgical instability, since it could be suppressed by overageing the alloy or by fatiguing at very low temperatures. Subsequent ageing of the alloy or fatiguing at 250°C indicated that the striations became depleted of solute.

Polmear and Bainbridge[24] made a similar observation in Al-Mg-Zn alloys without requiring the subsequent heat treatments of Forsyth or Broom. Forsyth[23] was able to observe the effect in thin films of Al-Mg-Zn as a depleted zone filled with dislocations arranged in a well-developed substructure. It is clear that the sequence of events leading to the concentration of slip into striations during the fatigue of age-hardening alloys is very different from that in pure metals. A further study of the literature reveals that the various age-hardening aluminium alloys respond differently to fatigue. Consequently, from the beginning of this investigation, attention has been concentrated upon one alloy, Al-4 wt.% Cu. The structure of this alloy and its precipitation behaviour are relatively well understood. Much is known about its response to uni-directional deformation, so that it is possible to base a study of its fatigue behaviour on a relatively firm foundation. Further, this investigation has been limited to the study of the earliest stage of fatigue, since this is of great fundamental interest and is the essential prerequisite to the later stages

of crack initiation and propagation. The greatest attention has been given to the mechanical behaviour of the alloy and how it alters during fatigue, since it is this aspect of the problem that has been least studied so far, although it must be known before any quantitative theory can be developed.

CHAPTER II

Products of Age-hardening in Al-Cu Alloys

1. Phase Change Leading to Precipitation

Age-hardening originates in the atomic rearrangements accompanying the break-down of supersaturated solid solutions. The changes are mostly submicroscopic and highly complex.

The free energy change provides the driving force for precipitation and the process is controlled by the thermodynamical factors of the solid solution state, diffusion, nucleation and the free energy relationships between the phases. Most age hardening systems transform with the conventional type of nucleation and growth process and thus there is a nucleation barrier which has to be overcome by composition fluctuation before there is a net decrease in the free energy of the system. Attention, therefore, must be focused on the diffusion coefficient of Cu in Al

$$D_{Cu} = A \exp - \left(\frac{E_F + E_M}{kT}\right)$$

where E_F and E_M are the activation energies for the formation and migration of vacancies respectively and A is a constant[25]. At 20°C, assuming that $E_F + E_M = 1.4$ eV, $D_{Cu} \simeq 10^{-24}$ cm.^{2}/sec. It is possible only to estimate the experimental diffusion coefficient since the size and spacing of the initial clusters are not sufficiently well known.

DeSorbo et al[26] have calculated $D_{Cu} \sim 10^{-16}$ cm.^{2}/sec. by assuming that the copper atoms move three or four atom diameters during clustering. Thus there is a discrepancy of $\sim 10^8$ between the experimental and theoretical figures. Now the excess vacancy theory attributes this discrepancy to the fact that diffusion is governed by a vacancy concentration and so

$$D_{Cu} = A \exp(-\frac{E_M}{kT_A}) \exp(-\frac{E_F}{kT_H}) \quad ,$$

T_H referring to the quenching temperature where the vacancy concentration is at equilibrium and T_A to the actual temperature. The second exponential is constant for the initial stages of ageing but decreases as vacancies are annihilated at sinks. D_{Cu} values of 5×10^{-16} cm.^{2}/sec. calculated this way are in good agreement with the value estimated from experimental data. The discrepancy between the theoretical and measured diffusion coefficients will depend on T_A and these ideas also explain why the rate of quenching has such a marked effect on the kinetics of clustering. If the quench is slow, some vacancies have time to migrate to sinks and the retained vacancy concentration will not be associated with T_H, but with some lower temperature.

In this analysis, therefore, phase change leading to precipitation is very much a vacancy concentration dependent process in the initial very rapid clustering stage, followed by a slow reaction and it is suggested from resistivity measurements that thus it takes a long time for the vacancy concentration to fall to its equilibrium value. Vacancy concentration ranks beside solute content, ageing time and ageing temperature as variables controlling precipitation.

2. Sequence of Precipitation

Most alloys precipitate at least one intermediate phase on ageing and the precipitation sequence at any temperature is simply determined by the principle that the alloy decomposes initially along the path of minimum activation energy rather than maximum loss of free energy.

Detailed arguments on the interpretations of X-ray diffraction patterns have led to a general acceptance of Guinier's theory[27] of a succession of precipitate types when each stage of ageing is associated with a definite precipitate type, but that the first precipitates were poorly defined and constituted a pre-precipitation stage. GP zones are a second phase in exactly the same way as the equilibrium precipitate is, the only difference lying in the nature of the interface which is coherent for the zones and possibly more diffuse than for the equilibrium precipitate. The origin of this distinction between GP zones and the intermediate precipitate lies in the interpretation of X-ray diffraction patterns since the former, having a structure very similar to that of the matrix, simply distorts the matrix reflections, whereas the latter produces a diffraction pattern which is well separated from the matrix pattern. Thus the distinction is an artificial one and in the electron microscope there is no difference in the images of GP zones, θ'' and θ' apart from one of scale and the effect of these precipitates on the surrounding matrix. Kelly and Nicholson[25] conclude, therefore, that the term GP zones is useful in describing the initial precipitate in a number of alloys where the structure of the precipitate is similar to that of the matrix, but the use of this term does not imply any fundamental difference from the subsequent intermediate precipitates.

At early stages in the ageing process, clustering of Cu atoms develops solute rich regions which are called GP zones. Later an ordered structure is formed, the θ". These two are fully coherent with the matrix. (Definition taken from (25): "A completely coherent precipitate is one in which all interfaces with the matrix are coherent and the Bravais lattices in the two crystal structures are identical if differences in chemical species and consequent small changes in atomic spacing are neglected".) The next type of precipitate θ' is only partially coherent and the product of overageing the θ equilibrium precipitate ($CuAl_2$) has only an orientation relationship with the matrix but is not coherent.

3. The Nature of the Precipitates

a) GP Zones

Clusters grow through a diffusion process by simple interchange of atoms on a fixed array of sites, until they give rise to the X-ray diffraction effects typical of GP zones. The first atoms formed must be completely coherent with the matrix. As the Cu atom is a little smaller than the Al atom, misfit must exist, so elastic strain is produced in the matrix and this strain governs the form of precipitate and the plane of the matrix on which it lies. Spheres are generally formed when the atomic misfit is $< 3\%$ and discs when the misfit is $> 5\%$.

It is clear that the copper atoms concentrate preferentially on {100} planes in the aluminium lattice, but according to Hardy and Heal[28], to what extent Cu atoms have replaced Al atoms and how many planes are enriched in Cu atoms, and also the extent of the distortion

caused by this concentration in adjacent Al lattice planes, is not yet determined accurately. From the work of Nicholson and Nutting[29] it is assumed that GP zones are disc-shaped with 3 - 6 Å or one atomic plane thickness and ~ 80Å diameter with an average separation of 100Å.

The nature of the interface--coherent--and the shape of the precipitate--disc--have a great influence on the mechanical properties of the resulting two-phase structure as it is shown in the next chapter.

b) Theta Double Prime (θ") Precipitate

The reference to this precipitate as GP 2 was pointed out by Nicholson[30] as not quite correct, since it has a definite crystallographic structure (Fig. 1) and is more like the intermediate precipitate θ' than the zone GP 1 . The correct structure of θ" has been worked out by several authors, viz., Gerold[31], Guinier[32], Silcock et al[33] and Guinier[34]. This phase also appears as plates on the {100} planes of the aluminium lattice with a tetragonal structure of a = b = 4.05Å and c = 7.6Å compared with the aluminium matrix of a = b = c = 4.04Å. As θ" grows by the decomposition of GP zones, c varies and decreases from 8.0Å to 7.6Å (Graf[33,35]). The orientation relationship between θ" and the aluminium matrix is {100}θ"//{100}Al. The plane is thought to be completely coherent with the matrix and thus the lattice is considerably strained, but only in the c direction--which coincides with the thin dimension of the plate--since the lattice parameters are the same as that of aluminium across a and b.

The dimensions of the particles vary with ageing time, being about 8Å thick and 125Å diameter to 30Å thick and 600Å in diameter.

There is a distribution in size and the width of this distribution increases with ageing time.

The average separation of these precipitates is only about 300Å[29] and this has great significance when energetical considerations are made on whether cutting, bending or climbing is the more probable when dislocations encounter the precipitates.

From the model of θ" strain field drawn[30] (Fig. 2), it becomes clear that with the increasing size, the strain to be accommodated in the matrix becomes larger and larger and eventually the whole of the regions between the precipitates will be strained. On electron micrographs it is noticeable that there are dark regions adjacent to some of the precipitates and Nutting[29] showed that these were due to diffraction contrast produced by elastic strains in the matrix. With high density of θ" which is typical near peak hardness, the strain fields stretch from one precipitate to another, forming a checkered pattern.

c) θ' Precipitate

The change of θ" to θ' and the homogeneous nucleation of θ' at high ageing temperatures have not yet been studied in detail. No strain fields have been observed near θ' precipitates and there is some metallographic evidence by Nicholson et al[36] for the existence of structural dislocations around the precipitates.

Thomas and Nutting[37] showed that the distribution of helical dislocations in the quenched alloy and the distribution of θ' precipitates as observed in oxide replicas is consistent with the theory that helical dislocations act as preferential nucleating sites for θ'

precipitates. More recently, Nicholson[38,39] has used the thin foil technique to study the actual nucleation process and confirmed earlier suggestions by Thomas and Nutting[40] and Wilsdorf and Kuhlmann[41] that only certain θ' orientations are present in each array of precipitates.

The heterogeneous nucleation of θ' accounts for an appreciable fraction of the total θ' precipitation, since large precipitates grow from each helix.

The structure itself is quite well established (Fig. 3), due to the work of Gerold[31] and Graf[33,35]. It is tetragonal with a = b = 4.05Å and c = 5.8Å. The orientation relationship of θ' and the aluminium matrix is $\{100\}\theta' // \{100\}$Al appearing as a disc on the $\{100\}$ planes of the aluminium matrix. It is only partially coherent--the face of the disc--while the c-b or c-a plane is incoherent, the c direction of the cell being the thin dimension of the disc. The particles change in size as ageing proceeds from about 50Å thick and 1000Å in diameter to 200Å thick and 4000Å in diameter. There is a very wide distribution of sizes.

d) θ Precipitate

This precipitate is not encountered at ageing times less than some thousands of hours at temperatures below 200°C according to Bonar[42]. It is the equilibrium precipitate in this system and has the chemical composition $CuAl_2$. It is also tetragonal with a = b = 6.066Å and c = 4.874Å; values have been published by many workers, e.g., Axon and Hume-Rothery[43].

The mode of formation of the θ phase has long been a matter of considerable uncertainty. Laird and Aaronson[44] reported that both morphological and crystallographic observations at foil surfaces indicate that the behaviour of θ formed in foils is qualitatively identical to that exhibited in bulk specimens and conclude the following:

Three reactions occur simultaneously during the formation of θ crystals: θ consumes θ' crystal at which it is nucleated, regions of the α matrix surrounding these θ' plates are simultaneously transformed to θ and θ' plates in the vicinity of growing θ crystals dissolve principally by shortening, but also by thinning. θ is blocky in shape except when formed at low ageing temperatures ($< 250^{\circ}C$) when it tends to appear as thick plates on the {100} planes of the matrix. These precipitates are completely non-coherent.

Vaughan and Silcock[45] report the formation of θ rods from θ' plates in an Al-4% Cu alloy, and from the shapes of θ and irregular gaps between the θ and θ' conclude that nucleation of θ within θ' plate and subsequent growth by dissolution of θ' is the transformation mechanism. (These rod-type precipitates are evident in this project, too.)

e) Transition States

In the previous sections, from the description of formation, it is obvious that at certain times in the ageing, there will be at least two types of precipitate present.

The transition of θ'' to θ' is of great interest, as it is in the vicinity of this transition that the mechanical properties alter drastically. It is suggested[30] that while θ'' is the predominant precipitate,

θ' can be nucleated on helical dislocations which have resulted from the quench. Precipitation of θ' in general seems to take place at random. Bonar[42], considering the large disparity in the mean particle diameter and growth rate between θ' and θ'', suggests that the growth process of θ' is quite independent of the presence of θ'', but nucleation of θ' may take place on certain θ'' plates.

CHAPTER III

Theories of Precipitation Strengthening

Before going into the discussion of effects and behaviour of precipitates, it seems appropriate to state that since initially the strength of the alloy is due to the short range interactions of solid solution strengthening and long range effects as caused by the non-uniform distribution of impurity atoms, then as the precipitation takes place and other interactions become dominant, the former constraints still have to be taken into account.

The magnitude of these constraints can be obtained from literature on the deformation of single crystals of pure metals and alloys, but care must be taken to use values obtained from comparable materials.

Regarding the impurity effect, from the composition (impurity $< 0.004\%$) and from the method of preparing the present test pieces, it appears reasonable to say that in this high purity material where the distribution of impurity is uniform, this type of constraint is negligible.

1. Strength of an Alloy Containing Coherent Precipitates

Is the initial flow stress of an alloy containing coherent precipitates due to shearing the particles by moving dislocations or because of bending of dislocation lines between them? The answer depends on

the spacing of the obstacles and on the stress necessary to shear them. The process requiring the smaller applied stress will occur.

According to Orowan[46], the dislocation is able to bow out between obstacles when the stress acting is:

$$\tau = \frac{T}{b\rho} \qquad \text{----------(III/1)}$$

where: T is the line tension of dislocation,

ρ is the radius of curvature of the loop and is equal to d/2, where d is the separation between obstacles,

and b is the Burgers vector.

Thus,

$$\tau = \frac{2T}{bd} \qquad \text{----------(III/2)}$$

and to make this equation more practical, the line tension has to be dealt with.

The concept introduced by Mott and Nabarro[47] is that a dislocation line will always tend to lie along a straight line, since this corresponds to the lowest energy position. The strain energy of a dislocation is a property of unit length and so an increase in length will correspond to an increase in energy.

Cottrell[48], expressing the line tension of an edge dislocation, gives:

$$T = \frac{Gb^2}{2\pi(1-\nu)} \ln\left(\frac{\lambda}{r_o}\right)$$

in his model which corresponds to

$$T = \frac{Gb^2}{2\pi(1-\nu)} \ln\left(\frac{d}{b}\right)$$

when dealing with dispersed particles and d is the equivalent of the cylinder radius in the model in which all the energy is assumed to be confined. G is the shear modulus and ν the Poisson's ratio.

Nabarro[49] derives a different formula, and a different one again[50] for a circular dislocation loop, but in all these equations,

$$T = \alpha\, Gb^2 \quad , \qquad \text{----------(III/3)}$$

and as uncertainty is involved in these expressions, a value of $\alpha = 0.5$ is generally used in this type of calculation. That is, (III/2) can be rewritten to get Orowan's criterion to estimate the flow stress:

$$\tau = \frac{Gb}{d} \qquad \text{----------(III/4)}$$

Values calculated and experimental measurements show agreement only when overageing of an alloy occurs (Hart[51]).

Kelly and Fine[52] estimated the stress required to shear zones in Al-Cu alloys from the heats of reversion.

In this work, on Al-2 at% Cu, an estimate is made of the applied stress enabling dislocations to break through the zones. If each atomic length of the dislocation must be separately forced through a GP zone, the shear stress necessary to do this is:

$$\sigma b^3 \approx \frac{\Delta E}{2} \qquad \text{----------(III/5)}$$

where ΔE is the energy difference between a Cu atom in GP zone and in solution in the Al.

If, however, the length of dislocation lying between precipitates is taken into account:

$$\sigma b^2 d = \frac{\Delta E}{2} \quad . \qquad \text{- - - - - - - - - - -(III/6)}$$

As in aluminium alloys of this composition, slip occurs on (111) planes in $[1\bar{1}0]$ directions, the zones (Fig. 4) being on the $\{100\}$ planes of the aluminium matrix, one-third of the zones lying perpendicular to the direction of motion of any dislocation. Thus (III/5) is an over-estimate and (III/6) an underestimate of σ value.

Suzuki[53] found the heat of reversion for a 2 at% Cu alloy to be 1.3 cal/g, giving a value of ΔE = 0.077 eV per atom of Cu and this gives, with (III/5): σ = 28 Kg/mm^2

and with (III/6): $\sigma \simeq 0.5$ Kg/mm^2 .

Experimental values of the flow stress in polycrystalline alloys vary between 9 and 17 Kg/mm^2 (Hardy[54]) within the range of values predicted by this analysis. Using either theoretical calculation to obtain the average distance between the centres of zones in the slip plane[52] or taking values obtained through microscopy work[29], the calculated flow stress using Orowan's criterion gives

$$\sigma \simeq 50 + \text{Kg/mm}^2$$

values when G is taken as 2.5×10^{11} dynes/cm^2 and $b = 2.8 \times 10^{-8}$ cm.

From this analysis, therefore, the conclusion is that the initial flow stress is more likely to be the stress necessary to shear the zones than that necessary to bend dislocation loops between them.

2. Factors Involved in Cutting the Precipitates

The work done in forcing the dislocations through the precipitate may be governed by any of the following factors.

a) Coherency Stresses

When the dislocation is at a distance from the precipitate of the same order as the precipitate spacing, a long-range interaction between the dislocation and precipitates is occurring, due to the coherency stresses in the matrix.

In a theoretical treatment, the difficulty is how to average over the whole dislocation line the effect of the individual precipitates.

Mott and Nabarro[55] evaluated the stress for the case of a completely coherent spherical inclusion of radius r_o containing material of atomic volume $(1+\delta)^3$ where the atomic volume of the matrix is unity. The stress in the precipitate is a uniform pressure of $P = 3K(\delta - \epsilon)$ where:

$$\epsilon = \frac{3K\delta}{3K + 2E/(1+\nu)} ,$$

K being the bulk modulus of the precipitate, E, Young's modulus of the matrix, and ν, Poisson's ratio of the matrix. The shear strain at a distance r from the precipitate is

$$\frac{\epsilon r_o^3}{r^3} ,$$

which has a constant value at the surface of the precipitate, independent of the radius of the precipitate r_o.

A crystal with N spherical inclusions per unit volume has an average distance of a point on the matrix from the nearest particle as $1/2\ N^{-1/3}$ and so the average shear strain is $\bar{\gamma} = 8\epsilon r_o^3 N$ and since $4/3\pi N r_o^3$ is equal to the volume fraction of precipitate f, which gives an average shear strain in the matrix

$$\gamma = 2\epsilon f \qquad \text{- - - - - - - - - - (III/7)}$$

The average shear strain in the matrix is independent of the size of the inclusion. Since the strain energy depends only on the volume fraction of the precipitate, then the formation of a smaller number of larger precipitates leads to no reduction in the total strain energy of a precipitating system.

Mott and Nabarro[47] identify the flow stress by multiplying the above expression by the shear modulus G and getting the critical resolved shear stress;

$$\tau = 2G\epsilon f \qquad \text{- - - - - - - - - - (III/8)}$$

They assume that this average should be taken to obtain the flow stress when the minimum radius of curvature to which dislocations can be bent by the internal stress is smaller than the mean separation of the precipitates in the glide plane. The minimum radius of curvature is given by:

$$\tau_i b = T\rho \ ,$$

where $\tau_i = 2G\epsilon f$ and $T \simeq 0.5\ Gb^2$, so the separation, d, of precipitates in the glide plane must fulfill the condition

$$d \geqslant \frac{b}{4\epsilon f} \ .$$

If d is much less than this value, then the flow stress should not be identified with the mean internal stress.

Hart[51] has pointed out that when this critical particle spacing applies, the dislocations must pass through the particles, as the stress necessary to expand dislocation loops between centres of

dilatation without their passing through these centres is given by

$$\tau_o = \frac{T2}{bd}$$

and taking $d = \frac{b}{4\epsilon f}$ and $\tau_i = 2G\epsilon f$ gives $\tau_o = 4G\epsilon f = 2\tau_i$.

As the interparticle spacing increases further, according to Mott and Nabarro's theory, the strength should remain constant and even if d becomes so large that dislocations can pass between obstacles, the flow stress will not be governed by the interparticle spacing, but by the equation $\tau = \tau_i = 2G\epsilon f$. Kelly and Nicholson conclude, then, that according to this theory, the flow stress is governed not by the mean internal stress, but by the forces on the dislocation due to the internal stresses when a dislocation is close to an obstacle. A much more detailed calculation than Mott and Nabarro's is then required to predict the flow stress.

The separation of the precipitates is often of the same order as the precipitate diameter and the process of finding the average force on a dislocation due to coherency stresses becomes very difficult. Franz and Kröner[56] have pointed out that the stress field of a thin disc-shaped precipitate is equivalent to that of a loop of edge dislocation and Saada[57] calculated the stress necessary to force a dislocation through a forest of dislocations cutting the glide plane against the forces of interaction between the moving dislocation and the fixed forest dislocations, $\tau = \frac{Gb_p}{5l}$, where l is the average separation of fixed dislocation threading the glide plane and b_p is their B. vector. Kelly and Nicholson[25] use Saada's method by setting b_p equal to the

discontinuity in elastic displacement obtained by making a Burgers circuit around the precipitate and approximating the stress field of a zone by that of a ring of edge dislocation. From Gerold's X-ray results[58] for the strains around a GP zone, the closure failure of a Burgers circuit is taken as 0.404×10^{-8} cm. and with Saada's equation, using the mean free path between precipitates as estimated from electron micrograph as 70Å, $\tau \sim 3.0$ Kg/mm^2 is obtained. It seems from this crude estimate that coherency stresses do not account for the total flow stress.

b) Internal Order of Precipitates

The precipitate may be ordered internally, in which case if the Burgers vector of the moving dislocation is not equal to the repeat distance of the ordered structure, then work must be done to create the disordered interface across the slip plane.

Griffith[59] and Fisher's[60] original idea applied to precipitation systems by Williams[61] and Kelly[62] gives the following results on the problem.

When a dislocation shears a particle, a surface consisting of two new interface regions is produced. If the precipitate is ordered internally, then an interface of energy γ_p per unit area is produced of area approximately πr_i^2, where r_i is the average radius of the circular section of a particle of radius r by the slip plane,

$$r_i = \sqrt{2/3}\ r \quad .$$

The energy of the additional particle-matrix interface produced by slip being γ_s per unit area and the area produced $2r_i b$, where b is the Burgers vector of the moving dislocation.

The work done by the applied stress in moving a dislocation across a unit area of the glide plane is γ_b and the increase in energy of the system due to the cutting of the particles is $n(\pi r_i^2 \gamma_p + 2r_i b\gamma_s)$ where n is the number of particles intersecting unit area of the glide plane.

Introducing f, the volume fraction of precipitate

$$f = \frac{2\pi r^2 n}{3}$$

and equating γ_b with the increase of energy expression due to cutting gives

$$\tau = \frac{f\gamma_p}{b} + \frac{3}{\pi}\sqrt{\frac{2}{3}}\,\frac{f\gamma_s}{r} \qquad \text{- - - - - - - - - - (III/9)}$$

If γ_p is much greater than γ_s, then the flow stress will be independent of particle size and depend only on the volume fraction of precipitate being given by

$$\tau \gg \frac{f\gamma_p}{b} \quad .$$

If the particles are not ordered internally, that is $\gamma_p = 0$ then

$$\tau \gg \frac{\sqrt{6}}{\pi}\,\frac{f\gamma_s}{r} \quad .$$

Williams estimated γ_p for Al-Ag alloys and calculated a value of 13.9 ergs/cm.^{2}

The value of γ_s for GP zones is estimated by Kelly[62], using heat of reversion figures as

$$\gamma_s \simeq \frac{\Delta E}{3b^2} \sim 150 \text{ ergs/cm.}^2$$

Similar results are reported by Byrne et al[63] (80 ergs/cm.^{2}) and Kelly and Fine[52] (200 ergs/cm.^{2}) obtained by using the same method.

Kelly and Nicholson, using (III/9) with the following values:

$$\gamma_p = \gamma_s = 200 \text{ ergs/cm}^2$$

$$f = 2 \times 10^{-2}$$

$$b = 2.5 \times 10^{-8} \text{ cm.}$$

$$r = 50 \times 10^{-8} \text{ cm.}$$

obtain

$$\tau \simeq 2.0 \text{ Kg/mm}^2$$

for spherical coherent particles as a lower limit and to obtain the upper limit, the energy balance must be performed at each particle leading to

$$\tau = \frac{\gamma}{2}\sqrt{\pi}\,\frac{f^{1/2}}{b}$$

and using values as above gives

$$\tau \simeq 9 \text{ Kg/mm}^2 \ .$$

A discussion between Hirsch and Kelly led Bonar[42] to investigate another mechanism of strengthening. If the particles have a stacking fault energy which is considerably lower than the stacking fault energy of the matrix, then the dislocation cutting the particle will tend to dissociate further while it is inside the particle than outside. This will produce a strengthening effect due to the work which must be done in constricting the partials back to their equilibrium matrix separation.

A sample calculation with the following formula:

$$\tau = \frac{Gb}{\bar{w}}\, f^{1/2} \ln \frac{w_2}{w_1} \ ,$$

where w_1 is the separation of partial dislocations in the matrix,

w_2 is the separation in the particle,

$$\bar{w} = \frac{w_1 + w_2}{2}$$

and taking $w_1 = 1b$

$$w_2 = 35\ b$$

leads to $\tau \simeq \frac{G}{500}$ value as a maximum, as w_1 and w_2 are extreme values.

Using $G = 2.5 \times 10^{11}$ dynes/cm.^{2}, this leads to:

$$\tau \simeq \frac{2.5 \times 10^{11}}{9.81 \times 10^5 \times 10^2 \times 500} = 5.1 \text{ Kg/mm}^2 \ .$$

c) Interface Effect

The lattice parameter of matrix and precipitate may be different and then even if stresses in the matrix are neglected, work will be done in shearing the precipitate, due to the formation of a misfit dislocation at the interface.

Fleischer[64] suggested the model and approximated the energy of the new interface produced to that of a non-coherent boundary.

The magnitude of the Burgers vector of the interface dislocation will be $|b_m - b_p|$, where b_m and b_p are the Burgers vectors of the moving dislocations in the matrix and in the precipitate. Even though $|b_m - b_p|$ may be small, Fleischer attaches physical significance to this dislocation. The energy per unit length will be approximately

$$\frac{G|b_p - b_m|^2}{4\pi(1 - \nu)} \ln R/r_o$$

R equals the precipitate diameter and it is supposed that a length b of interface dislocation is produced when the dislocation moves forward

distance b. The production of the interface dislocation then makes a maximum contribution to γ_s (energy of the additional particle matrix interface) of about 0.6 $Gb|\Delta b/b|^2$, where $\Delta b = |b_m - b_p|$

For precipitates in Cu and in Al and values of $\Delta b/b$ of 0.01, the contribution is only between 1 - 3 ergs/cm.^{2} According to Fleischer's model, only for values of $\Delta b/b \gtrsim 0.1$ does the contribution to γ_s become comparable to that due to changes in species of near neighbours estimated by Kelly and Fine[52].

3. Temperature Dependence of Flow Stress with Coherent Precipitation

Mott and Nabarro[47], Seeger[65] and Mott[66] treated the subject theoretically and the results of Seeger's analysis[67] are briefly presented. The energy of the system is increased by U_o if the dislocation cuts one of the obstacles in the absence of an applied stress. If the dislocation moves under the influence of an applied stress τ, the potential hill to be surmounted is reduced to U. The stress which must be applied to reduce the potential hill to zero is τ_o. Mott[66] derives two expressions as:

$$U = U_o - 4\, b l_o x_o \tau \qquad \text{- - - - - - - - - - - (III/10)}$$

when τ is much less than τ_o, and when $\tau \simeq \tau_o$

$$U = U_o\left(1 - \frac{\tau}{\tau_o}\right)^{3/2} \qquad \text{- - - - - - - - - - - (III/11)}$$

l_o is the average spacing of the obstacles, x_o, the equilibrium positions of the dislocation and x_o/l_o is small.

Seeger[67] writes the strain rate $\dot{\epsilon}$:

$$\dot{\epsilon} = \dot{\epsilon}_o \exp - U_{(\tau)}/kT \quad \text{- - - - - - - - - - - (III/12)}$$

where $\dot{\epsilon}_o = N\,Ab\,\nu_o$,

N = number of points per unit volume at which dislocations are held up at obstacles,

A = the area of slip plane swept out by a dislocation per activated event,

b = Burgers vector, and

ν_o = vibration frequency of a dislocation obstacle.

Substituting (III/10) into (III/12),

$$\tau = \frac{U - kT \ln \dot{\epsilon}_o/\dot{\epsilon}}{\nu} \quad \text{- - - - - - - (III/13)}$$

where $\nu = 4\,bl_o x_o$ is usually called the activation volume and substituting (III/11) into (III/12),

$$\tau = \frac{U_o}{\nu}\left\{1 - \left[\frac{kT}{U_o} \ln \frac{\dot{\epsilon}_o}{\dot{\epsilon}}\right]^{2/3}\right\} \quad \text{- - - - - (III/14)}$$

Kelly and Nicholson[25] consider the temperature or strain rate dependence of flow stress of alloys containing coherent precipitates. They say that when the obstacles are narrow and the temperature dependence of flow stress large, (III/13) should be used, and when the temperature dependence of flow stress is small, (III/14) should be used.

Byrne et al[63] worked on the temperature dependence of the C.R.S.S. and strain rate dependence of the flow stress over the temperature range 4.2°K to 373°K. The results of C.R.S.S. against $T^{2/3}$ gives

a straight line except at one point where there is a break and this point is expressed from (III/14) as

$$T_c = \frac{U_o}{k \ln \left(\frac{\dot{\epsilon}_o}{\dot{\epsilon}}\right)} \qquad \text{- - - - - - - - - - - (III/15)}$$

Above T_c, the slope is not very sharp and below T_c the temperature dependence is significant. To explain this type of behaviour, Byrne et al[63] suggest that dislocation interaction takes place with two differently oriented zones. One-third of the zones lying in $[\bar{1}10]$ lie parallel to the Burgers vector of a moving dislocation and present a thin barrier (Fig. 4), because a change in the number of like and unlike nearest neighbours is produced only as the dislocation enters and leaves the zone; there is also no elastic interaction to a first approximation, since the Burgers vector of the moving dislocation is normal to that of the zone. The zones at an angle of 60° (in $[0\bar{1}1]$ and $[\bar{1}01]$) to the Burgers vector of the gliding dislocation provide a large barrier. Thus the given explanation is as follows: there is a large barrier, and hence the contribution to the flow stress depends on temperature only slightly, giving a straight line, but at T_c and below one-third of the obstacles, the thin barriers become temperature sensitive and, therefore, their ever-growing contribution with decreasing temperature is superimposed. The critical resolved shear stress of Al + 1.7 at% Cu containing GP zones was found to be 14 Kg/mm^2 at 0°K.

Price and Kelly[68], on single crystals of Al-3.8% Cu alloy containing GP zones, conclude that after plastic deformation at room

temperature and 77°K. the temperature dependence of the yield stress due to the contribution of solid solution matrix is probably important. Further, the plastic deformation of zone hardened crystals resembles that of pure metals, except that the alloy crystals have slightly higher work hardening rates, especially in the early stages of deformation at room temperature where age hardening may occur during straining.

Fleischer[69], considering the strengthening factors of thin zones of copper in aluminium, finds the different elastic constant of the zone as the most important one. Further, with calculation he shows that the effect of the different modulus of the zone is capable of explaining the observed temperature variation of the flow stress producing a curve which is very consistent with the experimental values[63]. Kelly[70], however, doubts this prominent part given to the modulus effect and proves that the good agreement between the values obtained[63] and Fleischer's calculation is not real and arises only because in the calculation, altered values were used for the activation energy and length of dislocations considered.

4. Strengthening with Non-deforming Particles

As the precipitate particles increase in size and possibly change their internal structure or the nature of their interface with the matrix, the work done in cutting each particle increases. At the same time, their spacing increases too, so dislocations are eventually forced between the particles instead of through them.

a) Orowan's Criterion

Orowan[32] pointed out that an additional stress is needed to expand dislocations between hard particles, when gliding in a soft and ductile matrix.

Large enough stress bends dislocations in a semi-circular shape between particles so that the dislocations can by-pass the obstacles leaving rings of dislocations behind.

The initial flow stress, then, must be composed from the matrix yield stress (τ_s) and this additional stress, $\tau_A = \frac{T2}{bd}$, that is,

$$\tau = \tau_s + \frac{2T}{bd} \quad . \quad - - - - - - - - - - - \text{(III/16)}$$

To test quantitatively the validity of Orowan's criterion, the line tension T has to be evaluated more accurately. Nabarro[49] treated this problem most extensively and using his expression for line tension and substituting into (III/16),

$$\tau = \tau_s + \frac{Gb}{4\pi} \phi \ln\left\{\frac{d - 2r}{2b}\right\} \frac{1}{(d - 2r)/2} \quad - - \text{(III/17)}$$

which is the final form of Orowan's prediction, by which the initial yield stress should be given.

$\phi = 1/2(1 + \frac{1}{1 - \nu})$ is the mean of the factors for an edge and for a screw dislocation.

b) Ansell and Lenel's Plastic Flow Criteria

Ansell and Lenel[71] reject Orowan's idea and suggest that detectable plastic flow will occur only when the particles of the second phase are broken. The stress necessary to fracture the precipitates is

supplied from the pile-ups of dislocations against the precipitates.

Kelly and Nicholson[25] show that the pile-ups against the particles must be in the form of pinched-off loops. The back-stress from n loops stops the source from operating (Cottrell[48]) when

$$n = \frac{2(2R - 2r)}{Gb} \quad . \quad - - - - - - - - - - - - \quad (III/19)$$

Ansell and Lenel[71,72] maintain that detectable plastic flow occurs only when the particles break, i.e., when the stress on them, given by Fisher, Hart and Pry[73] as nGb/r, reaches the theoretical strength of the particle, i.e., G'/c, where G' is the elastic modulus of the particle and c is a constant approximately equal to 30. Inserting these values in (III/19), the yield stress is found to be

$$\tau_A = \frac{G'}{4c} \frac{r}{R - r} \quad .$$

Since for spherical particles $r/R = \frac{f^{1/3}}{0.82}$, where f is the volume fraction, then the final form of Ansell and Lenel's theory is

$$\tau = \tau_s + \frac{G'}{4c} \frac{f^{1/3}}{(0.82 - f^{1/3})} \quad - - - - - - \quad (III/21)$$

where τ_s is the yield strength of the matrix without the dispersion.

Kelly and Nicholson[25] criticize Ansell and Lenel's theory on the grounds that 1) the expression (III/19) is derived for straight dislocations and may not hold for pinched-off loops, 2) there is no experimental evidence that the particles are sheared at the yield strength (although, as Ansell points out, it is extremely difficult to detect shear in the particles).

Experimental evidence on Al-Cu alloys by Dew-Hughes and Robertson[74] indicated the validity of Orowan's criterion. θ particles were produced in Al-4wt.% Cu single crystal material and during tensile deformation, bowing out of dislocation occurred and the deviation from $\tau_c = \frac{Gb}{d}$ relationship was only assumed to be due to non-uniform distribution and non-spherical shape of the precipitates.

Bonar's work[42] supports the case represented by Fig. 5, where Orowan's criterion is satisfied after a certain ageing time and cutting takes place prior to that.

Byrne et al[63], on Al-1.7 at% Cu single crystals containing θ precipitates, measured the temperature dependence of the yield stress and found the results consistent with (III/17), supporting the validity of Orowan's criterion.

However, data calculated by Tyson[75] on the mean interparticle spacing and plotted against yield strength from results of Roberts et al[76] is quite consistent with Orowan's relation and also with Ansell and Lenel's relation. The difficulty in this matter is deciding the value of interparticle spacing for non-spherical particles and also that this value can vary with the temperature if the moving dislocations are not confined to a single plane, but may leave this by cross slip.

c) Kelly and Nicholson's Theory of the Interaction of Dislocations with Precipitates[25].

As the ageing time or temperature is increased and the precipitate size and spacing increases, there may come a point when a lower stress is required to expand dislocation loops between obstacles than

to shear the precipitate. When the precipitates are fully coherent and small, cutting occurs with high initial flow stress and a rate of work-hardening comparable to that of pure matrix metals. Non-coherent precipitates are usually not deformed and stress-strain curves show a very rapid rate of work-hardening initially, flattening off and becoming approximately parallel to that of the matrix metal.

Kelly and Nicholson attempt to find some criteria to account for this different behaviour and to predict when the transition should occur.

Considering non-coherent particles with an applied stress of

$$\tau_o = \frac{Gb}{d} \qquad \text{- - - - - - - - - - - - (III/22)}$$

By cutting, within the particle a high energy interface of energy γ per unit area is produced.

If the work done by the applied stress in moving the dislocation forward a distance 2r is equal to the interface energy produced (r = radius of particle), then the necessary applied stress is:

$$\tau_c bd2r = \pi r^2 \gamma$$

$$\tau_c = \frac{\pi r^2 \gamma}{2bdr} = \frac{\pi}{2}\frac{\gamma r}{bd} \qquad \text{- - - - - - - - - - - - (III/23)}$$

If $\tau_c > \tau_o$, bowing takes place leaving dislocation loops behind; if $\tau_c < \tau_o$, the particles will be sheared.

Since τ_c increases with particle radius and τ_o is independent of it, equating (III/22) with (III/23) gives

$$r_c = \frac{2Gb^2}{\pi\gamma} \qquad \text{- - - - - - - - - - - - (III/24)}$$

as a critical particle radius for cutting.

The energy of interface produced within non-coherent particles by quite a different vector b, will approximate to that of a high energy grain boundary. From Van Der Merwe's work[77], the energy for a tilt boundary about an arbitrary axis unrelated to the crystal structure is:

$$\frac{0.6}{2\pi^2} G'b' (1 - 2\nu') \text{ ergs/cm.}^2$$

and for a similar twist boundary:

$$\frac{0.9}{2\pi^2} G'b' \text{ ergs/cm.}^2,$$

where G', b' and ν' are the shear modulus, smallest lattice translation vector and Poisson's ratio, respectively.

Taking the arithmetic average of these two values with $\nu = 0.3$:

$$\gamma = 0.03\ G'b'$$

so

$$r_c = \frac{2Gb^2}{0.03\pi\ G'b'} \qquad \text{- - - - - - - - - - - (III/25)}$$

If G = G' and b = b', r_c = 20 b, so the largest particle to be sheared is

$$d \simeq 40b \simeq 100\text{Å} ,$$

if the perfect non-coherent particle has about the same elastic moduli as the matrix.

If the particles contain dislocations with a different Burgers vector, shearing will not create high energy interface, but a ring of dislocation of Burgers vector $|b_p - b_m|$ will be left at the interface. The energy of this loop is

$$\frac{G'|b_p - b_m|^2}{4\pi} \phi \ln \frac{r}{2b} 2\pi r ,$$

and if only particles greater than 1μ diameter contain dislocations, this reduces to $6G''|b_p - b_m|^2 r$, where G'' refers to some average of the shear modulus of the matrix and particle.

Now the work done by the applied stress in moving the dislocation forward a distance 2r must equal the energy of the loop of dislocation produced around the particle:

$$\tau_c bd\, 2r = 6G''|b_p - b_m|^2 r$$

or

$$\tau_c = \frac{3G''|b_p - b_m|^2}{bd} \qquad \text{- - - - - - - - - - - (III/26)}$$

τ_c is independent of particle size.

Thus if $|b_p - b_m|$ is less than b_m, large non-coherent particles will deform with the matrix if they contain dislocations.

For partially coherent precipitates and coherent precipitates which are ordered internally and do not contain dislocations, the same argument is used which leads to (III/24),

$$r_c = \frac{2Gb^2}{\pi\gamma}$$

and if the value of γ for an ordered precipitate which is fully coherent will be of the order of 100 ergs/cm^2 and depending on the G and b values, precipitates of diameter up to 200Å will be sheared but larger ones will not. The same behaviour is predicted with partially coherent precipitates.

Bonar[42] produced results indicating some validity of this analysis. Al-1.6 at% Cu crystals aged at 190°C for 2 hours giving predominantly θ'' and aged for 100 hours giving predominantly θ' showed the following:

With θ", the C.R.S.S. was large and dislocations passed through θ" particles. As θ' replaced θ", there was initially no change, but as the size of θ' plates increased and a size was reached when the initial dislocations moving on the matrix did not pass through θ' particles, the C.R.S.S. fell and simultaneously the rate of work-hardening increased. Between 40 and 100 hours ageing time, the behaviour was very variable.

5. Work-hardening Characteristics

Alloys containing coherent precipitates show very similar work-hardening characteristics to those of pure metals.

Very great differences are found if the alloy contains strong non-coherent particles which are undeformed at small strains whilst the matrix material deforms around them.

Fisher, Hart and Pry[73] treated this question theoretically, using a model where a Frank-Read source operates in the matrix and the particles collect dislocation loops around them, supposedly of glissile type. The loops encircling the particles exert a shear stress on the surrounding slip plane which opposes further slip. This back-stress is found to be fairly uniform over the slip plane and its value is calculated as

$$\tau_h = \frac{cf^{3/2}NGb}{r} \qquad \text{- - - - - - - - - - - (III/27)}$$

where Fisher et al give c = 3 value and

f = volume fraction of precipitate,

r = radius of particle,

N = number of loops.

NGb/r is a measure of the shear stress due to the encircling loops at

the centre of the particle and of the stresses in the surrounding matrix. When this reaches a critical value τ_c the increment of flow stress represented by τ_h reaches a maximum:

$$\tau_{h\,max} = 3f^{3/2}\tau_c \qquad \text{- - - - - - - - - - - (III/28)}$$

Limitations of this theory appear to be that the possibility of slip on many systems and cross-slip taking place is neglected. Also, when the maximum in the increment of work-hardening is attained which should correspond to τ_c, the particles of $CuAl_2$ are generally not sheared. Work on Al-Cu single crystals[74] containing θ phase also indicates that to satisfy the equation, the number of loops had to be between 30 and 100, and this high number, considering the shear stress of a particle and also that of the matrix within a volume of the same order as the particle volume, leaves doubt as to whether the stresses in the matrix would exceed the theoretical shear strength.

Thomas and Nutting[78] observed cross-slip around particles in Al-Cu alloys and Ashby and Smith[79] observed prismatic loops at the particles in internally oxidized Cu-Al alloys. Hirsch[80] proposed originally that prismatic loops can be left around particles due to cross-slip.

If cross-slip is easy, dislocations can glide and slip into another slip plane with the formation of jogs, leaving prismatic loops at the obstacles producing stresses of the same order as the glissile loops considered by Fisher et al[73].

These loops are dipoles or prismatic loops of edge dislocations which can act as a source of dislocations if one edge of the dipole lies completely in the slip plane when the stress upon it reaches the value

$$\tau \approx \frac{Gb}{2\pi(1-\nu)} \frac{1}{x} \qquad \text{- - - - - - - - - - - (III/29)}$$

x being the height of the loop.

The rapid rate of work-hardening in dispersion-hardened alloys must be attributed to prismatic loop formation, the dispersed particles catalyzing very turbulent slip on many systems which, in addition, leads to many dislocation interactions causing a rapid increase of dislocation density.

Ashby[81] develops a work-hardening theory applicable to metals with non-deforming particles as follows. Dislocations bow out to by-pass particles and cross-slip is one of the possible mechanisms (Fig. 6). The cross-slip path of a dislocation depends on the local stresses around the particle, thus the loop left around when by-passing is completed does not lie in the slip plane but at an angle to it. Also, there are at least three slip systems operating. Consequently, the loops are distributed in a fairly random way. Dislocation cells are formed during deformation with jogged and tangled walls segregating into regions of high density--the cell walls--and low density, the interior of the cells. Further, there are two contributions to the dislocation density at a given strain; one from the loops and the other from the glide dislocations. He argues that the average glide dislocation moves a distance, large compared to the cell size and so it has to go through a forest of dislocations forming the cell structure.

The stress needed to force dislocation to cut through the forest is the increment in flow stress caused by work-hardening. He calculates this increment with

$$(\Delta\tau)_{\epsilon,T} = 1/2\ G\sqrt{\frac{bf}{r_s}}$$

for tensile strain ϵ where

r_s is the mean planar particle radius $r_s = \sqrt{\frac{2}{3}}\ r_v$,

r_v being the particle radius,

f is the volume fraction of precipitate.

The equation relating the flow stress to tensile strain in dispersion-hardened alloys is well supported by experimental results when Ashby makes this comparison.

Barnby and Smith[82] found on the deformation of an austenitic steel containing a distribution of coarse precipitates that dense clusters of dislocations are nucleated at particles of $M_{23}C_6$, eventually link up to form a cell structure with dimensions comparable to the inter-particle spacing. They suggest and develop a model where the increase in work-hardening rate, due to the presence of the $M_{23}C_6$ particles, arises from the difficulty of moving dislocations through a matrix containing a cell structure.

Finally, Mitchell et al[92] report on low temperature deformation of an alloy containing θ particles that the thermally activated rate-controlling mechanism for the plastic deformation is determined by the dislocation intersection mechanism. A distinctive parameter of this mechanism is the distance L between forest dislocations. They find that

1/L is somewhat greater for dispersion-strengthened alloys than for high purity Al polycrystals and further that the much more rapid increase in 1/L with strain for dispersion-strengthened alloys is a major factor responsible for the strain-hardening of dispersion-strengthened alloys.

6. Effects of Deformation on the Precipitate Structure

a) Deformation of Supersaturated Alloys Before Precipitation

Kedzie and Dodd[83] report on cyclically strained age-hardening Al-Cu supersaturated solid solutions that the fatigue strength-tensile strength ratios determined at 150°C, 25°C and -195°C decrease with increasing alloy content, but at -195°C much more rapidly. This suggested that strain ageing and/or age-hardening occurred during tests at higher temperatures. Additionally, these ratios at 150°C exceeded those at 25°C for all compositions, indicating greater strengthening during fatigue at 150°C.

Gane and Parkins[84] observed on Al-4.2% Cu supersaturated alloy that if the material is cold-worked and then aged at various temperatures, the hardness first falls off, reaching a minimum at about 2 minutes in the case of 200°C treatment and then rises to peak hardness before over-ageing occurs and then the hardness falls again. With unstrained material, the case is different: the curve starts with horizontal section reaching a maximum well below the peak hardness obtained in the cold-worked sample. Tensile and compression tests show the same trend: 10% strain followed by 200°C treatment for 3 minutes results in a drop in yield stress of about 30-35%. These changes are attributed by the authors to changes within the solid solution, rather than precipitation effects, thus being a

strain-ageing phenomenon and the results are generally explicable in terms of Cottrell's theory of strain-ageing.

Further, they observe an increase in the number of Cu-rich regions if ageing at 200°C follows cold-working, whereas the undeformed specimens do not show such marked changes under the same conditions. Cold work, therefore, accelerates precipitation.

On Al-12.5% Mg alloy, Stubbington investigates the effect of cyclic straining and unidirectional straining on the subsequent ageing behaviour of the supersaturated solution. If solution treatment is followed by unidirectional deformation and then ageing takes place, the subsequent precipitation is not affected appreciably. However, if in the same sequence cyclic straining is used, a finer dispersion of particles and higher maximum hardness is the result in the fully aged condition, compared with a normally aged material.

b) Deformation After Precipitation

Broom et al[14] suggest that among other mechanisms, deformation creating lattice sites increases the diffusion rate leading to possible overageing comparable with that occurring isothermally at a "high" temperature.

McEvily et al[86], referring to Thomas and Hale, state that as a result of unidirectional loading, cold work brings about the fragmentation and disappearance of zones and coherent precipitates, that is, reversion takes place.

Thomas and Nutting[78,78a] suggest that the formation of GP zones makes it difficult for dislocation sources to become operative,

the slip path tends to avoid the copper enriched regions, so waviness of slip lines is increasing with more GP zones present. However, the slip displacement is 20-40 times greater than the size and spacing of zones, therefore the exact interaction of slip planes and zones remains obscure. With θ", fewer slip lines were observed and with θ precipitate, the slip lines were bent around the particles.

They also observed through oxide replicas that partially coherent particles deform with the matrix and with overaged non-coherent particles, the slip lines bent around the precipitates. However, at -184°C, these particles were sheared too, and deformed with the matrix.

Deformation of thin films of Al-4% Cu in the electron microscope by Forsyth and Wilson[87] suggests that GP zones and θ" precipitates are cut and this does not effect the number or behaviour of the dislocations. Specimen fully hardened at 130°C (for 50 days) showed evidence of fine straight slip within the grains, but no re-solution was observed, although the fracture occurred in the depleted zones. As ageing temperature is raised and the mean free path between particles becomes larger, more deformation takes place in the grain by cross-slip of the screw component in the foil. This deformation becomes very evident in the alloy containing θ' and θ precipitates. Besides loop and prismatic loop formations, the authors suggest that dislocations are emitted by the strained precipitates with the result that a multiplication of dislocations would occur on intersecting slip planes. Fracture of foils aged at higher temperature is transgranular and serrated by cross-slip of dislocations with θ' acting as both source and sink for dislocation.

It is suggested by the authors that this may be an important factor in causing a more rapid work-hardening rate of this structure than that of the alloy aged at lower temperature.

Koda and Takeyama[88] report evidence of cross-slip on the surface when a polycrystalline specimen--aged at 250°C for 2 1/2 hours and containing coherent θ' precipitates--was stretched 1-2%. As particles collected enough rings so that the stress reached a sufficiently high level, some rings passed through the precipitates and vanished, so that the precipitate was bent. The plate-like particles of precipitate are bent in the slip bands on the surface and similar bent particles were observed in the interior. It is, therefore, believed that in this alloy the slip bands in the interior have a structure similar to those on the surface.

Work on θ' precipitates by Clark and McEvily[89] indicates a creation of large numbers of tangled dislocations, but of a more complex type than reported by Koda et al[90], who found that after 5% tensile deformation, fracture occurred and numerous tangled dislocations and occasional loops were observed.

It is also interesting to note that Koda et al argue and show dark-field micrographs as evidence that fine striations appear on the precipitates which are nearly parallel to the foil surface. Their direction is consistent with ⟨110⟩ with ~100Å spacing, which would suggest a very fine slip in the matrix.

Nicholson et al[36] also report striations on θ' precipitates and interpret them as moiré pattern between the matrix and the precipitate.

With reversed straining[89], dipole and loop formation, and also cross-slip are observed. The fact that dipole loops and cell structure of dislocation tangles are seen in the dilute matrix after cyclic loading indicates that the matrix solute is appreciably reduced and thus the dislocation configuration more resembles pure aluminium than solution-treated alloy.

Rakin and Buinov[91] conclude on plastic deformation of Al-Cu alloys that partial dissolution of GP zones and particles of θ' and on the other hand the stabilization of a certain proportion of these precipitates takes place and also their transformation into θ' and θ particles respectively and the appearance of new GP zones is occurring. In some cases, the slip lines pass through particles of the θ' phase; in others they bend them. The θ particles are bent by the slip lines. Further, plastic deformation does not change the mechanism of precipitation, but only accelerates it.

CHAPTER IV

Response of Al-Cu to Fatigue

The pioneering work of Hanstock, Broom and co-workers and Forsyth and co-workers has already been described in the Introduction. More recently, the problem has been attacked by McEvily and his co-workers at Ford, who have published two important papers dealing with Al-4% Cu.

As evidence for reversion during cyclic loading of an aluminium alloy (4.5% Cu, 0.6% Mn, 1.5% Mg), McEvily et al[86] conducted an experiment where after cycling for 10% of the life at 25000 psi, ageing followed for 16 hours at 150°C and the specimens were then tested to failure and exhibited a marked increase in fatigue life. After reversion, the subsequent ageing at 150°C induces reprecipitation in the precipitate-free zones so that the weakened regions are strengthened and the fatigue life is extended. Statistical analysis showed that treatments other than the above-mentioned did not indicate significant differences from the control group. Average fatigue life of the control group at $\sigma = \pm$ 25000 psi 6,991,450 cycles and average on the heat-treated 18,480,000 cycles indicated a very remarkable increase in fatigue life indeed, far beyond the 10% increase which would have been expected if only the damage had been fully repaired.

To defend this anomaly, the authors refer to Stubbington[85], who has shown that a finer precipitate, more uniformly distributed, is

obtained if ageing follows cyclic loading of a supersaturated solid solution, as discussed above (III/6). This finer distribution of precipitate is believed to be, then, the reason for improvement in the fatigue properties. (Stubbington's work was done on Al-12.5% Mg and torsion fatigue and showed rapid softening during the early stage of ageing.)

Clark and McEvily[89] on Al-4 wt.% Cu alloy confirmed the hypothesis of Broom et al[13,14], that the metastable hardening precipitates are unstable in aluminium age-hardening alloys during cyclic loading. Interactions of the dislocations with θ" can generate soft regions within the microstructure where further deformation is concentrated and the probability of crack nucleation increased. It is stated that by repeated cutting of these precipitates, reversion takes place and, further, this finding is strengthened by electron micrographs showing a precipitate-free band about 1.5μ wide, filled with dislocation arrays. They suggest that with concentration of the strain, the passage of a large number of dislocations through a limited number of θ" precipitates fragments the zones to a size that offers little or no resistance to further dislocation motion. On GP zones, there is some evidence that the dislocations are slightly bowed, suggesting that the dislocations are impeded but not arrested by these weak zones, and although in a few foils, faint structures in the background suggested the formation of zone-free regions induced by the cyclic loading, the smallness of the GP zones precluded definitive evidence. It is important, too, that no evidence of cell formation, or precipitation of θ" or θ' indicating overageing was observed.

The large size of θ'' zones bordering the precipitate-free regions suggests that these zones had grown into a supersaturated solid solution and that the reversion of θ'', and not only fragmentation to a size below the resolution of the microscope has taken place.

In this case, of course, some knowledge of the solution-treated alloys offers some help and the same authors report that the character of the dislocation loops produced in the solution-treated alloy contrasts greatly with that seen after cyclic straining of pure aluminium, in which a definite cell structure and a large number of dipole loops elongated in the ⟨112⟩ directions are generated (Grosskreutz and Waldow[93]). These differences appear to be due to a lower stacking fault energy of the alloy with respect to aluminium. Such a reduction would inhibit the cross-slip required for dipole formation and for the formation of a cell structure.

Experiments were also made in which specimens cycled to develop reverted regions were reannealed at 160°C to see if the presence of the large number of dislocations which might act as nucleating sites would influence the precipitation process in these zones. The complete absence of reverted zones in these specimens indicated that the heat treatment eliminated the soft regions by reprecipitation of θ'' in normal size and dispersion.

However, it should be pointed out that Clark and McEvily, producing their thin films with window technique, used Lenoir's electropolishing solution so that the alloys have been heated up to 70°C during thinning after fatigue and this may have altered the observed structure appreciably.

These two papers constitute the latest thinking on the fatigue of Al-4% Cu alloy in age-hardened condition and it is seen that at present there is no direct unambiguous evidence of the effects of fatigue upon the detailed mechanical behaviour of this material. The only known experiment of this type, in which the mechanical response of the alloy is directly studied under fatigue conditions, is that described by Liu and Sachs[94]. In order to obtain information on the effects of straining cycles consisting of tension and subsequent compression, ϵ_T and ϵ_c were varied between 0.06 to 0.28 and -0.008 to -0.6 respectively.

The obtained results were not correlated with internal processes within the metal structure. The material used was commercial 24 ST and it was solution-treated, water quenched, aged at room temperature for 4 days and finally machined to the specimen size.

The Bauschinger effect reported depends on the magnitude of pre-strain. First, very rapid increase was observed with the increase of pre-strain, followed by a rather slow rate and finally it approached a constant value at very large pre-strains. The difference in Bauschinger effect for reversal from tension to compression and that from compression to tension was explained with the higher yield strengths needed for a certain pre-strain into compression than into tension.

However, since this work was carried out with polycrystals, the Bauschinger effect could arise largely from intercrystalline constraints, so that these results cannot demonstrate the true Bauschinger effect associated with precipitate structure. It is the purpose of this thesis

to assess this effect in single crystals and to extend the study to further cycles of strain, corresponding to fatigue conditions.

During plastic deformation the flow stress in opposite direction is smaller than for strain in the original direction (that is, after tensile cycle, the reverse flow stress is smaller in compression or vice-versa). This dependence of flow stress on the strain history of the metal is denoted and expressed by the so-called Bauschinger effect.

For the measure of the Bauschinger effect during the present project, the following method is used.

With constant strain amplitude cycling, the peak stress in tensile direction is measured and during unloading and on subsequent compression, the stress at which plastic deformation is detected that is the reverse flow stress is obtained. The difference in these stress values is the Bauschinger effect and half of this value is the elastic back stress as it is shown later.

CHAPTER V

Experimental Apparatus and Procedure

1. Experimental Apparatus

During the course of this project, the following equipment was used in chronological order. The ones marked 'S' are standard equipment and are not described in this thesis; the others are dealt with--according to their importance--primarily in the appendices.

i) S Stanat Model TA 215 6" rolling mill.
For grooved rolling ø 3/8" ø 2/8".

ii) S Tinius Olsen Tensile Machine.
Cold drawing from ø 2/8" ø 1/8".

iii) Salt pot furnace.
For critical annealing, single crystal growth and solution treatments.

iv) S Reichert Microscope.
For grain size determination, slip line observation.

v) Precise tensometer for 2-3 feet length.
Modification of Hounsfield for critical straining.

vi) Electropolishing device.
For producing pointed ends on rods.

vii) Lowering equipment.
For crystal growth.

viii) S Phillips 1010 X-ray Generator.
For orientation determinations.

ix) Goniometer for orientation corrections.

x) S Servomet Spark-cutter, producing gauge lengths on specimen; also cutting discs for electron microscopy.

xi) S Canlab drying oven for producing GP zones, θ", etc.

xii) S Eberbach electro-analyser unit for the polishing of gauge length.

xiii) Alignment jig.
For specimen alignment before fatigue. Designed by D. F. Watt.

xiv) Adapter for Instron, for fatigueing.
Designed by D. F. Watt.

xv) S Instron TTCL Precision Tester for fatigueing.

xvi) S Haake-Thermostat Unitherm.
For heat treatment during fatigue rest period.

xvii) S Bridge amplifier meter, for strain gauge check.
Supplied through the kindness of Dr. H. Robinson and Mr. T. Voogt.

xviii) "Thin film" Polisher.
Using Gates D. C. power supply and P.T.F.E. holder idea.

xix) S Siemens Elmiskop I. Electron Microscope. 100 KV.

2. Experimental Procedure

a) Production and Preparation of Single Crystals

(See detailed description of problems connected with crystal production in Appendix A.)

From a high purity Al-4.1 wt.% Cu alloy, by a combination of groove rolling and cold drawing, 1/8 inch diameter rods were produced. Using a modified strain anneal method, these rods were converted to single crystals with the [112] preferred orientation.

The single crystals were cut to 40 mm. pieces and a gauge length of 8 mm. with 2.5 mm. diameter was machined by the use of the spark-cutter.

Solution treatment followed at 540°C for 3 hours and the specimens were water quenched.

To obtain the various structures desired (Fig. 7), the following heat treatments[25,89] were adopted:

GP zones were produced using 130°C for 16 hours when the reported size is ~ 80Å in diameter and the Cu atoms are in disc shape concentration with ~ 3 - 6Å thickness and at an average separation of 100Å.

Theta double prime, θ", precipitates were obtained after ageing for 5 hours at 160°C and theta prime θ' precipitates treating the specimens at 220°C for 5 hours.

The equilibrium precipitate $CuAl_2$ Theta, θ, was attempted at 350°C for 3 hours and at 300°C for 5 hours as indicated later.

The limiting temperatures for various precipitates is shown in Fig. 7.

These treatments were carried out under atmospheric conditions. Also, because of the surface finish produced by spark-cutting, a polishing was advisable along the gauge length. After covering the ends with Microstop, the electropolishing was carried out in an electrolyte of 20% perchloric acid plus 80% ethyl alcohol at room temperature.

The specimens thus were ready for testing and to prevent any structural changes, they were stored in a freezer below $0^{\circ}C$.

b) Arrangements Made for Mechanical Testing

Techniques used in connection with mechanical testing are dealt with in more detail in Appendix B.

As the Instron testing instrument was already equipped with adapter for fatigue purposes (Fig. 8), it was decided to use the same system.

For this reason, the specimen had to be fitted with shoulders of around 10 mm. outside diameter. Aluminium shoulders were glued by Hysol epoxy on both ends leaving the polished section of the gauge length free.

The design of the fatigue adapter is such that the alignment of the test piece had to be carried out in the grips before fixing it into its testing position on the Instron unit. In Fig. 9, the jig used for this purpose is seen. The alignment had to be carried out with great accuracy to assure perfect cyclic loading and avoid buckling.

After the normal calibration of the testing machine--bearing in mind that for fatigue, the zero line had to be in the middle of the chart and thus tension and compression were on the right and left-hand

sides respectively--the test piece tightly held by the grips was placed in the adapter in such a way that the pre-load during this operation did not exceed 10 lbs. in tension and 2 lbs. in compression, which are well below the elastic limits observed in these tests.

Selecting the particulars such as chart speed, load scale and strain rate, the fatigue test could proceed.

For fatigueing under liquid air, a minor modification was needed to prevent ice crystal formation in the bearings at the bottom of the adapter. As part of the framework and connecting rod to the load cell were submerged with the specimen under liquid air, the icing resulting due to the heat conduction, evaporation and condensation created an intolerable uncertainty, especially for the very first cycle, where a high degree of accuracy was imperative.

With 10 cubic feet of nitrogen flow per hour and a porous rubber deflector, the pressure difference attained was good enough to prevent any moisture from getting into the tube containing the bearings.

To reach equilibrium temperature, at least three hours were needed and great difficulties were experienced in maintaining this equilibrium, as the level of the liquid air had to be kept constant manually.

Heat Treatment at Rest Periods

For certain reprecipitation experiments, a temperature bath was necessary, giving the possibility for heat treatment while the test piece is in working position. The Haake-Thermostat Unitherm used gave a temperature control of $\pm$ 0.1°C.

The container filled with "Kyro L" detergent was lifted up so that the specimen was completely submerged and after the treatment, repeated water baths took care of the detergent covering the surfaces.

c) Electron Microscopy

(More detail in Appendix C.)

The fatigue tests were generally carried out until fracture occurred. Then, after surface examination under light microscope, electron microscopic observations were made.

From the fractured specimen, discs 0.3 - 0.5 mm. thick were cut out to provide thin films from the deformed structure. The electropolishing was done by using the P.T.F.E. holder idea, but the technique had to be modified as described in Appendix C.

CHAPTER VI

Experimental Results

Introduction

To make the results more self-explanatory in this section, they are presented mostly graphically, while the exact data on the tests is tabulated in Tables 1 to 14.

As a general rule, the graphs obtained on the Instron chart are not very suitable for presentation, consequently mirror images and some other methods are used for their evaluation.

It is reported by several authors[94,95] that after a few cycles of reversed strain at constant amplitude, the stress-strain curve developed an assymmetry and that the peak compressive stress needed was larger than the peak tensile stress. In this project the same tendency was observed, as is clear from the contents of the tables. However, to avoid confusion, in the diagrams only one curve, the tensile curve or the average of the two, is given.

To be able to use the automatic cycling control, the constant strain was set and measured from the zero load point for both the tensile and compressive cycles. All the tests were carried out with constant strain cycling.

1. The Bauschinger Effect

To express the Bauschinger effect, the following method is used:

If σ_F is the stress applied to achieve a certain strain in Forward-tension-motion

and σ_R is the reverse flow stress (at which plastic flow is detected on the chart)

it can be said that

$$\sigma_F = \sigma_f + \sigma_B$$

$$\sigma_R = \sigma_f - \sigma_B$$

giving $\sigma_F - \sigma_R = 2\sigma_B$, where σ_f is the frictional term and σ_B the elastic back stress associated with the forces opposing the dislocation movement.

To obtain σ_R from the chart, a ruler is placed parallel with the elastic line representing the unloading and a reading is taken at the point (indicated on Fig.VI/1) where the curve deviates from the straight line. Although the method is not very accurate, the strain-gauge readings indicated that the error is small for the first few cycles.

Thus for the evaluation of the Bauschinger effect, the expression

$$\sigma_B = \frac{\sigma_F - \sigma_R}{2}$$

is used, giving the value of the built-up back stress. This value is then related to σ_F, so that comparison could be made with the different structures examined.

In some cases, the plastic work done during each half-cycle was measured, as the area under the forward or reverse stress-strain curve.

Values are under "A" in the tables. This, divided by the strain amplitude, "W", gives an average flow stress for that half-cycle: $\bar{\sigma}_F$ (forward) or $\bar{\sigma}_R$ (reverse). The results of such calculations are included for some of the Bauschinger tests.

Typical hysteresis curve of test piece containing GP zones as it appears on Instnon Chart when cycled at constant strain.

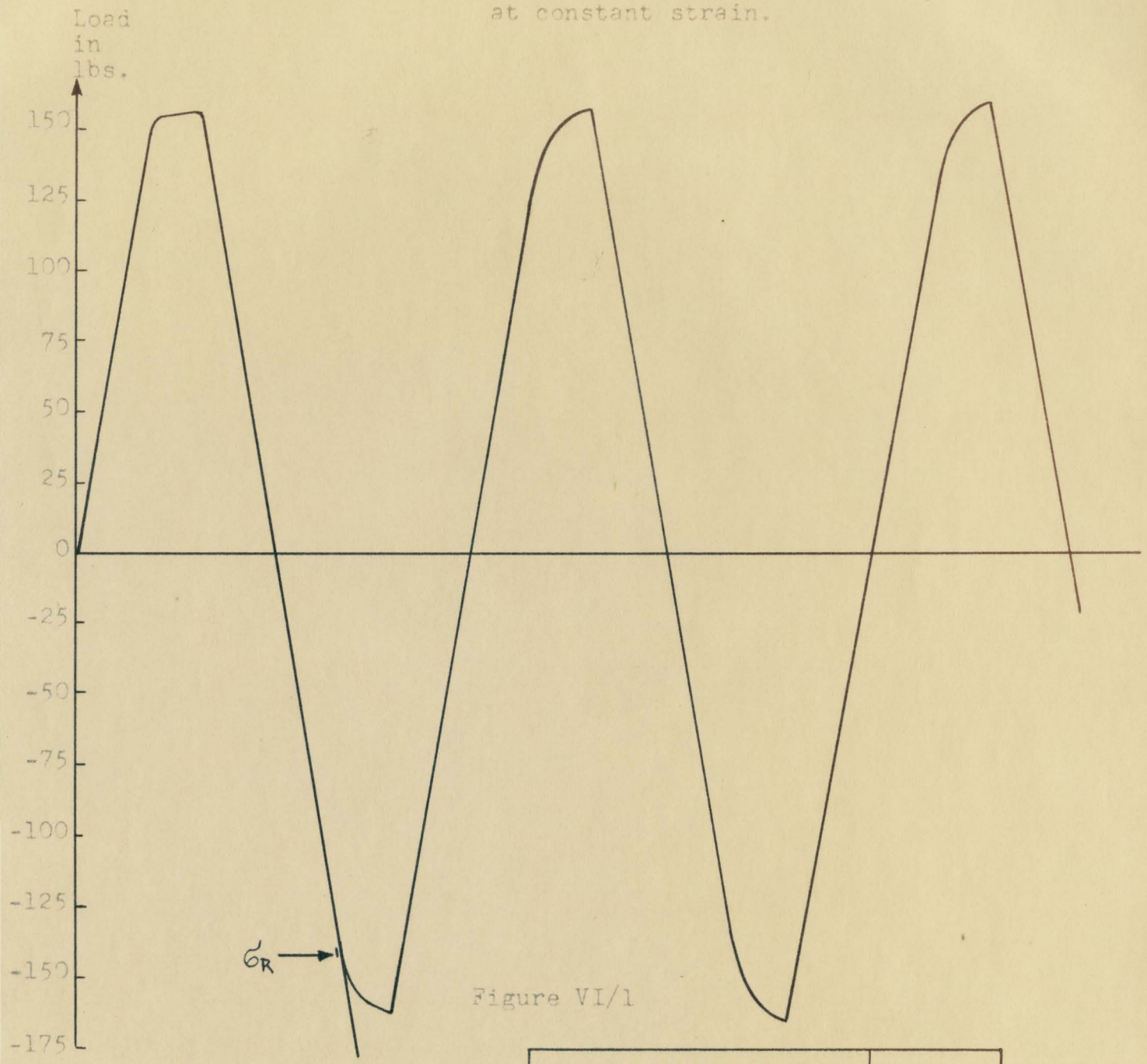

Figure VI/1

Test Number	6
Precipitate	GP zones
Temperature	Room T.
Strain Amplitude	2.4%
Data in Table number	1

Bauschinger effect in crystals containing GP zones.

Figure	VI/2	VI/3	VI/4
Test Number	6	25	27
Precipitate	GP zones	GP zones	GP zones
Temperature	Room	Room	Liquid Air
Strain	2.4%	0.66%	0.66%
Data in Table	1	2	3

σ_o = 15.75 kg/mm^2
σ_F = 16.2 kg/mm^2
σ_R = 14.0 kg/mm^2
$\sigma_B = \frac{\sigma_F - \sigma_R}{2}$ = 1.1 kg/mm^2
$\frac{\sigma_B}{\sigma_F} = \frac{1.1}{16.2}$ = 0.068 = 6.8%
σ_F = 16.15
σ_R = 15.00

σ_o = 11.58 kg/mm^2
σ_F = 12.45
σ_R = 10.55
σ_B = 0.95
$\frac{\sigma_B}{\sigma_F}$ = 0.076 = 7.6%

σ_o = 13.8
σ_F = 14.8
σ_R = 12.78
σ_B = 1.01
$\frac{\sigma_B}{\sigma_F}$ = 0.0675 = 6.75%
σ_F = 12.35
σ_R = 12.45

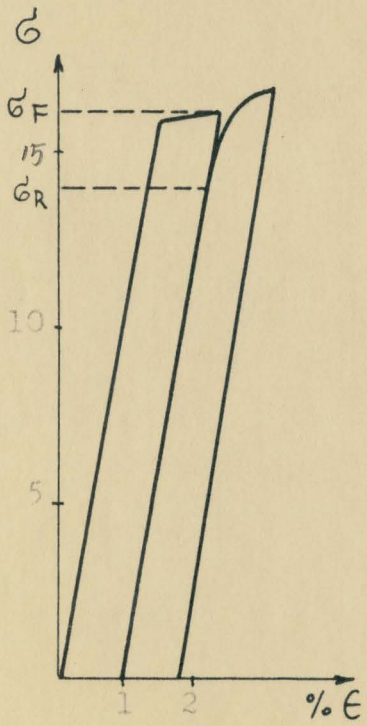

Fig. VI/2

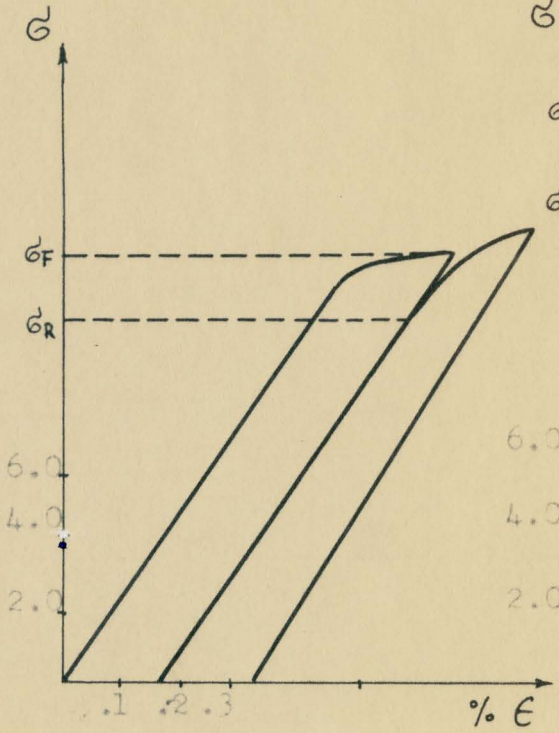

Fig. VI/3

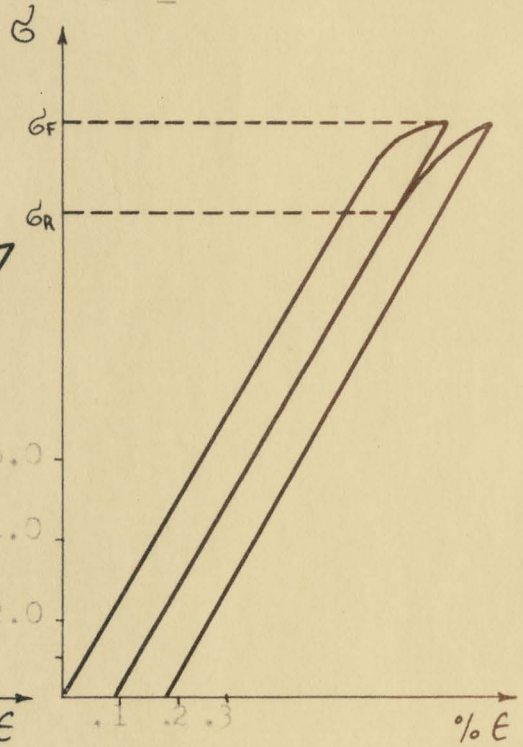

Fig. VI/4

σ_o = initial forward flow stress.

Bauschinger effect in crystals containing θ" precipitates.

Figure	VI/5	VI/6	VI/7
Test number	7	16	22
Precipitate	θ"	θ"	θ"
Temperature	Room	Room	Liquid Air
Strain	1.5%	0.64%	0.64%
Data in table	4	5	6

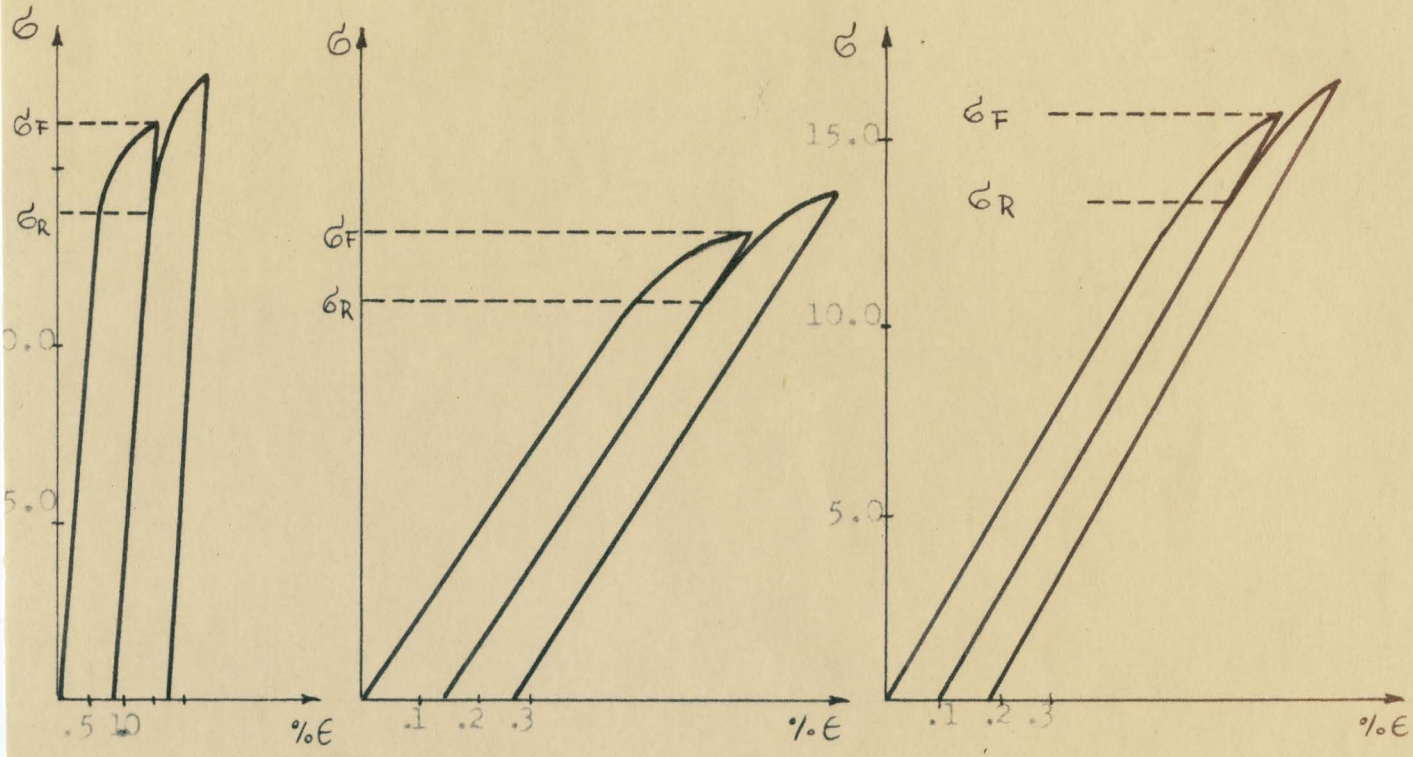

Figure VI/5

σ_o = 13.45 kg/mm²
σ_F = 16.25 "
σ_R = 13.45 "
σ_B = 1.4 "
$\frac{\sigma_B}{\sigma_F}$ = 0.086 8.6%

Figure VI/6

σ_o = 12.0 kg/mm²
σ_F = 13.95 "
σ_R = 12.00 "
σ_B = 0.975 "
$\frac{\sigma_B}{\sigma_F}$ = 0.07 7.0%
$\overline{\sigma_F}$ = 12.7 kg/mm²
$\overline{\sigma_R}$ = 12.57 "

Figure VI/7

σ_o = 13.0 kg/mm²
σ_F = 15.8 "
σ_R = 13.35 "
σ_B = 1.23 "
$\frac{\sigma_B}{\sigma_F}$ = 0.078 7.8%
$\overline{\sigma_F}$ = 14.1 kg/mm²
$\overline{\sigma_R}$ = 12.6 "

Bauschinger effect in crystals containing θ' precipitates.

Figure	VI/8	VI/9	VI/10
Test Number	8	17	20
Precipitate	θ'	θ'	θ'
Temperature	Room	Room	Liquid Air
Strain	1.27%	0.64%	0.64%
Data in table	7	8	9

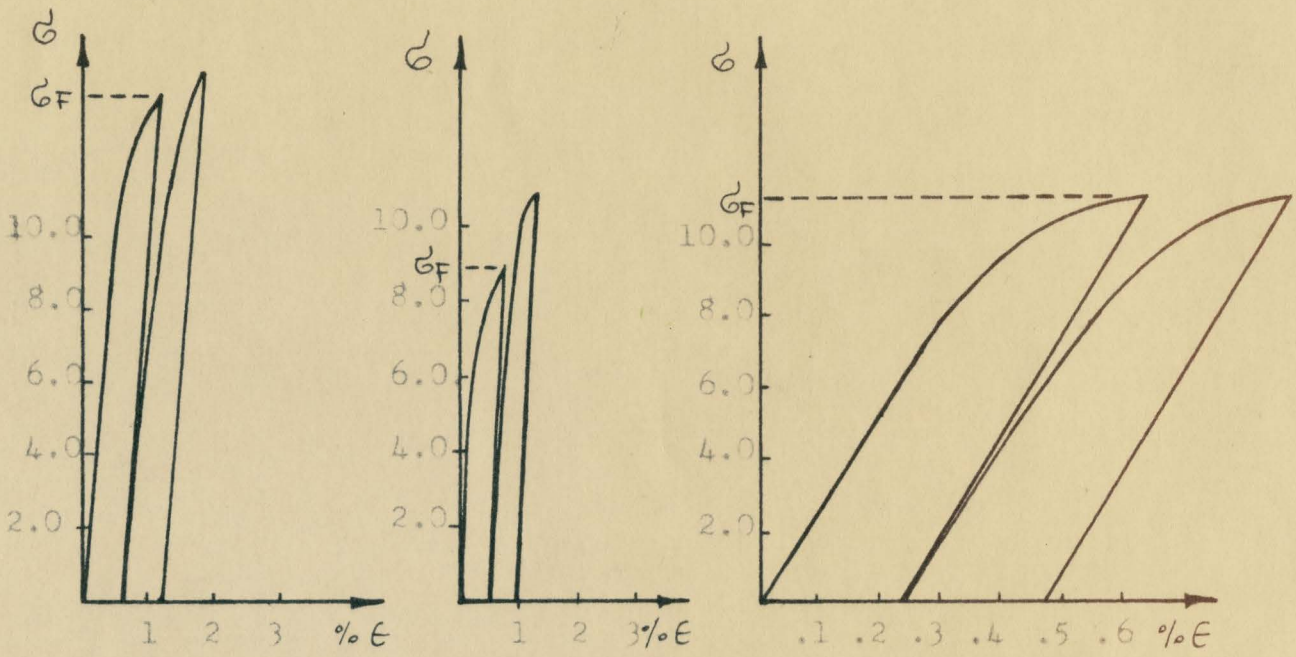

Figure VI/8

σ_o = 8.8 kg/mm²

σ_F = 14.45 "

$\sigma_R < 0$

$\sigma_B > 7.23$ "

$\frac{\sigma_B}{\sigma_F} > 0.5 = 50\%$

Figure VI/9

σ_o = 4.0 kg/mm²

σ_F = 8.8 "

$\sigma_R < 0$

$\sigma_B > 4.4$ "

$\frac{\sigma_B}{\sigma_F} > 0.5 = 50\%$

$\overline{\sigma_F}$ = 7.8 kg/mm²

$\overline{\sigma_R}$ = 8.8 "

Figure VI/10

σ_o = 7.35 kg/mm²

σ_F = 11.4 "

$\sigma_R < 0$

$\sigma_B > 5.7$ "

$\frac{\sigma_B}{\sigma_F} > 0.5 = 50\%$

$\overline{\sigma_F}$ = 9.95 kg/mm²

$\overline{\sigma_R}$ = 9.22 "

Bauschinger effect in crystals containing θ precipitates.

Figure	VI/11	VI/12	VI/13
Test Number	9	13	21
Precipitate	θ	θ	θ
Temperature	Room	Room	Room
Strain	1.2%	1.2%	0.64%
Data in table	10	11	12

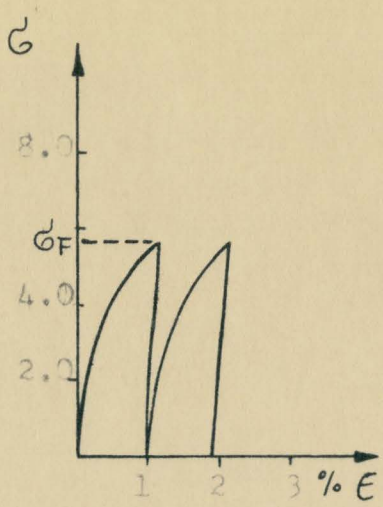

Figure VI/11

σ_o = 2.05 kg/mm²

σ_F = 5.4 "

σ_R = <0

σ_B > 2.7 kg/mm²

$\frac{\sigma_B}{\sigma_F}$ > .5 = 50%

$\bar{\sigma}_F$=4.26 kg/mm²

$\bar{\sigma}_R$= 3.94 "

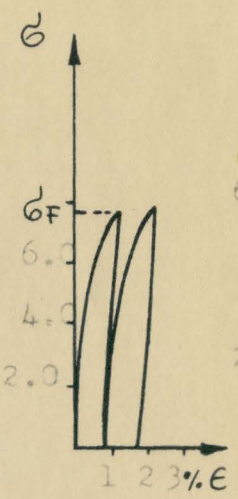

Figure VI/12

σ_o = 2.83 kg/mm²

σ_F = 7.56 "

σ_R <0

σ_B > 3.78 kg/mm²

$\frac{\sigma_B}{\sigma_F}$ > .5 = 50%

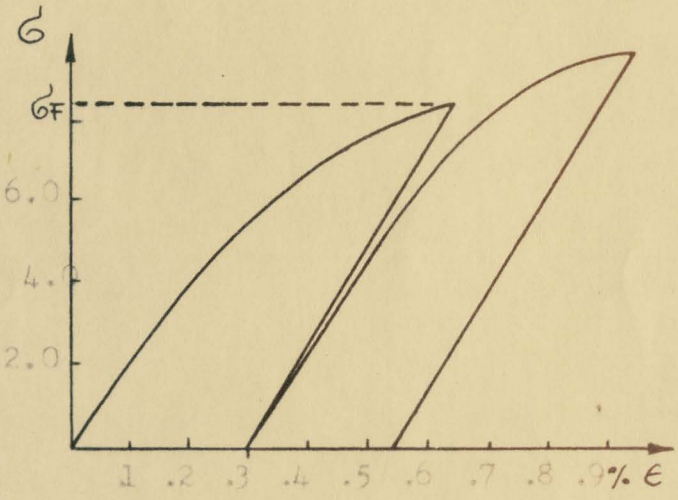

Figure VI/13

σ_o = 3.42 kg/mm²

σ_F = 8.3 "

σ_R <0

σ_B > 4.15 kg/mm²

$\frac{\sigma_B}{\sigma_F}$ > .5 = 50%

$\bar{\sigma}_F$ = 6.15 kg/mm²

$\bar{\sigma}_R$ = 8.35 "

2. The Cyclic Hardening Curves

The peak tensile stress for each cycle (or the average of the tensile and compressive peaks where these are significantly different) has been plotted versus the number of cycles. Also included on these graphs are two other curves for some specimens: 1) the value of σ_R determined as for the Bauschinger effect, 2) the mean flow stress around the hysteresis loop, $\bar{\sigma}$, calculated as the total loop area divided by the total loop width. These have been plotted versus the number of cycles. Such additional curves have only been included where they could be obtained with reasonable accuracy.

Peak stress versus number of cycles with crystals containing GP zones.

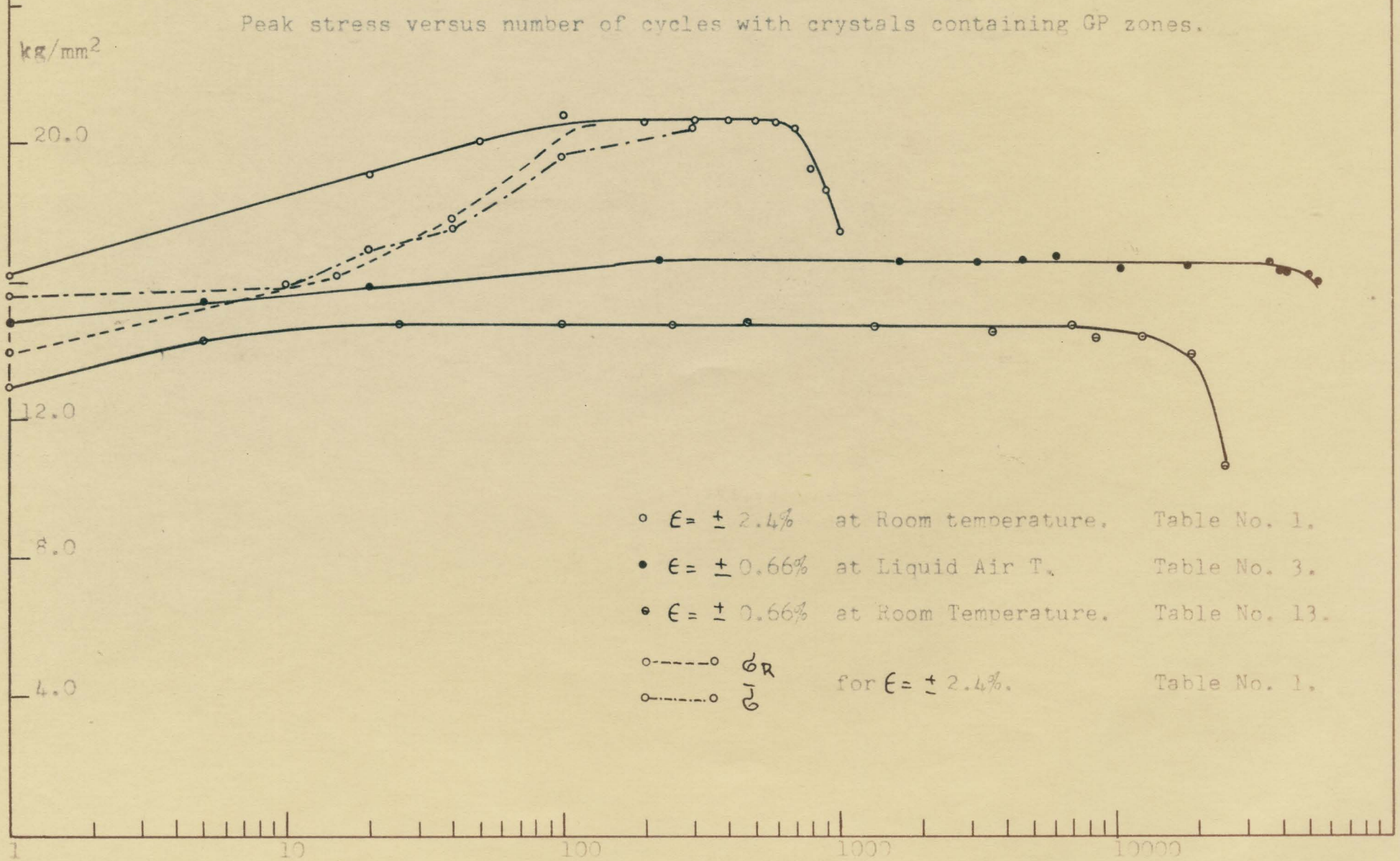

Figure VI/14

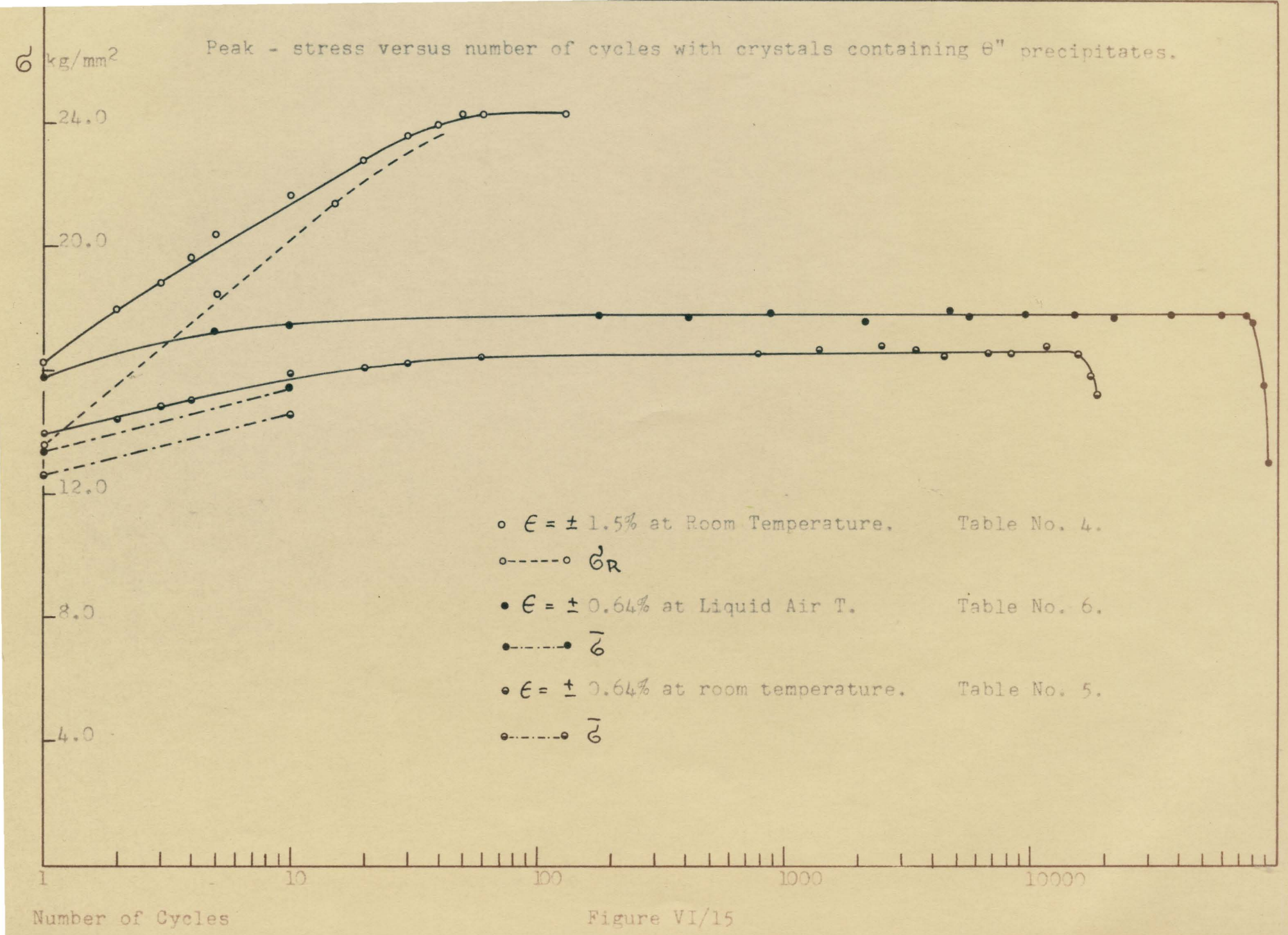
σ kg/mm²
Peak - stress versus number of cycles with crystals containing θ" precipitates.
24.0
20.0
12.0
8.0
4.0
1
10
100
1000
10000
Number of Cycles
∘ ϵ = ± 1.5% at Room Temperature. Table No. 4.
∘----∘ σR
• ϵ = ± 0.64% at Liquid Air T. Table No. 6.
•-·-·-• σ̄
• ϵ = ± 0.64% at room temperature. Table No. 5.
∘-·-·-∘ σ̄

Figure VI/15

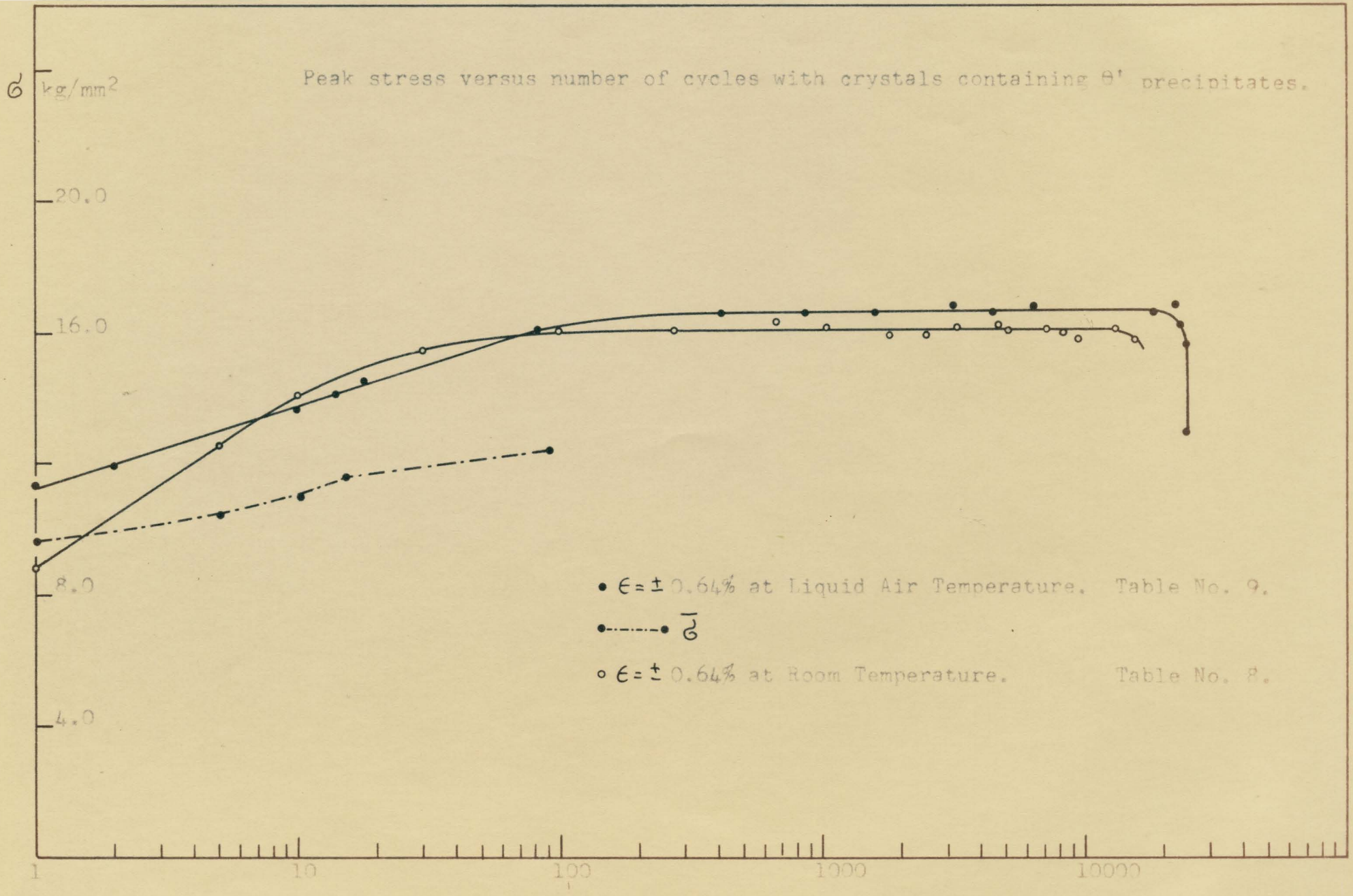
σ
kg/mm²
Peak stress versus number of cycles with crystals containing θ' precipitates.
20.0
16.0
8.0
4.0
• ε = ± 0.64% at Liquid Air Temperature. Table No. 9.
•----• σ̄
○ ε = ± 0.64% at Room Temperature. Table No. 8.
1
10
100
1000
10000
Number of Cycles

Figure VI/16

Peak stress versus number of cycles with crystals containing θ precipitates.

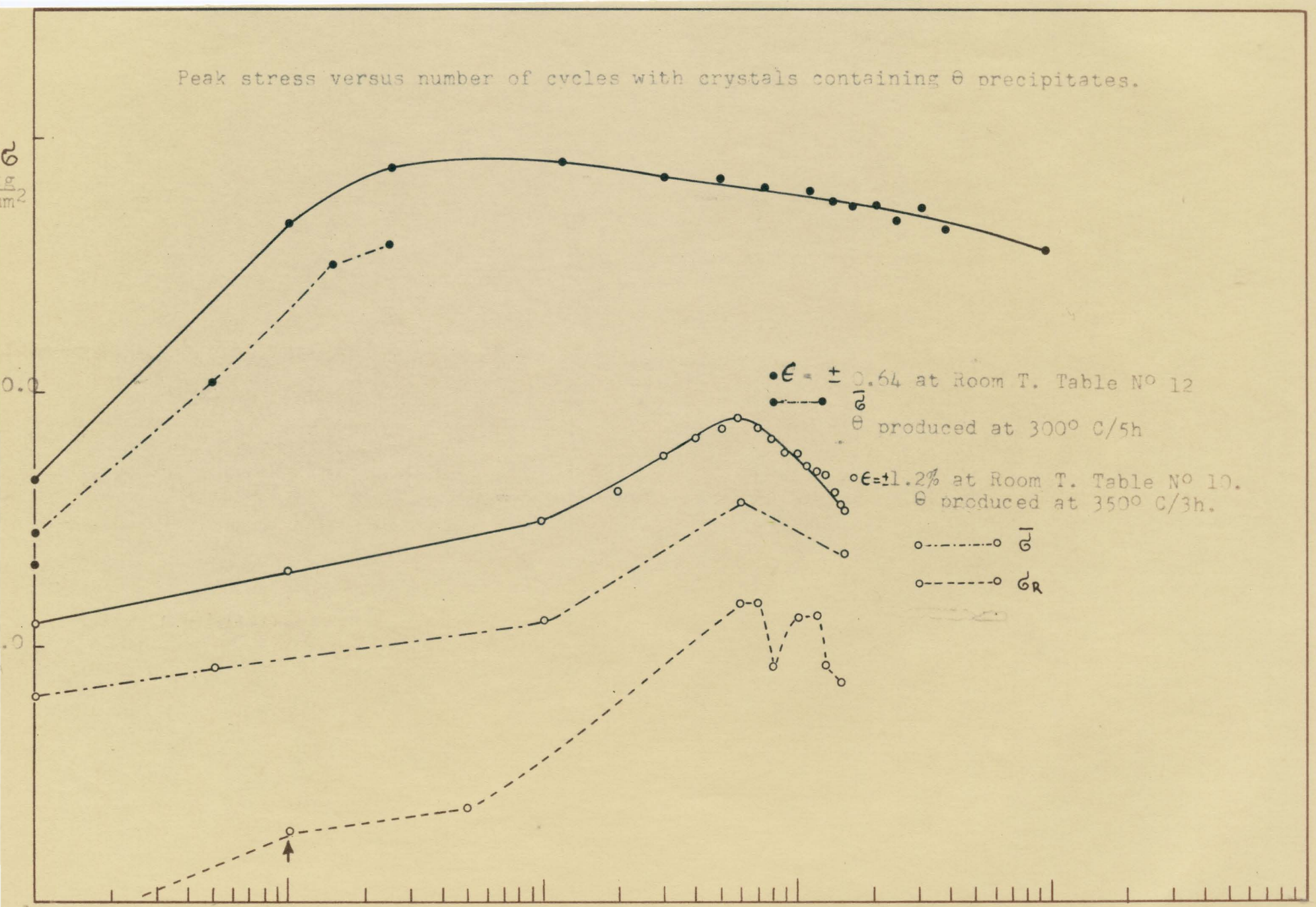

Fig. VI/17

3. Annealing Experiment

In the case of one specimen containing θ" precipitates, cycling was interrupted after 26 cycles and annealed at zero stress at 152°C for 12 hours. The same treatment was applied after 30 further cycles and again a third time when the annealing time was reduced to 1 1/2 hours. Finally, annealing was repeated at 152°C for 12 hours for the fourth time. The results are shown on the following graph and data is tabulated in Table 14.

From electron microscopy observation, the impression is that the precipitate became coarser and more widely spaced.

Peak stress versus number of cycles with crystals containing θ" precipitates when cycling is interrupted and specimen annealed at zero load.

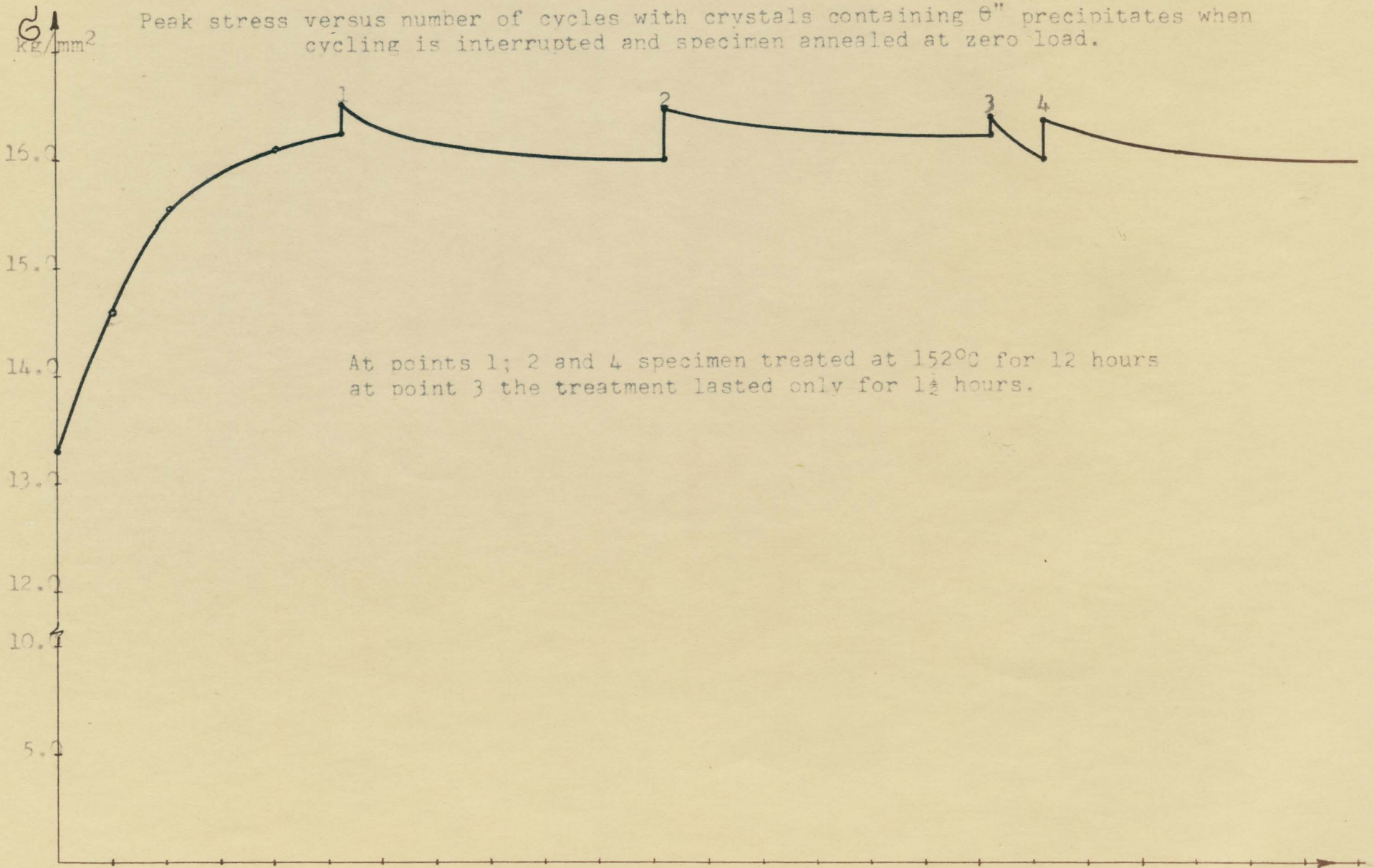

Figure VI/18

4. Observations of Relaxation under Stress

On reversing the cross-head movement, the Instron has a finite delay time at very low strain rates. During this time the stress-strain curve shows an interesting behaviour and reflects certain property or mechanism which can be characteristic of the various precipitates. The observations are as follows: When specimens containing GP zones are cycled in liquid air, on the very first cycle, the load relaxes with about 5 lbs. in 6 seconds (delay time with change-over from tension to compression when cross-head speed is 0.002"/mm.) showing equal values at the turning points of tension and compression cycles. This load drop increases slightly, reaching maximum within the first 10 cycles and then gradually decreases until it disappears completely at about 30 cycles. There was no observation of such load drop when working on room temperatures.

Specimens containing θ" precipitates showed the same type of effect, but relaxation took place even at room temperatures when straining to ±1.5%. In liquid air, the load drop lasted only on the first 10 cycles. The θ' and θ precipitates behaved differently, as at room temperature even at small strain amplitudes the relaxation started in the third or fifth cycle, building up to maximum at about 10 and gradually dying off. At liquid air temperatures, the load drop was observed from the very first cycle and followed the pattern described with GP zones. The following curves show some of the typical cases.

Typical cases of relaxation effects.
Numbers representing cycle number.

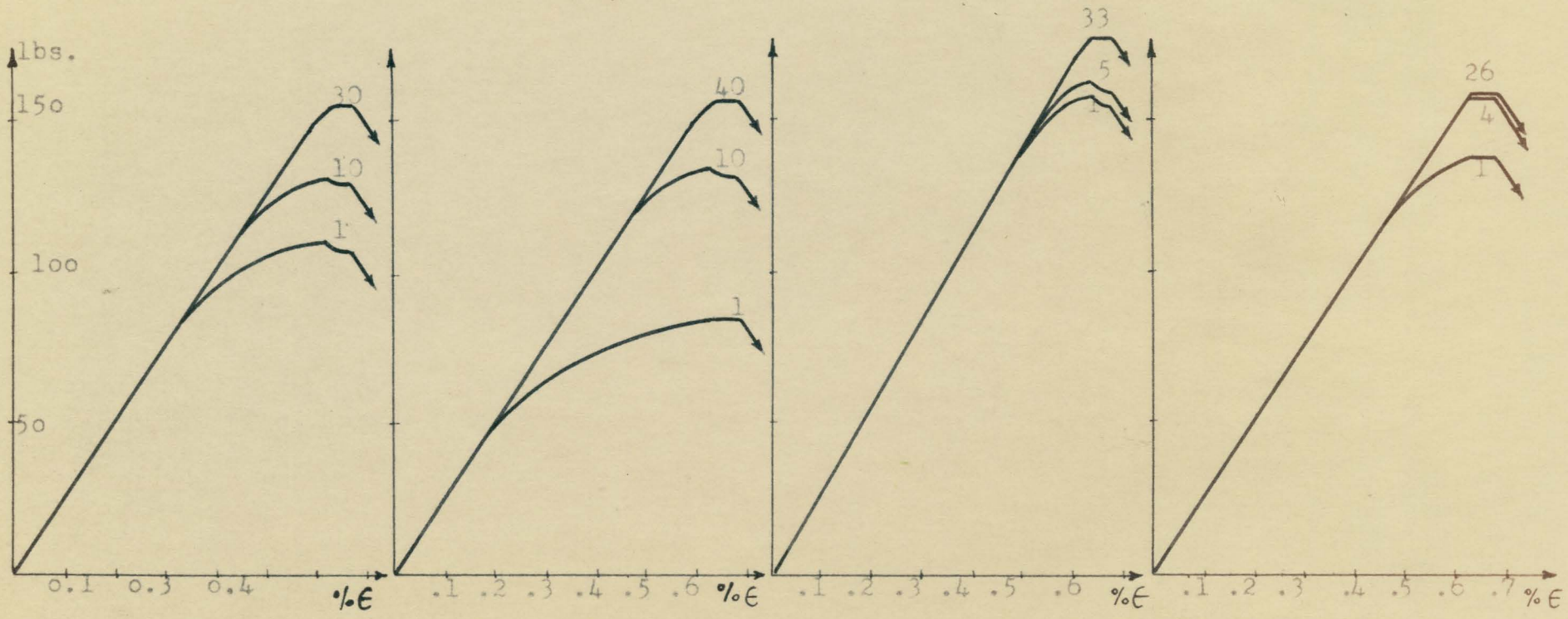

Fig.V1/19.
Test N°20.
Liquid Air T.
θ' prec.

Fig.V1/20.
Test N° 24.
Room T.
θ' prec.

Fig.V1/21.
Test N° 27.
Liquid Air T.
GP Zones

Fig.V1/22.
Test N° 15.
Room T.
GP Zones

5. Modes of Fracture and Observation of Slip Lines

Alloys containing zones tended to a cup-and-cone fracture with some necking, especially at high strain amplitudes. Alloys containing precipitates (θ", θ', θ) tended to give rather rough 45° shear fractures, for those specimens which failed far from the grips.

A few specimens on which the surface had not become too strained were examined with an optical microscope at 75x magnification and some micrographs are presented here (Fig. VI/23 - VI/27).

x 175

Fig. VI/23. Surface of a specimen containing GP zones after fracture at room temperature.

x 175

Fig. VI/24. Surface of a specimen containing θ" precipitates after fracture at room temperature.

x 175

Fig. VI/25. Surface of a specimen containing θ" precipitates after fracture at room temperature.
The area is near the fracture. Slip lines indicating cross-slip.

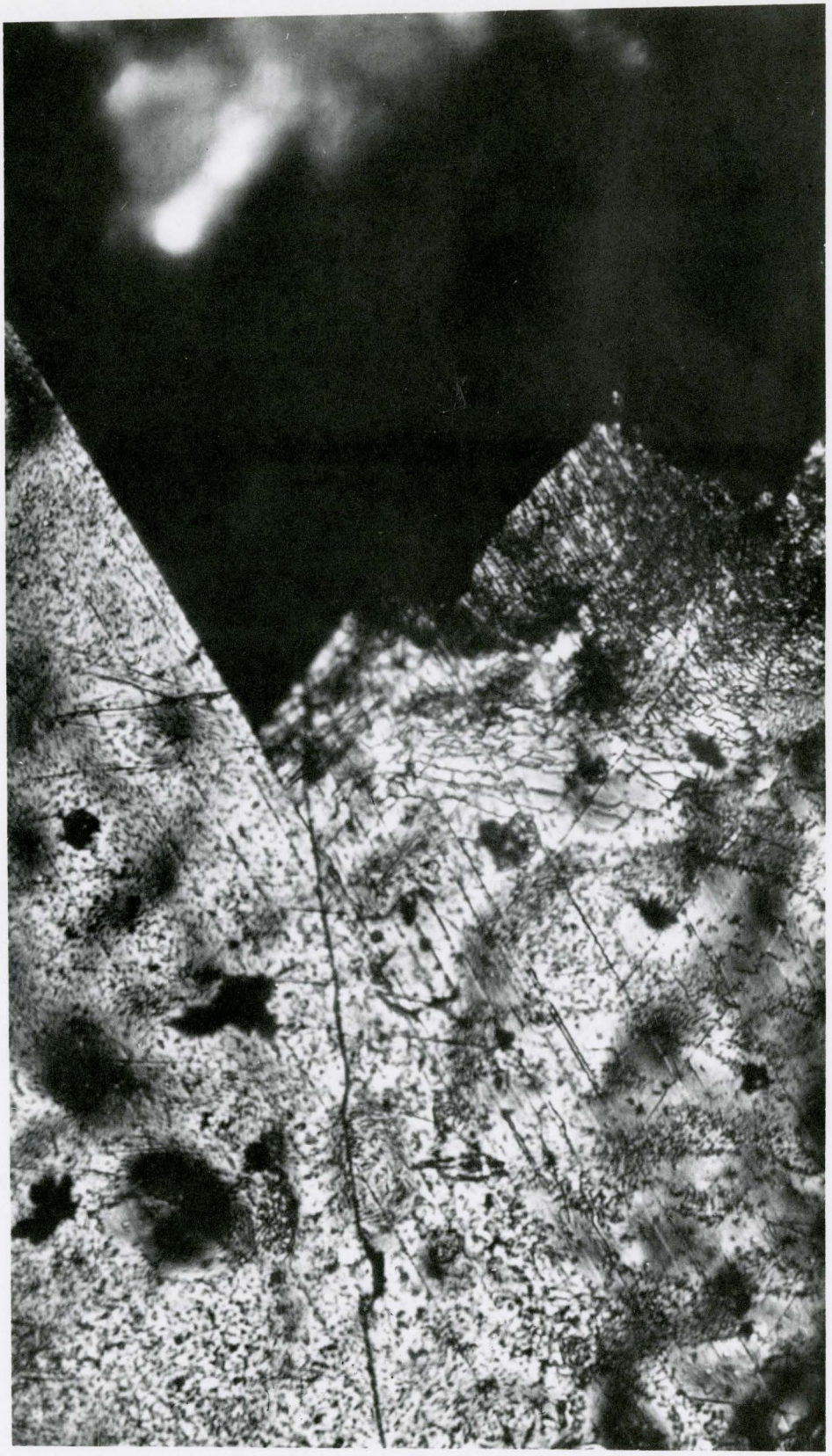

x 175

Fig. VI/26. Slip-lines and fractured area of a specimen containing θ' precipitates.

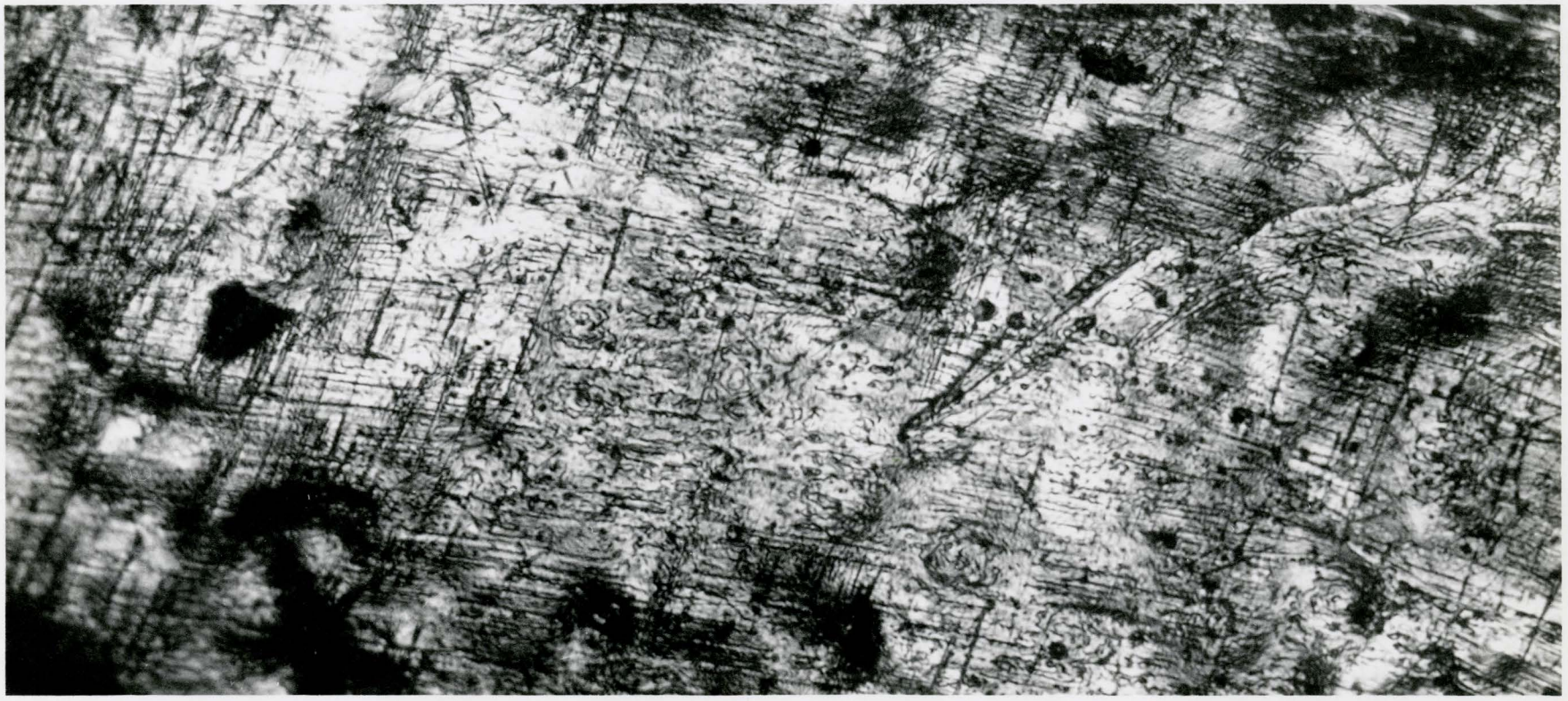

x 140

Fig. VI/27. Surface of specimen containing θ precipitates near the fractured area.

6. Electron Microscopy

Thin films were prepared from various specimens after fatigue. For alloys containing zones (Fig. VI/28 - VI/31), the zones themselves could not be resolved, but gave a general background mottling as reported by other workers[42,89]. A high density of dislocations was observed generally throughout the specimens, but as observed by Clark and McEvily the dislocations were not arranged in cells or piled-up formation.

For alloys containing θ'' precipitates (Fig. VI/32 - VI/36), the precipitates were observed directly and by tilting the specimen, dislocations could be brought into contrast. The measured dislocation density was 3.0×10^{10} lines/cm.^{2}, with an estimated thickness of 4000Å.

The dislocations appeared as a few isolated tangles but mostly in loops somewhat similar to the arrangements observed in fatigued pure aluminium[5,6,8].

For alloys containing θ' precipitates (Fig. VI/37 - VI/38), a very high density of dislocations entangled with the θ' plates was observed, similar to the observations of Clark and McEvily. Striation markings appeared on the faces of θ' plates as reported by Koda and Bonar on tensile deformation. However, the plates no-where appeared to be bent.

Alloys containing θ precipitates (Fig. VI/39 - VI/40) gave similar dislocation tangles, but the interfaces could not be studied.

The electron micrographs are presented on the following pages.

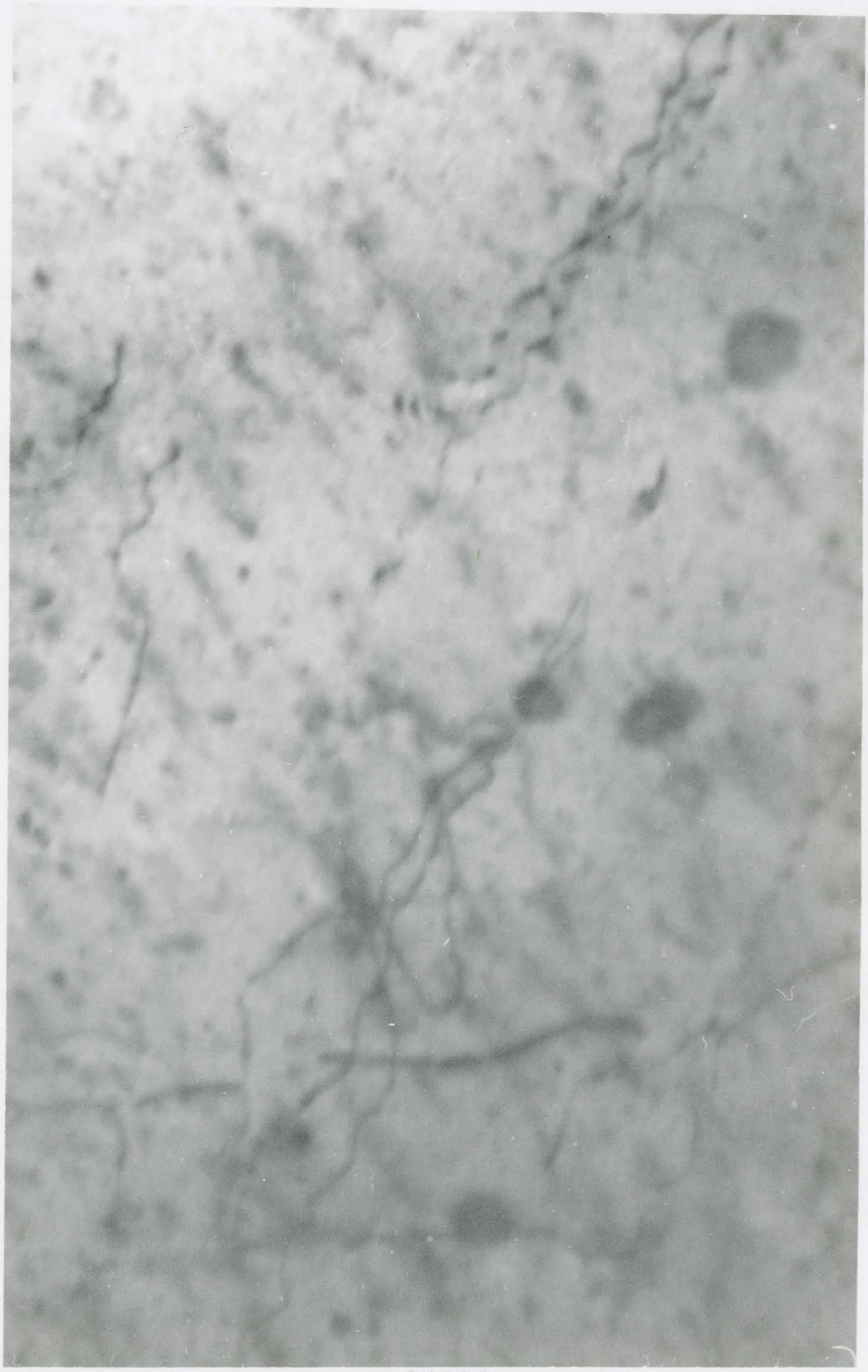

x 92000

Fig. VI/28. Dislocation configuration of a specimen containing GP zones after deformation. Test number 15.

x 120000

Fig. VI/29. Mottled background of GP zones with some dislocations. Test number 15.

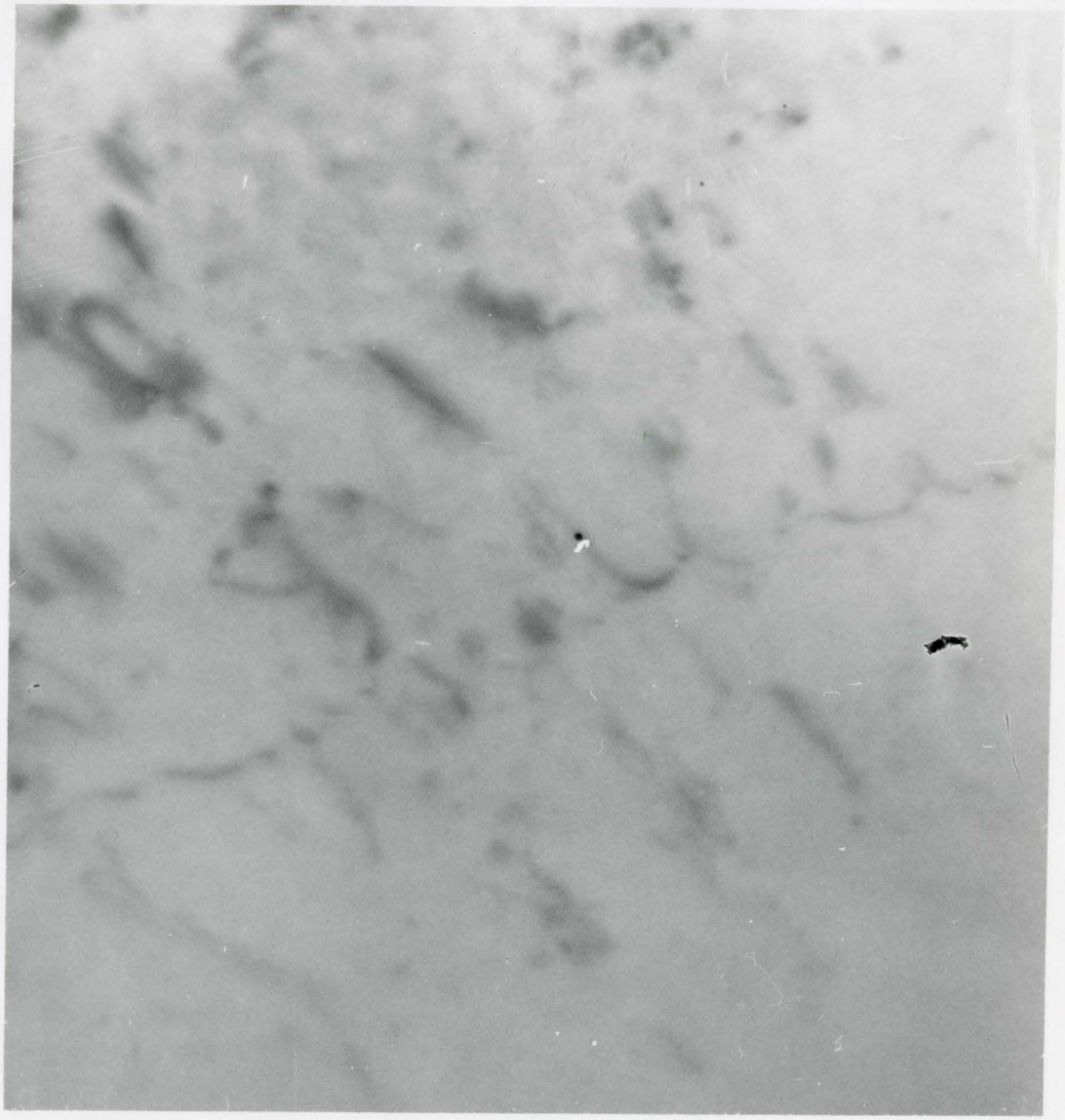

x 75000

Fig. VI/30. Arrested lines of dislocations in specimen containing GP zones. Test number 15.

x 75000

Fig. VI/31. Bowed out dislocations in specimen containing GP zones.
Test number 15.

x 55000

Fig. VI/32. θ" precipitates. Test number 22.

x 80000

Fig. VI/33. Specimen from test number 16 showing θ" precipitates with some dislocations.

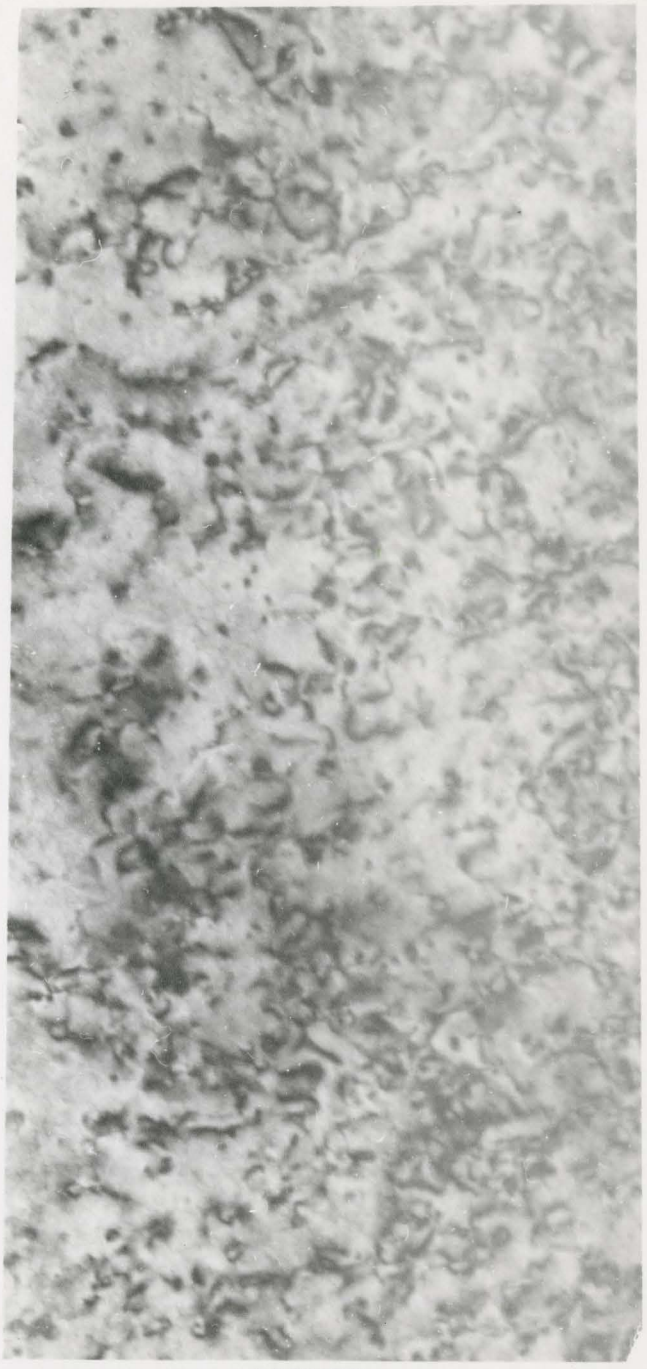

x 110000

Fig. VI/34. Specimen from test number 16 showing a higher density of dislocation.

x 85000

Fig. VI/35. A high density of dislocations is shown with θ" precipitates. It appears that the majority of dislocations are in loop forms. Test number 16.

x 46000

Fig. VI/36. A possible denuded zone is shown. Test number 7 contained θ" precipitates and was cycled at ± 1.27%.

x 46000

Fig. VI/37. θ' precipitates and dislocation arrangement as it appears in specimen 8 after deformation.

x 90000

Fig. VI/38. θ' precipitates from test piece used in test number 24.

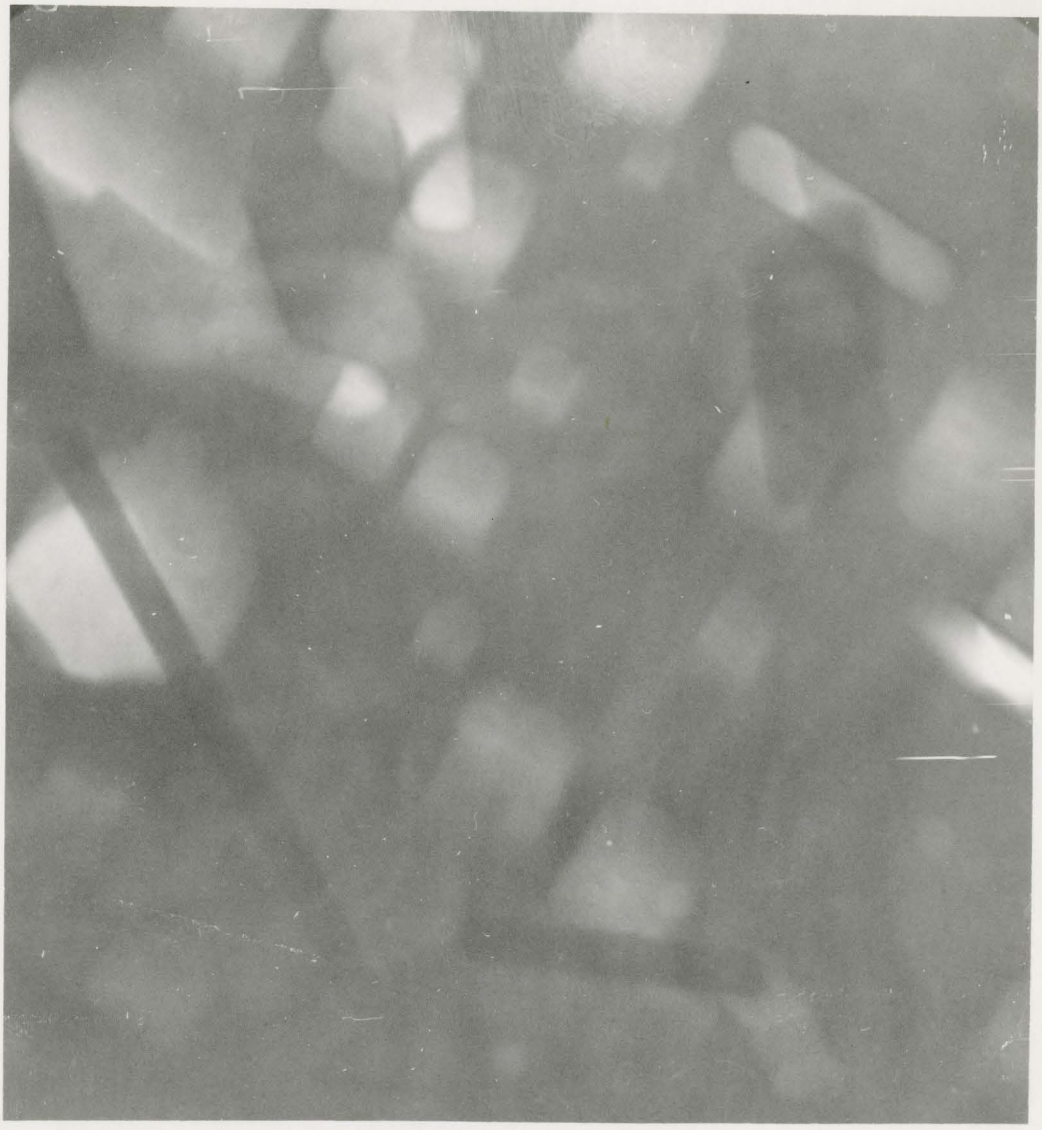

x 46000

Fig. VI/39. θ precipitates and the voids left by them due to thinning are visible from sample of number 9 specimen.

x 110000

Fig. VI/40. Dislocation arrangement in the vicinity of a θ particle. The particle-matrix interface can not be studied with these large precipitates.

CHAPTER VII

Discussion

On the Bauschinger Effect

From the results, the separation and discussion of two distinct groups, specimens containing GP zones and θ'' precipitates on the one hand and θ' and θ precipitates on the other, seems to be appropriate.

The first impression is that in the case of GP zones and θ'' precipitates the Bauschinger effect is relatively small, as $0.1\sigma_F > \sigma_B > 0.005\sigma_F$ and thus--not surprisingly--little long-range elastic back-stress is building up, strengthening further the belief that hardening is associated with the cutting mechanism.

If the amount of plastic strain is considered, it is clear that the absolute value of the back-stress is increasing with the strain amplitude in good agreement with Liu and Sachs' work on polycrystalline material.

It should be noted that the Bauschinger effect observed by Liu and Sachs[94] is larger, but this can be readily explained as due to Heyn stresses introduced by the grain boundaries (Woolley[117])*. The present results demonstrate the true Bauschinger effect in an alloy containing precipitates. The fact that the ratio σ_B/σ_F remains constant with increasing strain amplitude is interesting, but an explanation must await the development of a better theory of work-hardening.

* Heyn stresses: intergranular stresses set up in polycrystalline material during deformation as a result of different anisotropic deformation of neighbouring grains.

From the tests done at liquid air temperatures, it is evident that σ_B has higher values in both GP and θ" cases when taking into account that they had only ~ 0.1% plastic strain. This is entirely consistent with the view that cross-slip can more effectively relieve back-stresses at higher temperatures. On the micrograph of a θ" specimen fractured at room temperature (Fig. VI/25), there is evidence that cross-slip can occur readily under these conditions, although, of course, this specimen has undergone many cycles.

A striking difference is shown by the diagrams of GP material compared with θ" when the σ_o values are focussed upon. In all three cases of GP zones, it is observed that $\sigma_o > \sigma_R$. However, all three experiments on specimens containing θ" precipitates give $\sigma_o \simeq \sigma_R$. This may be analysed as follows. At any strain, the total forward stress is

$$\sigma_F = \sigma_{FA} + \sigma_{Fw.h.}$$

where σ_{FA} = forward flow stress required to overcome the alloy strengthening , σ_o = the initial forward flow stress, and $\sigma_{Fw.h.}$ = the work-hardening due to forward strain.

The total reverse flow stress is

$$\sigma_R = \sigma_{RA} + \sigma_{Rw.h.}$$

where σ_{RA} is the reverse flow stress of the alloy strengthening mechanisms, and $\sigma_{Rw.h.}$ the reverse flow stress associated with the work-hardening. It is known that for experiments in pure metals and solid solutions with comparable strain resolution to that of the present work, $\sigma_{Rw.h.} \simeq 0$ always. Hence we have

$$\sigma_F = \sigma_{FA} + \sigma_{Fw.h.} = \sigma_o + \sigma_{Fw.h.}$$

$$\sigma_R \simeq \sigma_{RA} \cdot$$

Thus when $\sigma_R = \sigma_o$, it means that $\sigma_{RA} = \sigma_{FA}$, and there is no Bauschinger effect associated with the alloy strengthening mechanisms. This appears to be the case with θ" precipitates. However, for GP zones, $\sigma_o > \sigma_R$, i.e., $\sigma_{FA} > \sigma_{RA}$ (after prestrain), so that there is a Bauschinger effect to be associated with the alloy strengthening mechanisms in this case. It is interesting to consider how this difference arises in terms of alloy strengthening theory.

Fleischer[69] and Dew-Hughes and Robertson[74] have considered a number of mechanisms for an alloy containing GP zones, viz., 1) chemical hardening, 2) interface dislocations, 3) coherency strains, and 4) the modulus effect, 5) impurity gradients in solid solution (Fleischer[64]). Of these, it is apparent that 3) and 4) and 5) cannot give a Bauschinger effect since the back-stress involved extends only over a distance 1/2 the zone spacing. The Bauschinger flow observed cannot be produced by dislocations moving backward such a small distance, unless the dislocation density is $> 10^{11}$, which is impossible at such small strain amplitudes. Mechanism 2) can give a Bauschinger effect, since a primary dislocation moving a long way forward through a number of zones will leave behind a set of interface dislocations which will attract it back over the same path, or one nearby. Also, mechanism 1) can give a Bauschinger effect, as has been predicted by Fleischer[69].

Fleischer points out that if the distribution of GP zones is such that one of the three sets of {100} planes have a preponderance of zones, then from the geometry of the zones--at 120° to one another--it follows that the dislocations for one of the three orientations will break Cu-Cu bonds, for the second it will make Cu-Cu bonds, and the zone of the third orientation is sheared in its own plane, either breaking one bond and making one, or breaking two. The breaking of Cu-Cu bonds as pointed out by Kelly and Fine[52] must increase the energy of the system, requiring, therefore, an applied stress to supply that energy during the slip. Thus if one type of zone predominates, then there is a Bauschinger effect, since the net Cu-Cu bond-breaking process is reversed on reversing the strain.

Turning now to θ", we note that the Fleischer argument for mechanism 1) above will not apply to the θ" structure, although a Bauschinger effect could arise if dislocations retraced their paths exactly. Since no Bauschinger effect of the alloy strengthening is observed for θ", it appears that dislocations do not retrace their paths exactly (not surprising in view of the conjugate slip and cross-slip occurring), and that the interface dislocation effect is negligible. Thus it now appears that the mechanism 1) is the explanation for the GP zone Bauschinger effect.

Turning to the other group of structures, a large Bauschinger effect is observed with θ' precipitates and perhaps even larger with the θ equilibrium precipitates. By simply stating that θ' or θ precipitates is not defining the "state of matter" and this is reflected very well indeed on the values of σ_B.

Test number 8 gives a value of $\sigma_B > 7.23$ Kg/mm.^{2} and $\sigma_o = 8.8$ Kg/mm.^{2} compared with test number 17 when the corresponding figures are $\sigma_B > 4.4$ and $\sigma_o = 4.0$ Kg/mm.^{2} The strain amplitude difference does not explain this and as the specimens were differently treated, 250°C for 2 1/2 hours for number 8 and 220°C for 5 hours for number 17, it seems that the particle size and spacing is affecting not only the strength of the material, but has a direct influence on the Bauschinger effect. This is demonstrated even more clearly when examining the details of tests number 9, 13 and 21. Here, specimen number 9 was treated at 350°C for 3 hours and the two others at 300°C for 5 hours.

The Bauschinger effect is greatest for a given strain amplitude when tested in liquid air as shown by the details of test number 20. Comparing tests 17 and 20, there is a great difference in σ_o, too, as the values are 4.0 and 7.35 Kg/mm.^{2} respectively. Although there is difficulty in measuring these values and the differences can be smaller, the back-stresses show similar differences as σ_B for the room temperature work is > 4.4 Kg/mm.^{2} for $\sim 0.40\%$ plastic strain, while $\sigma_B > 5.7$ Kg/mm.^{2} in liquid air when the plastic strain is about 0.27%. The cross-slip mechanism must be very active right from the beginning of the cycling.

These results also can be interpreted as very decisive in the question of the validity of Orowan's criterion and Ansell and Lenel's plastic flow criterion. Ansell and Lenel proposed that the bowing out of dislocation loops between particles will not lead to sufficient plastic flow to account for the observed strain and that the particles must be fractured before detectable plastic flow occurs.

Considering the tensile half of the cycle alone it can be argued that the yield stress coincides with the shearing of particles, and using the expression derived by these authors, reasonable agreement can be obtained. Supposing, therefore, that pile-ups form around the precipitates, and as σ increases, the number of piled-up loops increases up to the critical value when the particle shears.

At this stage, two possibilities arise: 1) All the piled-up dislocations run into this sink and the pile-ups disappear. Consequently, there would be no Bauschinger effect. 2) More likely, a balance is set up and as the stresses acting on the inner ring reach the critical value σ_{CR}, one of the rings disappears, the source reinforces the pile-up and plastic flow is increasing continually. When unloading, therefore, no plastic flow is expected until $-\sigma_{CR}$ is reached, according to this criterion. Purely with the relaxation of the rings--which movement must be limited--no plastic strain should be detected, just as when the pile-ups are found, no plastic flow was detected.

However, the experiments supply convincing evidence that plastic flow is occurring even during unloading. Further, σ_B values are generally greater than σ_o, which suggests that piling up during the tensile cycle continued after the yield stress, which is in accordance with the fast work-hardening taking place in these materials.

During electron microscopy examination, there was no evidence of sheared θ' or θ particles. This argument does not prove that these particles are not sheared, only that Orowan's criterion can explain the characteristics of the obtained hysteresis loops while Ansell and Lenel's theory is not consistent with the present results.

Peak Stress Versus Number of Cycles

The higher strain-amplitude-cycled GP and θ" samples show a much steeper work-hardening rate than the rest of the samples and it should be pointed out that the reason is partly due to the difference in strain rate and amplitude at which they were cycled and partly to the difference in orientation of these crystals. The rest of the results are thus more comparable as their orientation is uniformly [112].

It is seen that as is generally observed with pure metals and solid solutions, the peak stress rises gradually during cycling until it reaches saturation at about 100 cycles or so, and then remains constant until near fracture. The rates of hardening and the total amount of hardening up to saturation, are a little higher for GP crystals than for θ". It should be noted that while the total strain amplitude is the same for both sets of tests, the plastic strain amplitude is actually somewhat greater for the GP crystals, since these have a lower flow stress. The saturation hardening, and hardening rate, are greater for larger plastic strain amplitude. This is generally observed for pure metals and solid solutions, and is also demonstrated by the present results at higher amplitudes. Hence the difference between GP and θ" crystals is readily explained as due to the difference in work-hardening produced by the effective difference in amplitude. Also, at liquid air temperature, the rate of hardening is slower, while the total hardening to saturation is much the same. This is also consistent with results on pure metals,(e.g. Feltner, McMaster University, Metallurgy Seminar, March 1965). Hence the cyclic hardening appears to be chiefly due to the same work-hardening mechanisms that operate in pure

metals or solid solutions, just as the strain-hardening in tension of the alloy can apparently be nearly accounted for in this way (Price and Kelly[68]). A further check on this explanation can be made by comparing the present results with those of Snowden[8]. He cycled crystals of pure aluminium of orientation [112] at ±.74% total shear strain. Converting this to tensile strain, and noting a difference between Snowden's definition of reversed strain and the one used here, it is seen that this is equivalent to ±0.6% tensile strain amplitude, and hence comparable with the present conditions. Snowden observed saturation in about 100 or 200 cycles, and the total hardening obtained was about 800 gm/mm^2, increase in peak shear stress, or about 2 Kg/mm^2 increase in peak tensile stress, allowing for the fact that our amplitude is a little larger than Snowden's. It is seen that the agreement with our results is very good, considering the variability to be expected for this type of experiment, especially with this orientation. Hence it appears that the cyclic hardening results for GP and θ'' crystals can be attributed to normal work-hardening processes, so that any precipitation (overageing) or re-solution of precipitates during cycling does not have a large effect on the observed mechanical behaviour. This interpretation is supported by the observation that low temperature saturation hardening is similar to that at room temperature, and by the two further observations. First, the intermediate annealing experiment, illustrated in Fig. VI/18--a θ'' crystal was given 25 cycles, and then annealed at 152°C for 12 hours. On recycling, it was found that the peak stress had increased by about 0.25 Kg/mm^2. This strengthening was temporary, however, and faded away after about 25 further cycles. A second

anneal produced another transient increase of 0.5 Kg/mm^2. A third shorter anneal produced less strengthening which fell off more quickly. Thus it is seen that intermediate anneals produce only a small strengthening effect. Such an effect is consistent with the hypothesis of McEvily et al discussed in Chapter III. Thus it is reasonable to say that when cycling commences, there is a general deformation, but the persistent slip bands characteristic of fatigue soon develop, and in these there is fragmentation and re-solution of precipitates. Since the bands still give considerable resistance to flow, it appears that in addition to work-hardening, some re-precipitation of solute also occurs, either by nucleation or on existing fragments, until the specimen reaches a steady state in which small precipitates are continually created and destroyed, or the size of the fragments remains constant. This is the situation when saturation is reached. This balance may be disturbed in favour of larger precipitates by anneals, but the specimen returns to its steady state again in a few cycles. It should be noted also that dislocations may rearrange significantly during the anneal, so that the effect of this is included in the annealing result. However, the effect should be small in this alloy, and will be wiped out in the first subsequent cycle. In fact, the anneal may cause a persistent band to stop operating, and lead to the development of a new one elsewhere. In addition to this, which would increase the life of the specimen by roughly the number of cycles it has already endured, the alloy as a whole may be strengthened by the further ageing. There is some evidence for this from the thin film observations, and this would explain the 300% increase in fatigue life observed by

McEvily et al[86]. Now it is evident that the weakening of the alloy by cycling is more than compensated for by work-hardening, otherwise the peak stress would not rise to a saturation value. The work-hardening required is not large, as we have seen. The second observation which supports this view is that the back-stress observed as $(\sigma_F - \sigma_R)/2$, does not increase appreciably during cycling. There is a general increase in the frictional stress, to be associated with the usual debris of loops formed during cycling (see electron micrograph), which indicates that the loss in friction due to alloy weakening is more than compensated for by the increase in friction due to the debris. The $\bar{\sigma}$ curves indicate a similar trend, but can be extended to ranges in which σ_R cannot be measured. It even appears that the back stresses become considerably smaller near saturation, although the measurements become relatively inaccurate at this point.

Turning to the cyclic hardening of θ' and θ crystals, we find a much higher rate of cyclic hardening, and a much greater total hardening. This is entirely consistent with the view that the particles are impenetrable and cause very rapid multiplication of dislocations. This is seen in the electron micrograph. Again hardening is slower in liquid air, presumably because cross-slip is inhibited, so that the debris formation is slowed down, as in the pure metal case (Feltner, loc. cit.).

It appears from the measurements of σ_R and $\bar{\sigma}$ that the back-stress remains constant throughout these tests, which is to be expected if the principal source of internal stress is the elastic particles restraining flow in the plastic matrix. This appears to be true right up

to fracture, which suggests that the particles never break or tear away from the matrix during fatigue, but that the crack forms and grows between particles in this alloy.

Surface Observations

The observation of slip lines on specimens containing GP zones and θ" precipitates was not difficult at all (Figs. VI/23-VI/25) and they appeared at an early part of fatigue life (~300 cycles or less). The reports on θ" are rather contradictory (Thomas and Nutting[78] observe few slip lines, Silcock[116] many), but the differences may be due to the various states of the precipitates used in their experiments. It may be noted that the fracture surfaces for θ" are parallel to slip lines, as has been reported by other workers (Broom et al[14]).

The slip lines of deformed specimens containing θ' in the present experiment indicate that the primary slip planes are very active, as in θ"; however, some waviness can be observed. This and the similarity in peak stress versus number of cycles curves for θ' and θ" indicates that perhaps these θ' precipitates were in an early stage of growth and thus in a way resemble θ".

Specimens containing θ precipitates showed slip lines only near the fractured area and thus interpretation would be very difficult.

Electron Microscopic Observations

The electron microscopic observations generally do not offer anything new except, perhaps, in the case of θ" precipitates. The lack of published micrographs of θ" precipitates with the high density of

dislocations after cyclic deformation justifies the statement that the observed and presented dislocation configuration (Fig. VI/35) appears to be new. Very little was known about the dislocation arrangements between the particles in the matrix and study has, in the past, concentrated on the configuration in the slip bands. The work-hardening demonstrated, however, must be due to this general increase of dislocation density and the many observed loops suggest the possibility that a limited amount of contribution to deformation during the later stage of cycling can be due to Feltner-type flip-flop motion.*

Relaxation

The circumstances presented an unexpected phenomenon during the course of the experiment and it is felt that some very characteristic mechanism is manifesting itself by these relaxation curves, which could add to the knowledge of response of the various precipitates during cyclic loading. However, the available data does not permit detailed interpretation and further investigation was beyond the scope of this project.

* Feltner[6] proposed that the saturation stress in FCC metals is determined mainly by a flip-flop motion of elongated dislocation loops. The basic motion of the edge dislocation loop is a flip-flop motion from one stable equilibrium position to another. Therefore, the saturation condition is attained when the flow stress of the cyclically strain-hardened crystal is high enough to flip a sufficient number of dislocation loops to accommodate the enforced strain limits.

CHAPTER VIII

Conclusions

1) The Bauschinger effect of single crystals of Al-4% Cu containing GP zones and θ" precipitates is relatively small. The elastic back-stresses building up amount only to about 5 - 10 per cent of the applied stresses in the forward motion.
2) With precipitates containing θ' and θ precipitates, the back-stresses building up are more than 50% of the applied stress in the forward direction, and the Bauschinger effect is very large.
3) With constant strain amplitude cycling, specimens containing GP zones, θ" precipitates and θ' precipitates (aged at 220°C for 5 hours) reach saturation within the first 200 cycles and maintain constant peak hardness throughout 80 - 90% of their fatigue life.
4) Specimens containing θ particles reach maximum strength for a very short period during cycling and the peak hardness tends to fall until finally fracture occurs.
5) Cycling in liquid air causes lower work-hardening rates, but about the same work-hardening increment as cycling at room temperature.
6) Heat treatment applied at zero load with the interruption of fatigue after 20 - 30 cycles causes a strengthening with θ" precipitates, but this is only temporary, as further cycling tends towards a slightly lower, constant peak stress.

7) A large density of dislocation loops was observed in cyclically strained material containing θ" precipitates.

CHAPTER IX

Suggestions

The difficulty in comparing results arises partly because the various precipitates can be in many different states. Future experiments should be carried out with fully hardened specimens. Test pieces aged at certain temperatures would give hardness versus ageing time plots and the experiments could be carried out with specimens obtained with the help of these curves.

1) With a fully hardened θ" containing specimen then an annealing treatment would give important and more reliable information. After the fifth or so cycle where the precipitates should be only damaged partly $\pm \Delta\sigma$ on annealing would indicate whether the dislocation rearrangement has any appreciable effect. Knowing this more accurately, treatments resulting in changes along the peak stress curve could be interpreted with more certainty. Also with this experiment if electropolishing were carried out after the appearance of slip lines, it would be possible to correlate the new slip lines appearing after treatment with the strengthening in the denuded zones.
2) The question as to whether re-solution is taking place or only fragmentation could be elucidated by experiments on solution-treated specimens. As the active slip lines with θ" specimens are the weakest parts in the specimen, their strength represents the peak stress on

the cycling chart. If therefore σ values of solution-treated alloy are comparable and the long parallel part of the peak stress curve is characteristic of solution-treated alloys too, then re-solution is more likely than fragmentation.

3) Extending the study of the effects of temperature to higher temperatures would be interesting. An ageing temperature which results in a long parallel peak hardness curve should be used to produce θ'' precipitates and ageing cut off as soon as the peak hardness is reached. Then fatigue could commence with strain amplitudes such that fracture takes place on the "dummy" run within the time corresponding to the fall in the ageing curve.

4) It is felt that the mechanism responsible for the crack initiation of overaged precipitate-containing material could be best studied with the use of electron microscopy when the θ' peak stress versus number of cycles curves change over from the type demonstrated by θ'' to the one observed with θ. That is when there is a definite peak in this curve and a relatively extended life on the downward slope of the curve. Observation of the matrix-particle interface, $\bar{\sigma}$ determination and σ_R measurements could be all applied.

5) To investigate the relaxation, the combination of very low strain rates (possible on the Instron) and high chart speeds at various temperatures, could be used for opening a new approach to dislocation mechanism.

6) A further suggestion is made in Appendix A.

APPENDIX A

The Growth of Single Crystals with Preferred Orientation

A/1 Selection of Method

In this consideration, the dictating factor was that our material is an alloy of Al + 4.1% Cu and thus any melt method was overruled, for fear of segregation problems.

Solid state methods generally offer the following advantages, according to Honeycombe[96]: 1) segregation for all practical purposes eliminated, 2) contamination and 3) alloy losses due to volatilization minimized, so chemical composition is controlled, 4) less defect is produced in the form of subgrain, and 5) accurately shaped specimens can be prepared prior to the growth.

The other problem arising with single crystal testing (Chalmers[97]) is due to the design of the testing machines, which do not allow the specimen to deform freely by uniform glide on every slip plane, causing rotations near the center of the gauge length, so that the slip planes tend to align themselves parallel with the acting forces. This leads to buckling under cyclic loading and to prevent this, it was decided that the single crystals should be grown with [$\bar{1}12$] orientation.

Thus the choice was severely limited and the strain-annealing method had to be applied.

The growth of single crystals by the strain-anneal method depends: 1) on the growth of a recrystallized nucleus in a slightly deformed matrix, and 2) on the principle that the recrystallized grain size increases with decreasing amount of prior deformation. The so-called "critical strain" is needed to allow a few, or even one, nucleus to grow in the deformed matrix. The driving force for this growth is the strain energy of the deformed specimen which is released on recrystallization. However, if the original crystals are randomly oriented, then the resulting single crystal will have random orientation.

The technique, therefore, had to be modified to gain control over the orientation. The pre-strained rod is lowered into a salt pot and the crystal growth is temporarily interrupted and its orientation determined. A correcting bending is carried out on the rod above the crystal and growing is resumed, through the bend, so that it assumes the desired orientation.

A/2 Review of Previous Work

In this section, both the crystal growing itself and the orientation, too, is followed up very briefly.

The strain-anneal method for growing metal single crystals was first used by Carpenter and Elam[98] in 1921.

Specimens of fully annealed metal were strained a small amount, just sufficient to initiate recrystallization on subsequent annealing. In some cases, slow heating of the strained specimen to a predetermined maximum temperature is adequate to give a good yield of single crystals.

In more recent years, the travelling gradient furnace improved this method as grain growth starts at one end of the specimen and the temperature gradient ensures the nucleation monopoly.

Kelly and Chiou[99] produced single crystals of Al + 4% Cu with the strain-anneal method, using a salt pot furnace into which the specimens were lowered. However, as they converted only the gauge length (1.5" x 0.1" x 0.07") into single crystals of any orientation, the process was more like a conversion into coarse grains with restrictions that the grain boundary must be on the shoulders of the specimen.

The measure of success reported on iron by Andrade[100], on aluminium by Fujiwara[101], Mögg and Karlsson[102] and Tiedema[103] and finally on silicon ferrite by Dunn[104], was much greater.

Tiedema describes a method for the preparation of Al single crystals with a definite orientation. His work was done on hard drawn wire of 2 mm. diameter, where the texture in the wire axis had a more or less pronounced [111] orientation. After annealing and straining, the growing single crystal always possessed a [210] direction, parallel within a few degrees to the wire axis.

To prepare a single crystal with a different orientation, the recrystallization was interrupted when the crystal had grown to a certain length. After mounting into a bending apparatus and Laue transmission photograph analysis, a correcting rotation and bending was carried out on the polycrystalline part in such a way that the wire axis became parallel to the desired crystallographic direction and so the growth was resumed. (An exception they found was correcting to [111] direction.

A growing crystal cannot consume grains which possess almost the same orientation as the crystal.)

They also did this experiment on rolled aluminium sheet of 1 mm. thickness. The maximum bending permissible was 40°.

Hägg[102] reports on 1 mm. cold-rolled Al sheet, a maximum permissible bend of 15°.

The question of purity was raised by Talbot[105] and has recently shown that very pure iron, 99.99%+ does not yield single crystals because of its marked tendency to polygonize and so lower the strain energy. Introduction of 0.035% C eliminates the difficulty.

It is also more difficult to grow single crystals in very pure aluminium than in less pure material, because the deformed metal polygonizes easily.

Beevers[106] has found that in high purity Al-Cu alloys single crystals grow less readily than in material made from commercial Al, indicating that impurities present as a fine second-phase dispersion are more effective than certain amounts of Cu in solid solution. This may be due to locking of the grain boundaries to prevent strain-induced migration as found in Al and now recognized as a form of recovery.

Garstone et al[107] produced up to 22" long Al single crystals, so that after cutting the square rod (1/8" x 1/8") to 4" pieces, they had 5 test pieces with identical orientation.

Experiments on Al and Al alloys made by Williamson and Smallman[108] are perhaps the most successful. They describe a furnace in which strip 1/2" x 0.04" and up to 2 feet in length can be converted to single crystals using speeds of growth up to 10 cm./min.

They produced 1 mm. thick high purity (99.992%), commercial purity (99.7%) Al single crystals and alloys of Al containing less than 2% of either copper, zinc or silver.

Bonar[42], in his Ph.D. thesis, describes the method where he produced Al + 1.6 at% Cu alloy single crystals in sheet form with 0.5 mm. thickness. During the annealing, a fairly uniform grain size of about 0.5 mm. was produced! and the success described by him was rather erratic. Single crystals as long as 45 cm. were obtained several times. Lesser lengths were obtained frequently.

A/3 Theory

Although the amount of work directly involved with strain-anneal technique is very little indeed, some of the principles are tackled by various authors.

With the strain-induced grain boundary migration, Beck and Sperry[109] dealt intensively, experimenting on high purity aluminium.

The recrystallization of cold-worked metals proceeds by means of boundary migration. The moving boundaries separate strain-hardened grains from annealed grains and the direction of the movement is such that the volume of the annealed material increases with time at the expense of the cold-worked material. The familiar concept of recrystallization involves the formation of nuclei of new strain-free grains in the midst of the strain-hardened material. During the growth of these new grains, their convex boundaries move in a direction opposite to their centres of curvature.

The total free energy is still decreasing and equilibrium is approached as the strain-hardened grains of high free energy content are replaced by low energy annealed grains.

This is contrary to the migration of grain boundaries resulting from surface energy where the direction is towards the center of curvature.

It was also found that certain strained grains serve as nuclei for strain-free grains of the same orientation which grow at the expense of neighbouring strained grains. Most of the strain-free grains formed during the annealing of high purity aluminium cold-rolled to 40% are produced by this mechanism of strain-induced boundary migration without the formation of new nuclei.

Thus, strain-induced boundary migration may be considered as recrystallization without the formation of new nuclei.

In a further investigation, Beck et al[110] came to a conclusion about the orientation dependence of the rate of grain boundary migration. They found that in slightly deformed high purity aluminium crystals, the rate of growth of recrystallized grains of various orientations varies over wide limits.

Those growing with highest rate have relative orientation with respect to the matrix corresponding approximately to a 40° rotation around a common [111] axis. The recrystallization texture can be accounted for by the orientation dependence of the rate of grain boundary migration.

Williamson and Smallman[108] have undertaken a thorough theoretical and experimental study of the growth of crystals by the travelling-gradient strain-anneal method.

For the production of a single crystal, all growth must originate from a single nucleus and the investigation undertook to examine the factors which may affect, directly or indirectly, the formation of other active nuclei.

Consider a travelling furnace moves with $v = dl/dt$ and has a temperature gradient $S = dT/dl$, where l is measured along the specimen length. The temperature of the interface where the crystal growth is taking place, T_g, is related to the steady state growth, which equals v, and if growth is an activated process with activation energy Q_g, then

$$(1)\quad v = B \exp(-Q_g/kT_g)$$

and

$$(2)\quad T_g = Q_g/k \ln(B/v).$$

B is a limiting growth velocity factor.

Let the probability of forming a nucleus in unit volume at a temperature T during an increment of time dt be $p(T)dt$. Then, assuming for simplicity that S is a constant from $T = 0$ to $T = T_g$, a small element of volume $A\,dl$, which at time $t = 0$ is at the lowest point of the temperature gradient, will have a probability of nucleation given by:

$$(3)\quad A\,dl \int_{T=0}^{T=T_g} p(T)\,dt = A\,dl \int_{t=0}^{t=T_g/S_v} p(tS_v)dt$$

The total probability of nucleation in the entire sample will be:

$$(4)\quad P = \int_0^L A\,dl \int_0^{T_g/S_v} p(tS_v)dt = V \int_0^{T_g/S_v} p(tS_v)dt \quad ,$$

where V is the volume of the specimen.

If nucleation is also an activated process, only those regions having the lowest activation energy Q_n need be considered, and if the probability of finding such regions in unit volume is C, then

$$(5) \quad p(T) = C \exp(-Q_n/kT) \quad .$$

p(T) is such a steep function of temperature that the integral in equation (4) is reasonable, even if S is constant only at temperatures just below T_g, as in most experimental arrangements.

Equation (4) has an asymptotic solution if Q_n/kT_g is large (as it must be if the probability of nucleation is to be small). Thus, according to Whittaker and Watson[111]:

$$(6) \quad P = \frac{T_g^2 \exp(-Q_n/kT_g)\, CVk}{S_v Q_n} = \frac{(v/B)^{Q_n/Q_g}\, CVQ_g^2}{S_v \ln(B/v)^2 k Q_n} \quad .$$

For the growth of single crystals, conditions must be maintained so that the value of P is vanishingly small.

Some of the factors can be dealt with and the importance of temperature gradient is directly shown. The higher it is, the greater the chance of producing single crystals. The importance of V, the volume of the specimen, must have been discovered long before this equation was derived, as most of the experiments were carried out on very thin sheets of specimens. An interesting feature disclosed by this equation is the strong influence which the activation energy ratio Q_n/Q_g exerts on the importance of the velocity v. If this ratio is appreciably greater than unity, then a furnace with either too small a temperature gradient, or too great a velocity may fail to produce single crystals, but this defect

can be remedied by a practicable reduction in the velocity. However, if Q_n/Q_g is equal to or less than unity, no change in velocity will result in an appreciable reduction in the probability of nucleation and attention must be directed towards improvement of the preparation of specimens so that Q_n/Q_g is raised.

The limiting growth velocity B is very sensitive to the crystal orientation as shown by Beck[109,110]. Where due to the orientation relationship B is high, single crystals are readily grown because of the great increase in the permissible velocity v. Equation (6) shows that v/B is absolutely critical as from $[\ln(B/v)]^{-2}$ it is evident that no single crystal can be grown if v approaches B, as the term approaches infinity.

If it is assumed that B depends on the degree of disorder at the crystal boundary, at 30 - 40° rotation, each atom in the boundary may be thought near to an irregularity analogous to a vacant site, so that atomic migration in the boundary layer is rapid. The effective density of vacant sites in this layer is about 10^{-1}. It is unlikely that a low angle boundary contains any such disordered layer, since it may be considered as a wall of dislocations. Thus it is not surprising that it has been reported that crystals cannot be grown into "low angle" orientations. This is a great disadvantage of the secondary recrystallization method.

Where a crystal is grown into a material with little preferred orientation, the value of B varies as the interface moves from grain to grain.

Nucleation and the effect of specimen shape is examined next. In a polycrystal, every grain is constrained to a certain extent to deform equally with its neighbours, this constraint being exerted through the boundary where it joins these neighbours. At places in the grain which are remote from this boundary, the deformation is unconstrained until the strain gradient, which is set up near the grain boundary, reaches back to them. Grains totally enclosed in the specimen have boundaries over a solid angle 4π, those at the surface are enclosed over 2π, and those at the free edge over π. Hence most heterogenity and thus nucleation, is most probable at the edges and least probable inside the specimen.

The factors Q_n and C are both sensitive to the preparation of the specimen. The presence of a grain-refining element, as in commercially pure aluminium, raises C, and stress concentrations at defects produced during rolling or casting lead to low values of Q_n. Perhaps the most critical part of the preparation process is the annealing treatment prior to straining. Any recovered but unrecrystallized regions remaining in the specimen after annealing will almost certainly serve as active nuclei during the subsequent attempt to grow a single crystal. One way of achieving complete recrystallization is to retard the dislocation movements necessary for large-scale recovery by introducing 0.1% or more impurity. In this sense, C and Q_n are sensitive to purity, high C/Q_n values tending to be obtained with high purity materials.

The control of orientation described[108] is dealing with strips and bends of up to 20° and twists of 30° are considered feasible.

A/4 Experimental Procedure

a) Preparation of Material

The material received was a high purity Al-Cu alloy with the following composition in weight per cent:

Cu - 4.1%

Fe - 0.002%

Si - 0.001%

Mg - 0.001%

and Al 95.896% (Al + Cu 99.996%)

An homogenization at 500°C for four hours was carried out before extruding to 3/8" rod at 400°C from a 5" diameter chill ingot. By a combination of groove rolling and cold drawing, the diameter was reduced to 1/8". One annealing treatment was carried out when at 0.24" diameter at 520°C for two hours. Thus the reduction in area due to cold work from here was 73%. For cold drawing, the Tinius Olsen tensile machine was used.

b) Salt Pot Furnace Construction and Annealing

To be able to produce long single crystals up to 24" length, a new salt-pot furnace had to be assembled. The framework of dexion on moveable four-wheel base contained fire bricks enclosed within panels of galvanized sheet. The salt container was a mild steel material having 2.9" inside and 3.5" outside diameter with 24" depth.

Two Kanthal heating elements (REH 7-30 type) with ceramic embedding cement on the outside surface and 8" of heating length were applied in such a way that the longest equilibrium temperature resulted.

The composition of the salt used was 45% $NaNO_2$ + 55% KNO_3, which has a melting point of 290°F and its recommended heating range is between 325 - 1200°F. The temperature control of about ±5°F was achieved by a system of mercury relay and Honeywell Pyr-O-Vane.

Various annealing times (5 seconds to 5 minutes) and temperatures (515°C to 560°C) were used to find the optimum conditions of 515°C and 30 seconds, a treatment which resulted in a fully recrystallized structure with an average grain size of about 0.05 mm. After annealing, the specimens were air-cooled (see A/5(c)).

c) Modification of Hounsfield Tensometer and the Critical Straining

As the two-foot-long rods were beyond the capacity of the standard Hounsfield Tensometer and a high degree of accuracy in straining had to be achieved, a modification seemed to be necessary. A framework was built, into which the parts of the above-mentioned equipment could be placed, such as the gripping jaws and driving rod, and thus the straining was carried out in the same way and under very similar conditions as in the original arrangement. The tried strain values are between 1 and 3%, and 1.75% was the most successful, with about ±0.25% deviation, leading to failure to produce single crystals.

d) Electrochemical Polishing and Etching the Specimen

In order to increase the probability or yield of single crystal production, the two-foot-long rod of 0.125" diameter was pointed at one end to a needle-like and polished finish. First, the damaged end which was due to the Tensometer grip was cut off by a jeweller's saw, then the polishing operation was carried out with the help of a device in which the specimen was rotated at 1 r.p.m. in a 6° angle to the horizon. The

electrochemical removal took place until the contact broke at the intersecting plane between electrolyte and specimen. The electrolyte was made up from a NaOH + 85% H_2O solution. Although the rods prepared this way gave good results, for certain reasons (explained later) the following modification was introduced before the single crystal production ended.

Once the point was formed, the level of the electrolyte was increased so that the greatest intensity of metal removal was somewhere on the conical part above the point and lead to a form of body which is obtained when a spear-like shape is rotated around its longitudinal axis. Thus, if on the tip of the rod, two or more crystals started to grow, the narrow "neck" further up the specimen helped to force a competition from which, generally, one crystal only came out. By this time, the electrolyte was changed also to 20% perchloric acid + 80% ethyl alcohol, using about 20 volts at room temperature.

Before lowering the rod into the salt bath, each specimen was etched very lightly in Flick's etch (10 ml. HF, 15 ml. HCl, 90 ml. H_2O), dipped in concentrated nitric acid, rinsed in water and dried to remove the surface oxide layer that might have provided preferred nucleation sites due to dislocation pile-ups at the oxide layer.

e) Establishing the Single Crystal

The pointed specimens were lowered with various speeds by a small variac controlled electric motor, driven through reduction gear. The temperatures tested were 560°C to 590°C and lowering rates were between 0.4 and 3.0 cm./hr. Best results were obtained and consequently adopted for production with 585°C and 0.6 cm./hr. lowering rate, but during the preliminary tests, the 0.4 and 0.9 cm./hr. speeds gave single crystals too.

This initial growth took place for about three or four hours when the specimen was lifted out from the bath and air cooled.

f) Techniques Involved in Determining and Changing the Orientation of the Single Crystal

After dissolving the salt from the surface of the specimen by water, Tucker's etch was used (HCl conc 45 ml. HNO_3 conc 15 ml. HF(48%) 15 ml. H_2O 25 ml.) to reveal the macrostructure by grain contrast. In the case of single crystal, on the cylindrical part of the rod a cut was made by jeweller's saw and the surface lightly polished. The rod was then mounted in an X-ray goniometer and photographed with the back reflection Lane technique at a distance of 3 cm. The rod is in a position so that its cross-section is parallel with the film and the X-ray beam strikes it perpendicular to the surface that is parallel with its axis. The target used was Cu and exposure lasted for 30 minutes. After developing in the normal manner, the pole positions were determined. Superimposing the film on a Greninger chart the diffraction spots are given directly in angular co-ordinates γ and ρ of the normal to the plane causing the spot. Knowing the co-ordinates of any plane normal, the pole of the plane can be plotted on a stereographic projection using the Wulff net. Great circles are drawn through poles that obviously represent planes of a zone. The intersections of these great circles are poles representing important planes, since they lie on more than one zone. The angles between these important planes can be measured and identified by reference to a table of interplanar angles. The method is essentially one of trial and error. Once (111), (110) and (100) poles are identified, it is relatively easy

to find (112) on the unit stereographic triangle, as this pole must be located 35° from (100) on the great circle passing through (100) and (111).

Now the co-ordinates of (112) pole have to be determined from the center of the projection, which corresponds to the cross-section normal and the correction must be such that when the crystal grows past the bend the pole of (112) should coincide with the center of the projection.

The goniometer built for this purpose gave complete freedom as the specimen was rotated so that the pole of (112) lying either in the northern or southern hemisphere was transformed into the east-west horizon. The next step to be taken was the bending, when moving along E-W to the right or left the N-S is reached that is the transformation is complete and the growing can be resumed. The bending must be carried out with the greatest care on the polycrystal section and the radius of curvature used was 9.0 cm. Thus the losses depending on the amount of bending can be considerable.

The majority of corrections were around 10° bending going down to 4° and up to 38°. Bendings over 25° gave difficulty and generally failed to produce single crystals.

The crystal was lowered back into the salt pot and the normal speed was applied from just below the single crystal - polycrystal interface.

As soon as the crystal grew round the bend, a further check was necessary to see if any new nucleation took place as a consequence of bending. In most cases, these new crystals--frequent especially with larger bendings--could be stopped by removing them with electropolishing and thus the corrected crystal grew alone through the length of the rod. At the end, a further check was necessary with X-ray and the crystals generally had (112) orientations within the accuracy of 2°.

A/5 Notes on Technical Difficulties in Growing the Crystal

(For possible assistance in future work.)

a) The reductions in cross-section from 3/8" to 1/8" carried out under relatively primitive conditions were not only uneconomical regarding time, but did not result in surface finish such as could be expected from normal wire drawing conditions, promoting surface nucleation.

b) The annealing furnace did not give uniform temperature along more than 18" of its length and consequently the longest single crystal produced was 17" (from which, due to pointing and bending losses, only 12" oriented single crystal was obtained as maximum). The bottom part of the pot was very much colder and any manipulation with placing the heating coils at various positions could not remedy this problem. Therefore, a stirring mechanism should be tried, but only for the first annealing, where uniform temperature is imperative along the whole length and turbulence at the surface is not harmful.

c) After the first anneal from the fear of precipitation and its consequence on the consecutive crystal growth, at the beginning, water quenching was applied. No single crystal was produced this way and from the following, it can be seen why.

The critical strain, producing single crystals from air-cooled material, was 1.75%, and the corresponding load producing this was 70 - 80 Kg. The diameter being 0.125" gives a cross-section of 7.9 $mm.^2$ and thus the critical strain is $\frac{70-80}{7.9} \simeq 9 - 10$ Kg./$mm.^2$

If, however, after annealing quenching follows, then a high supersaturation of vacancies is retained, leading to high chemical stresses

(Smallman[112]) and the precipitation of vacancies on dislocations or in the form of loops. Also, there is a rapid clustering of the Cu into zones (DeSorbo et al[113], Turnbull et al[114] and Matyas[115]), so that a form of precipitation cannot be suppressed by quenching. As a result, it was found that a stress of 19 - 20 Kg./mm.^{2} was required to produce the strain of 1.75% in quenched material. Thermal quenching stresses may also contribute to this change in the behaviour of the material. Also, because of this quenched structure, the strain of 1.75% was no longer suitable for producing crystals. In fact, no critical strain could be found in quenched material.

d) Pointing the end of the specimen before growth is not because the grains at the tip have boundaries over a solid angle of π, as during the critical straining the grains in this area were totally enclosed and had the least amount of heterogenity during deformation. The reason is purely to reduce the number of candidate grains for the growth. This improvement, however, is far from perfect, as due to the surface tension of the liquid salt bath the following happened:

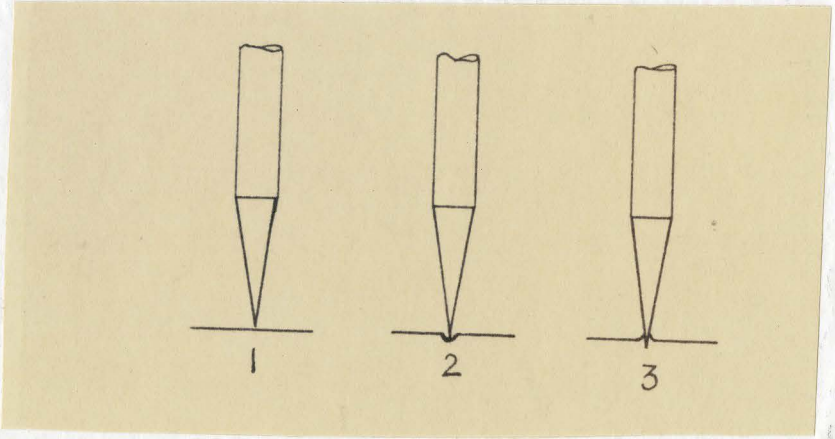

The growth started at the tip when at '2' position and even if by the time of '3' it was well-established, due to the meniscus of the liquid, new crystals had a good chance to start to grow from the sides ahead of the growing interface.

The modification adopted as described earlier

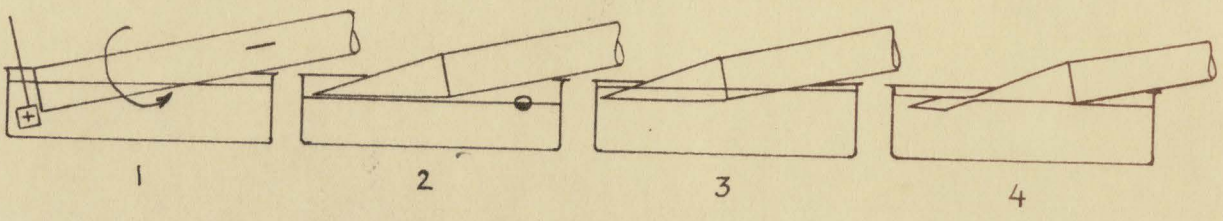

helped to diminish this problem, as through this neck generally only one crystal managed to grow.

As from the formula derived earlier, the effect of volume on nucleation probability is obvious. It is proposed that for diameters of this size and larger, a manipulation with the starting end of the crystal is necessary to ensure the best geometrical conditions for the successful start of the process.

Therefore, the probability of growing single crystals may be expressed as: $P = P_g \times P_{th}$, where g refers to geometrical, th to thermodynamical conditions, and the yield is one hundred per cent when both components are equal to one. However, even if P_{th} is one, but P_g is less than one, the chances are down, also when vice-versa.

e) During bending, depending on the amount of correction, an extra stress is superimposed on the one causing the critical strain in a

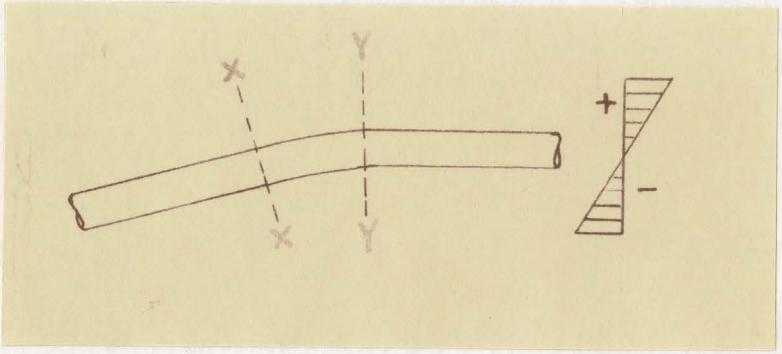

continuously changing fashion in three dimension between X-X and Y-Y. If, therefore, 1.75% strain is not the optimum value for growth conditions, it is almost certain that somewhere in this section, strain value nearer to the optimum will be set up.

To understand the governing factors better, it was considered advisable to study the form of advancing interface

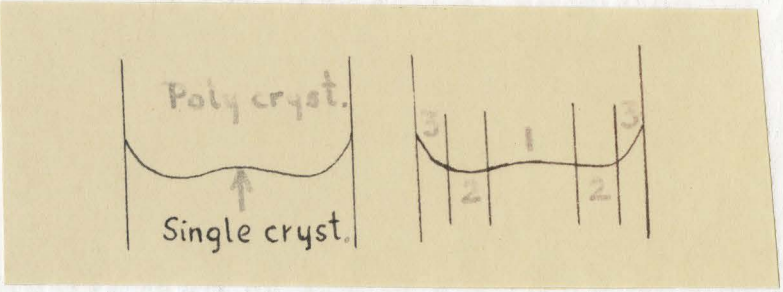

It seems reasonable to split this interface into three sections: in section 1, the superimposed strain is negligible and the difference it creates in growth condition is hardly enough to compete with the well-established advancing section (nucleation is least probable in the inside of a specimen having boundaries over a solid angle 4π, anyhow).

Section 2 receives, perhaps, the optimum amount of strain; however, it is not only inside the specimen, but between and behind two advancing boundaries. This handicap is enough to offset any danger from this zone. The third section gives the most trouble, fortunately, as this seems to be the only one where interventions are possible.

Strain deviation here is the largest, so the occurrence of nucleation should be small, but as it is at the surface quite frequently new grains are going to grow. Generally when the growth passed the bend, the arrangement is as follows:

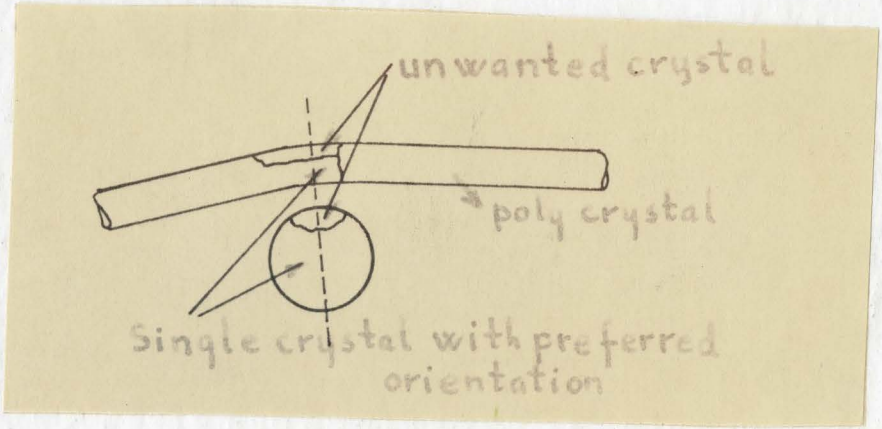

Using Miccrostop for protection, this volume can be removed and

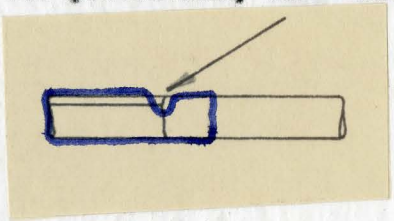

the growth continued, so that the rest of the rod is converted to the chosen orientation.

A/6 Suggestion for Future Work

When a cut was applied by jeweller's saw to stop the growth of unwanted crystal, a recrystallization followed on a length of 6 - 7 mm. across the whole volume of the specimen. From the recrystallized grain size, it is evident that the damage done is greatest near the cut and the grain size is increasing as the distance from the cut is increasing. If the strain anneal method is so sensitive, perhaps an investigation on summer thesis level, using the spark cutting machine's seven different settings would reveal some valuable information about the propagation of damage and depth of damage induced by cold work.

APPENDIX B

Mechanical Testing Techniques

a) Adapter for Fatigue

The vertical motion of the adapter was made possible with the Thomson die-set Ball Bushings. These bearings were housed in the moving part of the device attached to the cross-bar and gave practically friction-less motion on the surface of the static rod which was connected to the load cell.

b) Gluing

After considering methods such as soldering and trying various glues, the Hysol Epoxi-Patch Kit was found to be the most suitable. On tensile tests made with this glue, no failure occurred under 350 lbs. on the glued-in polycrystalline specimen and during fatigue the load hardly exceeded 200 lbs. Regarding the fatigue properties, no information was available, but as all the fractures happened in the specimen, its reliability under conditions used has been proven.

In the aluminium shoulders, four grooves were cut with a jeweller's saw, parallel to the axis to give better wetting possibilities for the surfaces and to overcome the surface area. Both parts, the test pieces and the shoulders, were thoroughly degreased in methanol before the glue was applied to the surfaces.

c) Load and Strain Reading

The load was directly read from the chart in pounds according to the scale setting and readings were accurate to ±1 pound.

All the fatigue tests were done at constant strain amplitudes and the strain was calculated in the following way: after deciding on the amount of straining, the extension to be applied in inches was calculated from the dimensions of the specimen. Selecting the strain rate, that is, the cross-head speed---which is the moving part---a time is given. The chart speed is now selected from these considerations to give a convenient length of record. The divisions on the chart thus replace time for the measure of strain.

The method used in the present experiments was to start with slow strain rate, 0.002"/min., to be able to obtain accurate recording on the behaviour of the alloy and repeat this at certain intervals, while in between time the strain rate was increased to 0.1"/min. During this fast straining, the automatic extension cycling was operated.

d) Low Temperature Cycling

A Dewar flask filled with liquid air was lifted up so that the specimen, held by the outer cage and the inner rod, was submerged. Due to the uneven contraction of the parts involved, a very quick and changeable correction had to be applied manually so that the forces acting on the specimen remained near enough zero. This manual correction, by turning a knob, caused the movement of the cross-head up or down, according to the acting forces visible on the chart. Finally, when thermal equilibrium was reached, only the level of the liquid air needed attention.

To keep constant liquid level manually over a testing period of days is very difficult indeed, and not quite satisfactory.

e) Strain Gauge Check

An SR-4 type strain gauge on the gauge length, connected by 2 strain gauge arms to BAM-1 type self-contained bridge amplifier and meter unit indicated that the stress-strain curves obtained on the chart faithfully follow the plastic behaviour of the crystal, but with a large superimposed elasticity in the system due, probably, to the deflexion of glue, grips, etc.

APPENDIX C

Electron Microscopy Techniques

a) Cutting Discs from the Specimen

Having a specimen with 2.5 mm. diameter, the only possible solution was to produce thin films from discs of the same diameter. For cutting discs, with minimum amount of damage to be imposed, the spark cutter was available. There is no information on the electrical conductivity of the glue, but as some specimens were not receiving spark-discharge across the work gap, it proved that there is a continuous layer of glue between the test piece and its shoulder. After breaking up partly this insulation, machinery did not give difficulties and discs of 300 - 500μ width were cut in about five minutes.

b) Electropolishing

Several attempts were made to produce thin films with the P.T.F.E. holder, but perhaps because of slight dimensional differences, success was very seldom attained. However, the idea seems to be perfect, and with modification it was used. The discs were sandwiched between two thin plexi-glass slabs (teflon would be better) and held there by the flexible force of rubber band, while the edges were sealed off by Miccrostop. Thus the electropolishing took place on the two faces of the disc being in contact with the electrolyte through two conically formed holes.

Two solutions were tried:

20% perchloric acid

80% ethanol

and

40% acetic acid

30% nitric acid

20% phosphoric acid

10% water,

both at 0°C and with an applied voltage of 20 V. Both of these solutions gave thin enough films for transmission electron microscopy observations. However, the specimens were randomly clean or dirty on their surface and the various cleaning operations tried did not solve this problem. As standard practice, the surfaces were washed vigorously with a jet of methanol after perforation, when work on the project ended.

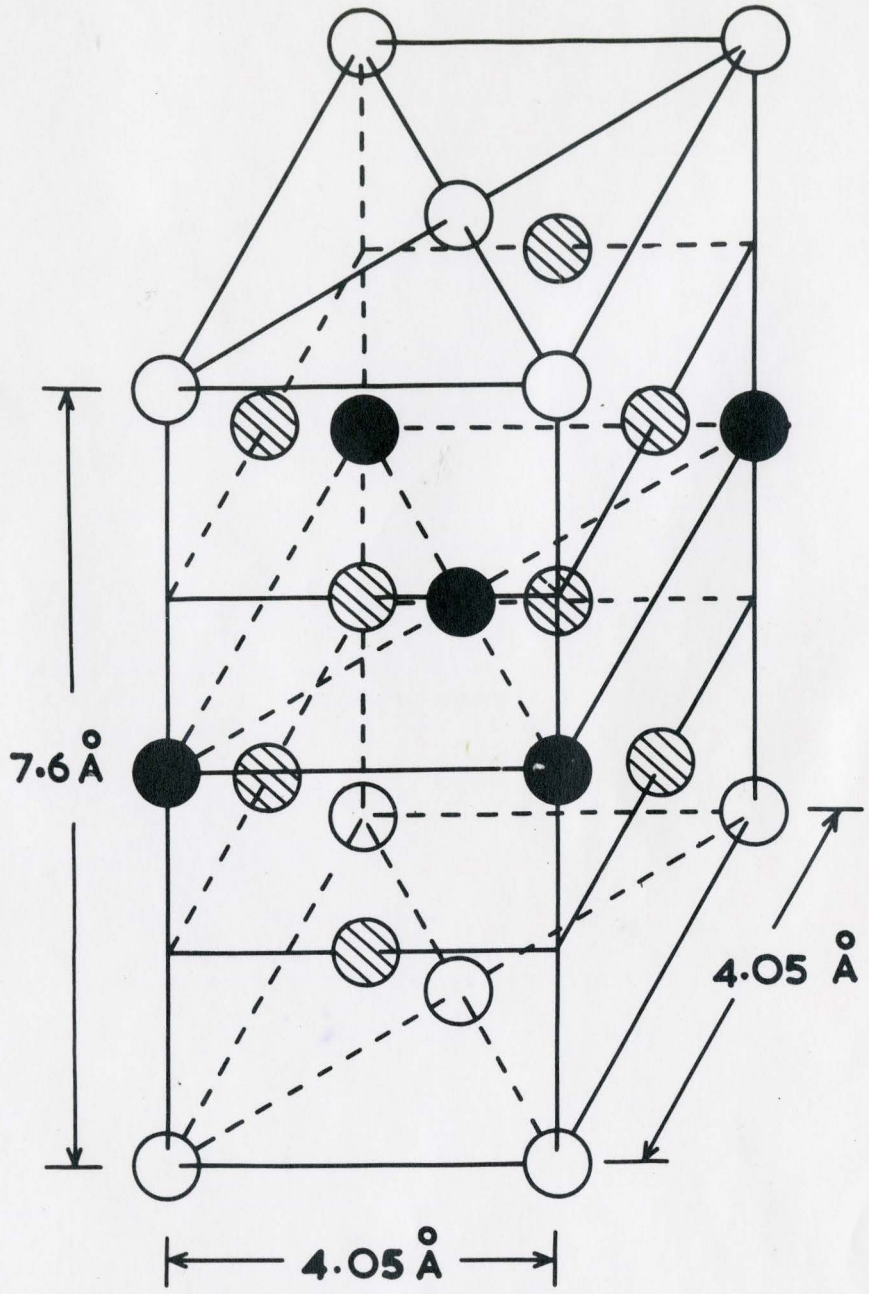

STRUCTURE OF θ" (AFTER GRAF)

ALUMINIUM

75 % ALUMINIUM
25 % COPPER

COPPER

(NOT TO SCALE)

Fig. 1. The Structure of θ" Precipitate.

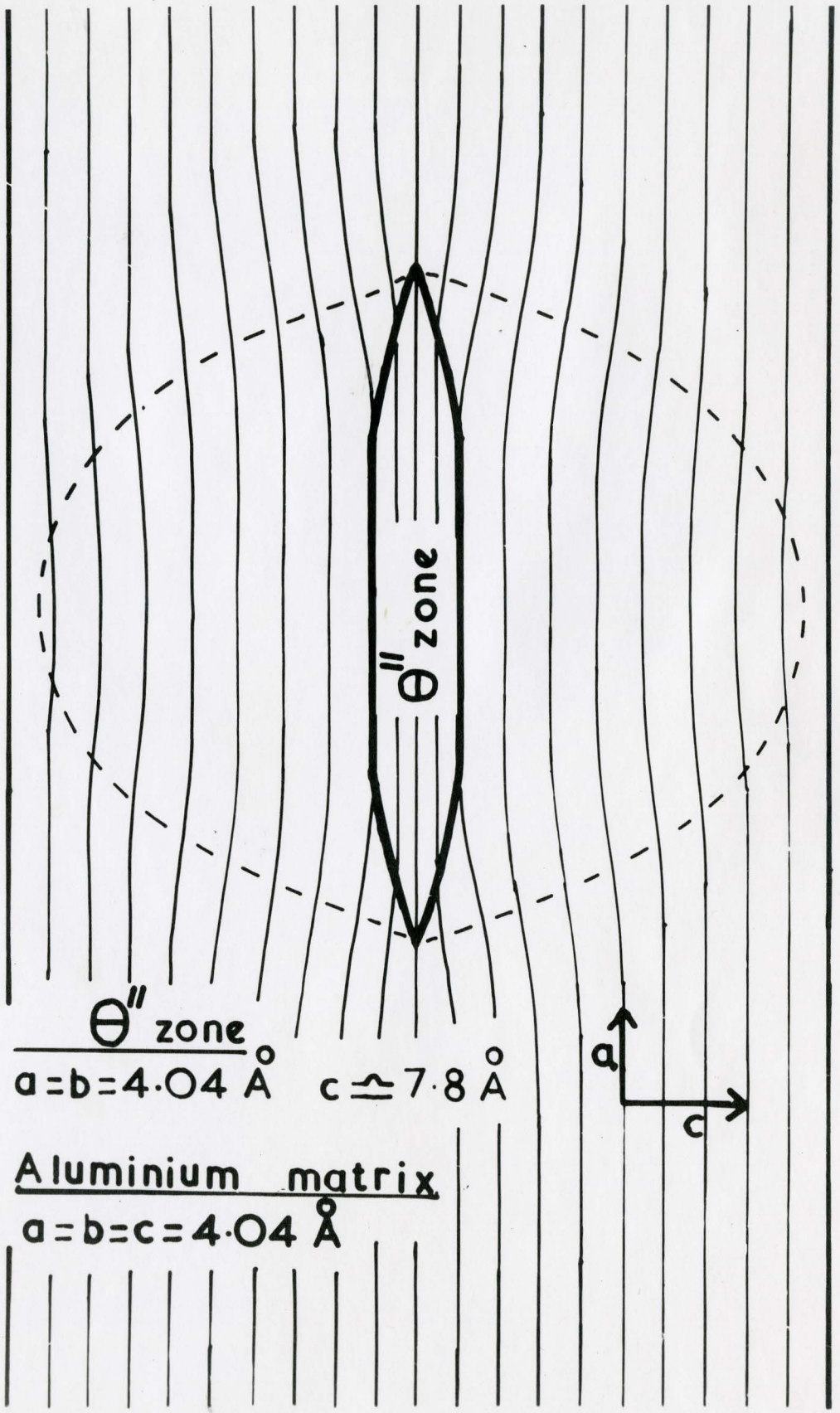

Fig. 2. Nicholson's[30] model of the strain field about a θ'' plate.

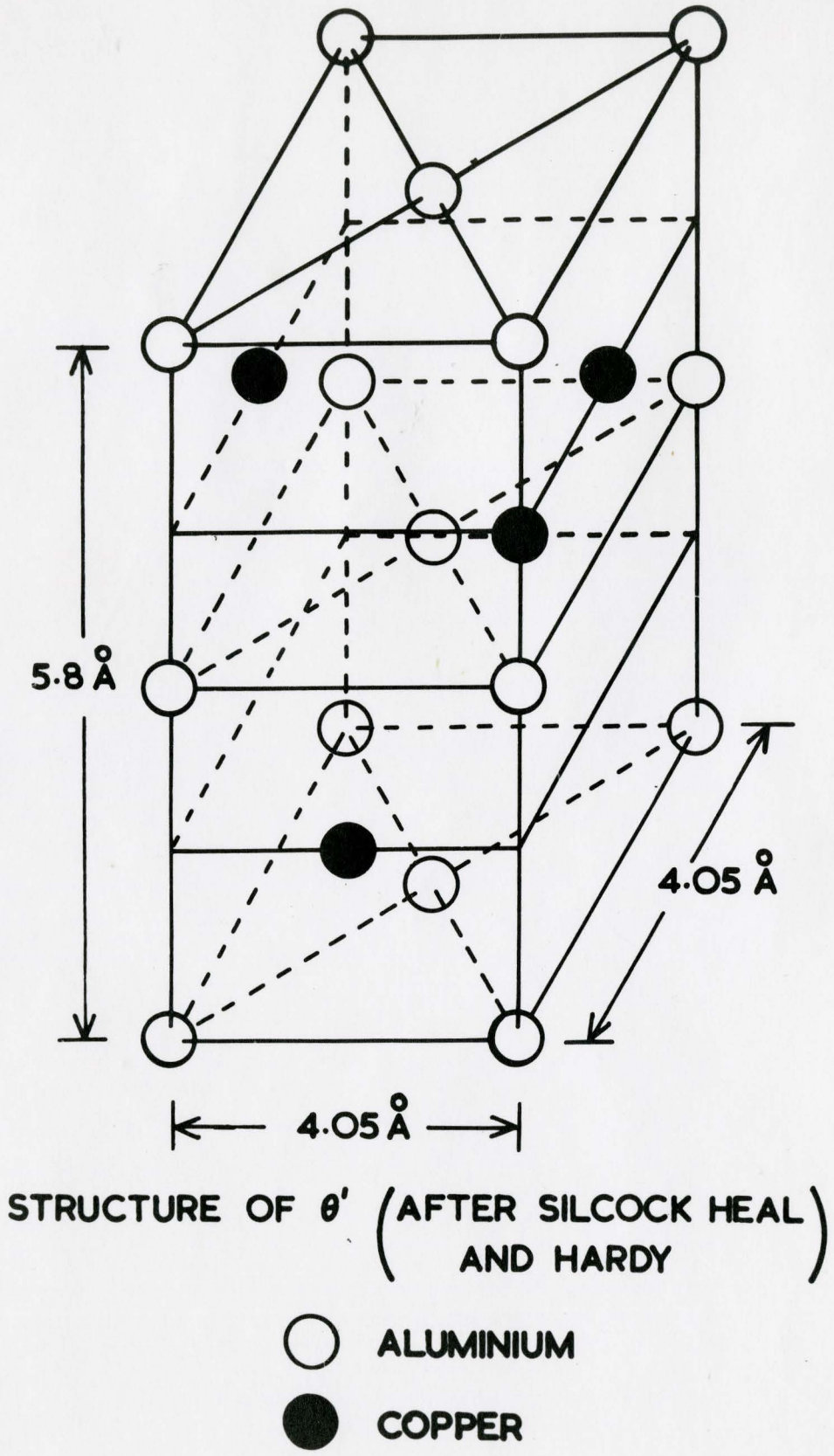

Fig. 3. The structure of θ' particle.

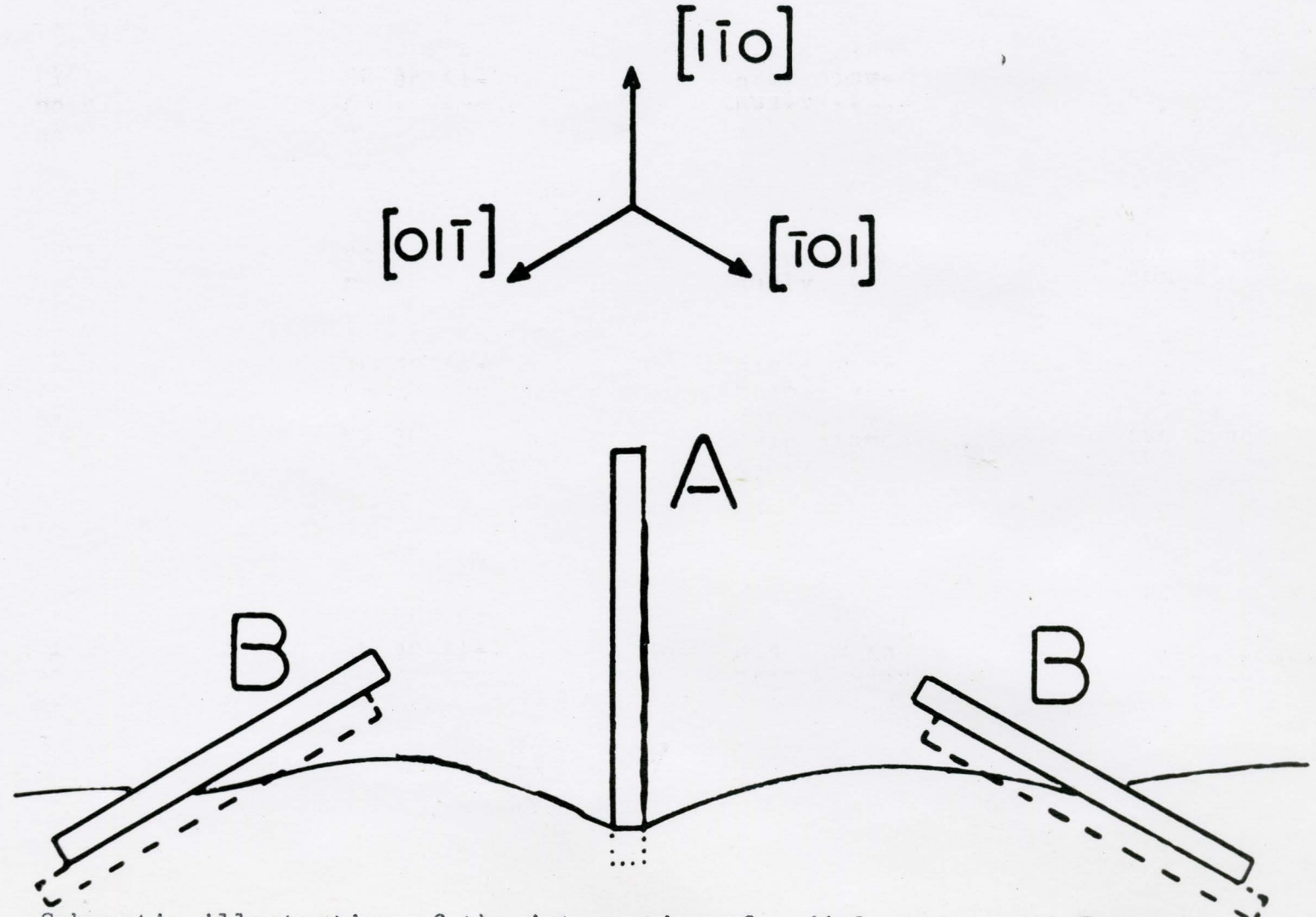

Fig. 4. Schematic illustration of the interaction of a dislocation with Burgers vector a/2 [1$\bar{1}$0] with GP zones in an Al-Cu crystal. Zones A with traces in the glide plane parallel to [1$\bar{1}$0] are sheared parallel to their diameter; zones B with traces parallel to [01$\bar{1}$] or [$\bar{1}$01] are sheared obliquely. (Kelly and Nicholson 25)

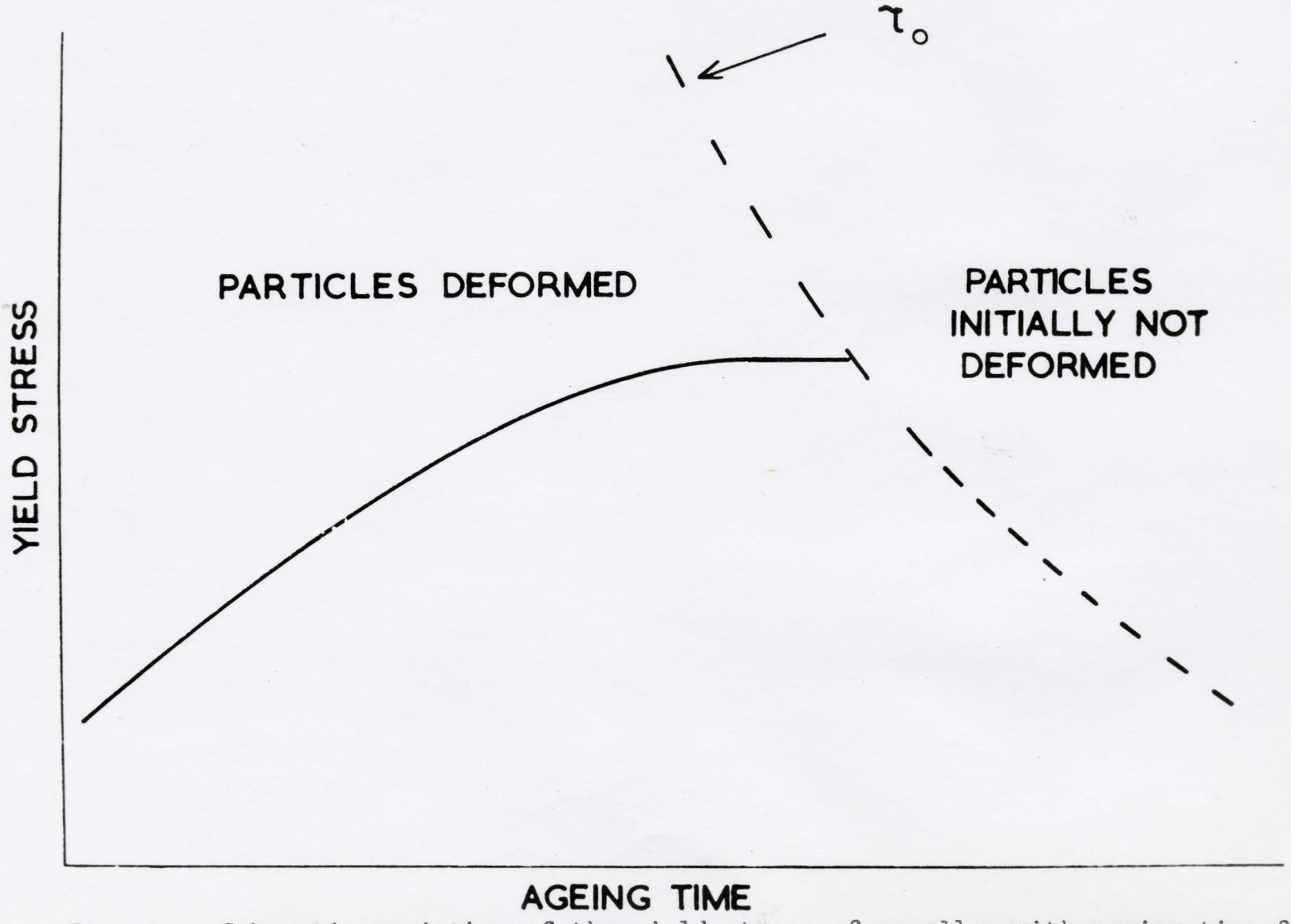

Fig. 5. Schematic variation of the yield stress of an alloy with ageing time for a typical age-hardening system. τ_o is the stress necessary to force dislocation between precipitates (Kelly and Nicholson 25.)

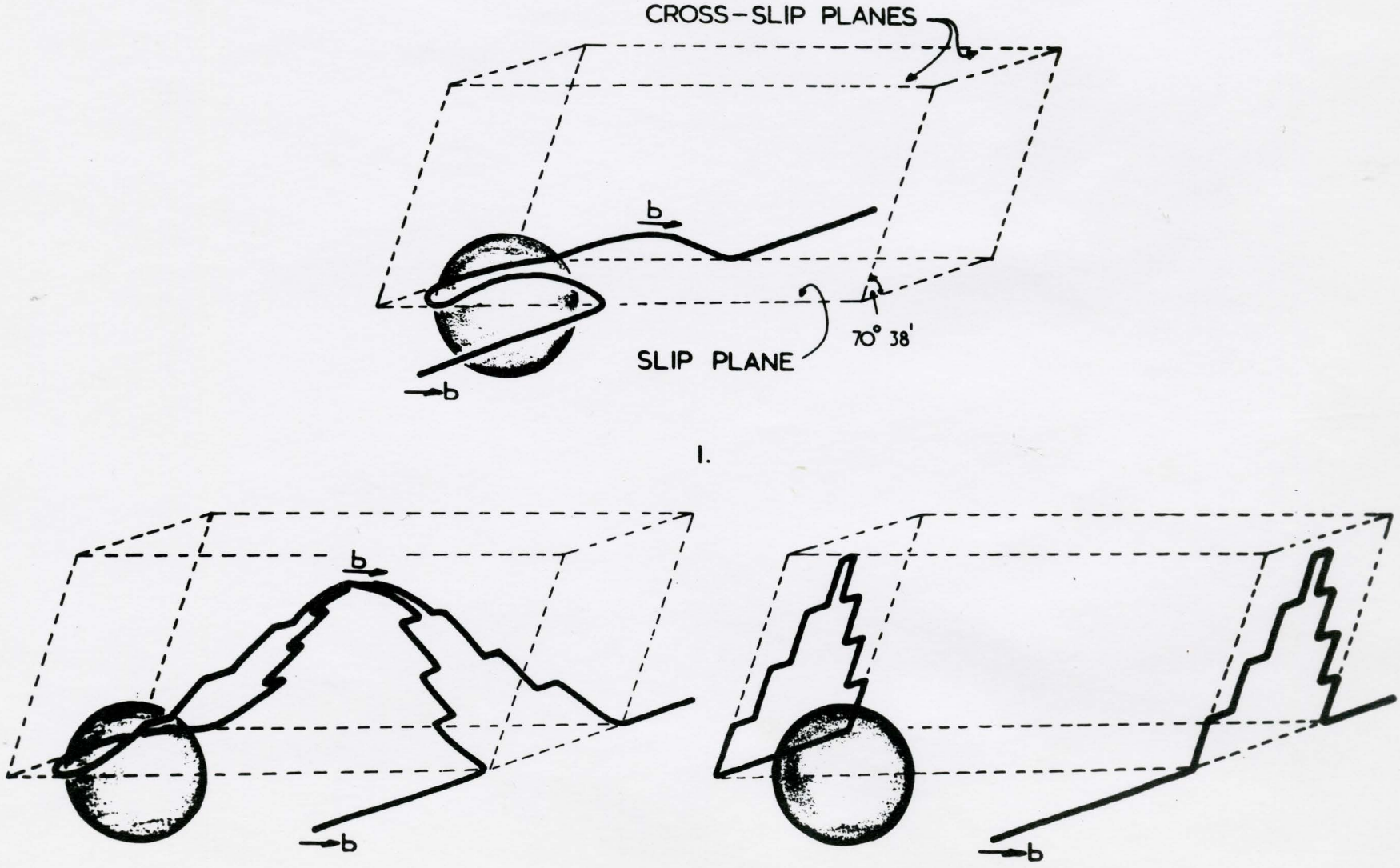

Fig. 6. Illustrating a cross-slip mechanism. From Ashby (79)

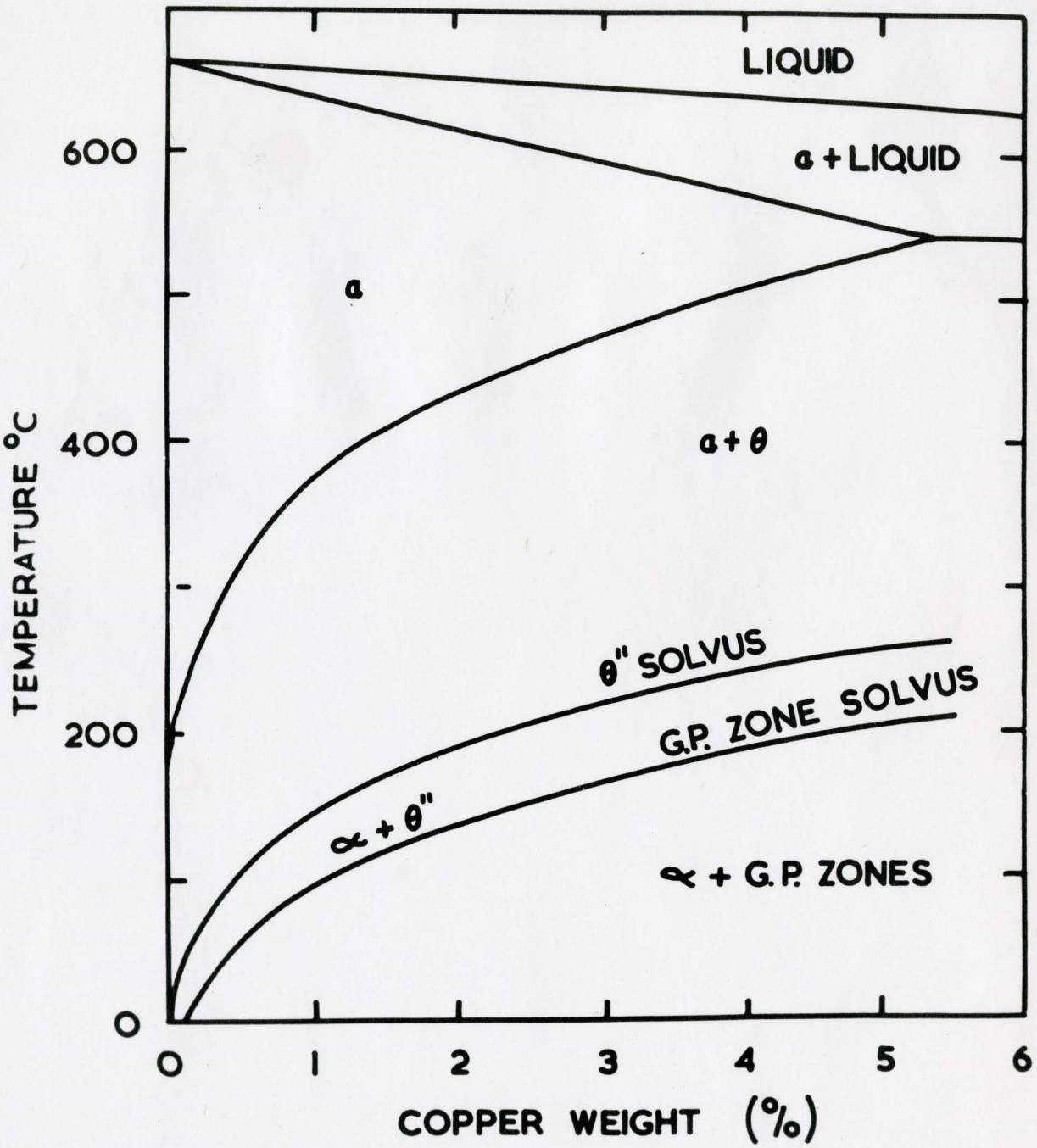

Fig. 7. Metastable and stable equilibrium diagram for various precipitates in aluminum-copper alloys (Beton and Rollason: J. Inst. Met. 86, 1957, 77.)

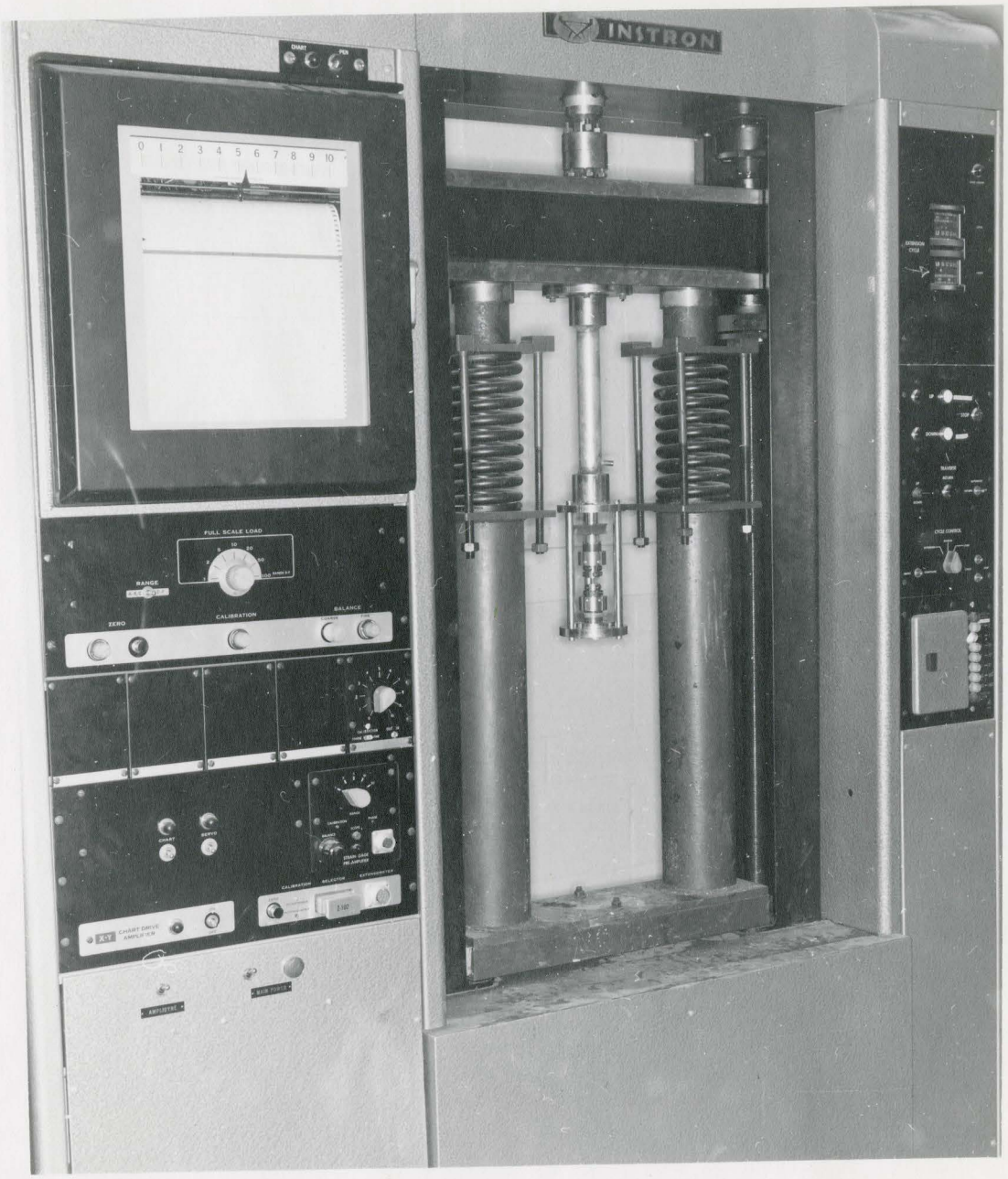

Fig. 8. "Instron" and the adapter for fatigueing.

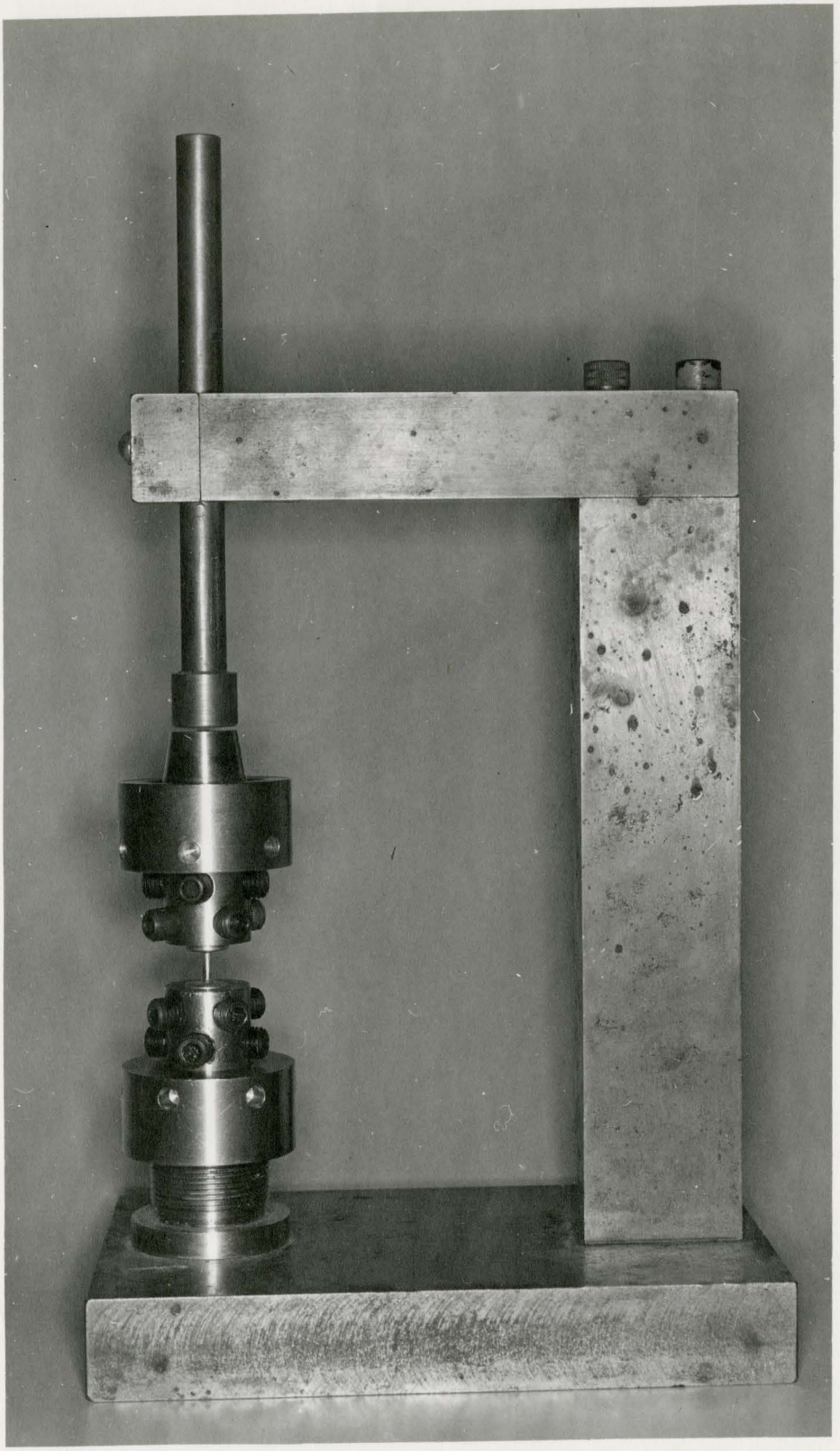

Fig. 9. Alignment jig used for specimen alignment before fatigue.

TABLE 1

Specimen			Instron			Deformation	
Diameter	Cross-section	Gauge length	Chart speed	Cross-head speed	Extension on chart	Extension	Strain amplitude
mm	mm^2	mm	in/min	in/min	inch	inches	%
2.37	4.4	8.5	2	0.02	0.8	±0.008	±2.4

Test No.	6
Precipitate	GP
Temperature	Room
Strain ampl.	±2.4

Cycle No.	Load in lbs.			Stress in Kg/mm^2 factor: lbs.x.0947			A	H	W	A/W	H/A/W	$\frac{\Sigma H}{\Sigma A/W}$	Remarks
	Tens.	Comp.	Rev.	σ_F	σ_C	σ_R	mm^2	mm	mm				
1	157	160	136	16.2	16.5	14.0	591	79.5	7.5	79.2	1.002		Orien-
							537	82.0	7.24	74.5	1.1	1.05	tation
10							426	89.4	5.84	73.0	1.245		≠[112]
							436	93.4	5.33	81.8	1.14	1.18	
15			157			16.25							
20	185	190		19.1	19.7		349	94.2	4.19	83.3	1.131		
							381	97.3	4.31	88.3	1.1	1.115	
40			171			17.7	294	99.0	3.42	86.0	1.15		
							332	101.5	3.81	87.1	1.168	1.158	
50	195	200		20.1	20.6								
100	202	208		20.8	21.4		245	102.5	2.54	96.4	1.063		
							284	106.5	2.92	97.3	1.093	1.082	
300	200	206		20.6	21.3		258	102.0	2.54	103.0	0.99		
							323	102.5	3.3	98.0	1.04	1.038	
500	200	206		20.6	21.3								
700	198	204		20.4	21.0								
800	187	194		19.3	20.0								
900	181	187		18.7	19.3		304	93.5	3.3	92.2	1.015		
							458	96.2	7.61	60.15	1.565	1.245	
1000	170	174		17.5	18.0								
1050	150	157		15.5	16.2		317	65.3	6.35	50.0	1.27		
							349	68.0	7.6	46.0	1.48	1.39	
1095	55			5.7									

TABLE 2

Specimen			Instron			Deformation		Test No.	25
Diameter	Cross-section	Gauge length	Chart speed	Cross-head speed	Extension on chart	Extension	Strain amplitude	Precipitate	GP
								Temperature	Room
mm	mm^2	mm	in/min	in/min	inch	inches	%	Strain Ampl.	±0.66
2.37	4.4	8.0	2	0.002	2.0	±0.004	±0.66		

Cycle No.	Load in lbs.			Stress in Kg/mm^2 factor: lbs.x0.103			A	H	W	A/W	H/A/W	$\frac{\Sigma H}{\Sigma A/W}$	Remarks
	Tens.	Comp.	Rev.	σ_F	σ_C	σ_R	mm^2	mm	mm				
1	120	122	102	12.45	12.55	10.55							

TABLE 7

Specimen			Instron			Deformation		Test No.	8
Diameter	Cross-section	Gauge length	Chart speed	Cross-head speed	Extension on chart	Extension	Strain amplitude	Precipitate	θ'
								Temperature	Room
mm	mm^2	mm	in/min	in/min	inch	inches	%	Strain Ampl.	±1.27
2.37	4.4	8.5	2.0	0.02	0.4	±0.004	±1.27		

Cycle No.	Load in lbs.			Stress in Kg/mm^2 factor: lbs.x0.103			A	H	W	A/W	H/A/W	$\frac{\Sigma H}{\Sigma A/W}$	Remarks
	Tens.	Comp.	Rev.	σ_F	σ_C	σ_R	mm^2	mm	mm				
1	140	142	<0	14.45	14.65	<0.					Orien-	tation	≠[112]
											Treated	at 250 °C 2½ h	

TABLE 11

Specimen			Instron			Deformation		Test No.	13
Diameter	Cross-section	Gauge length	Chart speed	Cross-head speed	Extension on chart	Extension	Strain amplitude	Precipitate	θ
								Temperature	Room
mm	mm^2	mm	in/min	in/min	inch	inches	%	Strain Ampl.	±1.2
2.2	3.8	8.0	2.0	0.02	0.4	±0.004	±1.2		

Cycle No.	Load in lbs.			Stress in Kg/mm^2 factor: lbs.x0.12			A	H	W	A/W	H/A/W	$\frac{\Sigma H}{\Sigma A/W}$	Remarks
	Tens.	Comp.	Rev.	σ_F	σ_C	σ_R	mm^2	mm	mm				
1	63	64	<0	7.55	7.6	<0							

TABLE 3

Specimen			Instron			Deformation	
Diameter	Cross-section	Gauge length	Chart Speed	Cross-head speed	Extension on chart	Extension	Strain amplitude
mm	mm^2	mm	in/min	in/min	inch	inches	%
2.47	4.8	8.0	2.0	0.002 0.1	2.0	±0.002	±0.66

Test No.	27
Precipitate	GP
Temperature	Liquid Air
Strain Ampl.	±0.66

Cycle No.	Load in lbs.			Stress in Kg/mm^2 factor: lbsx0.0947			A	H	W	A/W	H/A/W	$\frac{\Sigma H}{\Sigma A/W}$	Remarks
	Tens.	Comp.	Rev.	σ_F	σ_C	σ_R	mm^2	mm	mm				
1	156	156	135	14.8	14.8	12.78	510	80.7	7.61	67.0	1.205		
							487	78.8	7.36	66.2	1.19	1.195	
5	162	161		15.35	15.35		426	82.0	6.35	67.1	1.22		
							336	81.4	5.07	66.2	1.227	1.225	
10	165	165		15.65	15.65								
20	167	170		15.85	15.85		278	86.4	4.45	62.5	1.38		
							194	86.8	2.54	76.3	1.13	1.25	
223	175	175		16.6	16.6								
1673	175	175		16.6	16.6								
3154	170	180		16.6	16.6								
4631	171	182		16.7	16.7								
6098	171	185		16.8	16.8								
10461	170	175		16.4	16.4								
18231	176	173		16.55	16.55								
36449	175	176		16.6	16.6								
39260	172	173		16.35	16.35								
41730	175	170		16.35	16.35								
50501	173	170		16.25	16.25								
52000	170			16.1									

TABLE 4

Specimen			Instron			Deformation		Test No.	7
Diameter	Cross-section	Gauge length	Chart speed	Cross-head speed	Extension on chart	Extension	Strain amplitude	Precipitate	θ"
								Temperature	Room
mm	mm^2	mm	in/min	in/min	inch	inches	%	Strain Ampl.	±1.5
2.35	4.4	8.5	2.0	0.02	0.5	±0.005	±1.5		

Cycle No.	Load in lbs.			Stress in Kg/mm^2 factor: lbs. x 0.1035			A	H	W	A/W	H/A/W	$\frac{\Sigma H}{\Sigma A/W}$	Remarks
	Tens.	Comp.	Rev.	σ_F	σ_C	σ_R	mm^2	mm	mm				
1	157	173	130	16.25	17.9	13.45							Orien-
2	174	184	150	18.00	19.0	15.5							tation
3	183	192	160	18.9	19.8	16.5							≠ [112]
4	191	199		19.7	20.5								
5	197	205	180	20.4	21.2	18.6							
6	202	209		20.8	21.6								
10	210	215	206	21.7	22.3	21.3							
15	216	220	208	22.4	22.7	21.6							
20	221	226	218	22.8	23.3	22.6							
25	227	230	225	23.4	23.7	23.3							
30	228	233	228	23.6	24.0	23.6							
40	232	237.5	235	24.0	24.4	24.4							
50	235	240	237	24.3	24.8	24.5							
60	235	240	237	24.3	24.8	24.5							
130	Fractured in tension at 318 lbs. =						32.5	Kg/mm					

TABLE 5

Specimen			Instron			Deformation	
Diameter	Cross-section	Gauge length	Chart speed	Cross-head speed	Extension on chart	Extension	Strain amplitude
mm	mm^2	mm	in/min	in/min	inch	inches	%
2.32	4.2	8	2.0	0.002 0.1	2.0	±0.002	±0.635

Test No.	16
Precipitate	9"
Temperature	Room
Strain Ampl.	±0.635

Cycle No.	Load in lbs.			Stress in Kg/mm^2 factor: lbs.x 0.108			A	H	W	A/W	H/A/W	$\frac{\Sigma H}{\Sigma A/W}$	Remarks
	Tens.	Comp.	Rev.	σ_F	σ_C	σ_R	mm^2	mm	mm				
1	129	138	111	13.95	14.9	12.0	668	65.7	11.2	59.6	1.1		
							482	71.0	8.0	60.2	1.182	1.141	
2	133	145	116	14.4	15.65	12.5							
3	137	148	120	14.8	16.0	12.95							
4	139	150		15.0	16.2								
10	147	153	142	15.9	16.5	15.3	248	74.4	3.94	63.0	1.18		
							213	78.8	2.8	76.0	1.035	1.1075	
20	149	156		16.1	16.8								
30	150	160		16.2	17.3								
60	152	162		16.4	17.5								
790	158	160		16.75	16.75								
850	160	160		16.75	16.75								
1400	156	166		16.75	16.75								
1820	152	161		16.75	16.75								
2550	156	156		16.85	16.85								
3400	155	155		16.75	16.75								
4550	153	153		16.5	16.5								
6700	154	154		16.65	16.65								
8270	153	153		16.5	16.5								
11510	156	156		16.85	16.85								
12380	157	157		17.0	17.0								
16170	152	152		16.40	16.40								
17400	147	147		15.9	15.9								
18800	142	143		15.3	15.3								
19000	Fracture												

TABLE 6

Specimen			Instron			Deformation		Test No.	22
Diameter	Cross-Section	Gauge length	Chart speed	Cross-head speed	Extension on chart	Extension	Strain amplitude	Precipitate	0"
								Temperature	Liquid Air
mm	mm^2	mm	in/min	in/min	inch	inches	%	Strain Ampl.	±0.64
2.44	4.66	8	2.0	0.002 0.1	2.0	±0.002	±0.64		

Cycle No.	Load in lbs.			Stress in Kg/mm^2 factor: lbs. x 0.0975			A	H	W	A/W	H/A/W	$\frac{\Sigma H}{\Sigma A/W}$	Remarks
	Tens.	Comp.	Rev.	σ_F	σ_C	σ_R	mm^2	mm	mm				
1	162	169	137	15.8	16.5	13.35	462	81.3	6.35	72.7	1.12		
							374	85.5	5.72	65.4	1.131	1.205	
2	173	176	150	16.8	17.15	14.5							
3	178	181	170	17.3	17.6	16.5							
4	178	184		17.3	17.9								
5	178	183	175	17.35	17.8	16.9	118	91.5	1.52	77.6	1.18		
							134	93	2.03	66.0	1.4	1.29	
10	179	183	180	17.45	17.8	17.4	96.5	91	1.27	76.0	1.195		
							76.2	94	1.02	74.8	1.255	1.225	
180	183	193		17.8	18.8								
420	182	193		17.7	18.8								
900	184	184		17.9	17.9								
2100	180	180		17.6	17.6								
4716	185	185		18.0	18.0								
6872	183	183		17.8	17.8								
7712	182	182		17.7	17.7								
9536	184	184		17.9	17.9								
11386	182	182		17.7	17.7								
19306	182	182		17.7	17.7								
37000	184	184		17.9	17.9								
60000	184	184		17.9	17.9								
75000	184	184		17.9	17.9								
80000	182	182		17.7	17.7								
90000	160	160		15.6	15.6								
92000	135	135		13.15	13.15								

TABLE 8

Specimen			Instron			Deformation		Test No.	17
Diameter	Cross-section	Gauge length	Chart speed	Cross-head speed	Extension on chart	Extension	Strain amplitude	Precipitate	θ'
								Temperature	Room
mm	mm^2	mm	in/min	in/min	inch	inches	%		
2.46	4.75	8.0	2.0	0.002 0.02	2.0 0.2	±0.002	±0.64	Strain Ampl.	±0.64

Cycle No.	Load in lbs.			Stress in Kg/mm^2 factor: lbs. x 0.0957			A	H	W	A/W	H/A/W	$\frac{\Sigma H}{\Sigma A/W}$	Remarks
	Tens.	Comp.	Rev.	σ_F	σ_C	σ_R	mm^2	mm	mm				
1	92	112	<0	8.8	10.7	<0	970	45.8	23.8	40.7	1.125		
							905	55.9	19.8	45.7	1.22	1.18	
5	132	141		12.6	13.5		587	67.2	9.6	61.2	1.095		
							452	71.3	7.16	63.0	1.13	1.11	
10	147	153		14.1	14.65								
30	162	166		15.5	15.5								
100	168	169		16.1	16.2								
275	168	168		16.1	16.2								
665	171	171		16.3	16.4								
1050	170	170		16.25	16.25								
1735	166	166		15.9	15.9								
2535	166	166		15.9	15.9								
3318	170	170		16.25	16.25								
4055	172	172		16.4	16.4								
4805	171	171		16.3	16.3								
5180	168	168		16.1	16.1								
6420	165	165		15.8	15.8								
7645	168	168		16.1	16.1								
8339	167	167		16.0	16.0								
9575	165	165		15.8	15.8								
13230	169	169		16.15	16.15								
14710	168	168		16.1	16.1								
15235	165	165		15.8	15.8								
15985	162	162		15.5	15.5								

TABLE 9

Specimen			Instron			Deformation		Test No.	20
Diameter	Cross-section	Gauge length	Chart speed	Cross-head speed	Extension on chart	Extension	Strain amplitude	Precipitate	θ'
								Temperature	Liquid Air
mm	mm^2	mm	in/min	in/min	inch	inches	%	Strain Ampl.	±0.64
2.36	4.37	8	2.0	0.002 0.1	2.0	±0.002	±0.64		

Cycle No.	Load in lbs.			Stress in Kg/mm^2 factor: lbs. x 0.104			A	H	W	A/W	H/A/W	$\frac{\Sigma H}{\Sigma A/W}$	Remarks
	Tens.	Comp.	Rev.	σ_F	σ_C	σ_R	mm^2	mm	mm				
1	110	111	<0	11.4	11.5	<0	952	55.9	19.45	48.9	1.145		
							820	56.6	18.00	45.6	1.242	1.19	
2	115	116		12.0	12.0								
3	118	119	25	12.3	12.4	2.6							
5	123	125	40	12.8	13.0	4.15	772	62.4	15.1	51.1	1.22		
							745	63.3	13.95	53.4	1.188	1.20	
10	132	128	50	13.75	13.3	5.2	710	66.7	13.95	50.8	1.312		
							632	65.5	11.4	55.4	1.182	1.245	
15	136	131	70	14.14	13.76	7.28	650	69.3	12.7	51.2	1.35		
							565	660	10.3	54.8	1.2	1.275	
90							330	78.7	5.59	59.2	1.33		
							291	73.6	5.08	57.4	1.281	1.305	
436	160	156		16.65	16.2								
874	160	156		16.65	16.2								
3146	162	154		16.85	16.0								
4640	160	156		16.65	16.2								
6485	162	156		16.85	16.2								
9674	166	157		17.2	16.3								
13094	168	156		17.4	16.2								
18825	160	156		16.65	16.2								
22140	162	155		16.85	16.1								
24096	151	147		15.7	15.3								
24500	125	135		13.0	14.0								

TABLE 10

Specimen			Instron			Deformation		Test No.	9
Diameter	Cross-section	Gauge length	Chart speed	Cross-head speed	Extension on chart	Extension	Strain amplitude	Precipitate	⊖
								Temperature	Room
mm	mm^2	mm	in/min	in/min	inch	inches	%	Strain Ampl.	±1.2
2.5	4.9	8.5	2.0	0.02	0.4	±0.004	±1.2		

Cycle No:	Load in lbs.			Stress in Kg/mm^2 factor: lbs. x 0.0928			A	H	W	A/W	H/A/W	$\frac{\Sigma H}{\Sigma A/W}$	Remarks
	Tens.	Comp.	Rev.	σ_F	σ_C	σ_R	mm^2	mm	mm				
1	58	58	<0	5.4	5.4	<0	178	30	7.5	23.7	1.268		Orien-
							172	30	7.87	21.9	1.375	1.315	tation
2	63	63		5.85	5.85								≠[112]
5	67	67		6.21	6.21		184	34	7.36	25.0	1.36		
							199	33.8	7.87	25.3	1.335	1.348	⊖
10	70	70	15	6.5	6.5	1.39							Treated
50	73	74	20	6.85	6.9	1.85							350°C
100	80	80	30	7.45	7.45	2.78	226	40.7	7.36	30.7	1.325		3 h
							213	40.7	7.1	30.0	1.355	1.34	
200	87	88	42	8.05	8.1	3.9							
300	94	95	50	8.74	8.8	4.63							
400	98	100	52	9.1	9.28	4.81							
500	100	105		9.28	9.6								
600	103	103	62	9.5	9.5	5.75	286	50.8	6.73	42.5	1.195		
							255	50.8	6.1	41.8	1.215	1.205	
700	100	100	63	9.28	9.28	5.84							
800	98	98	50	9.1	9.1	4.63							
900	95	95	58	8.85	8.85	5.38							
1000	95	95	60	8.85	8.85	5.56							
1100	92	94	60	8.54	8.74	5.56							
1200	91	91	60	8.45	8.45	5.56							
1300	90	90	50	8.35	8.35	4.63							
1400	87	87	48	8.07	8.07	4.45							
1500	84	84	46	7.8	7.8	4.27	209	42.7	5.33	39.2	1.09		
							223	42.7	6.35	35.5	1.2	1.143	
1521	83	Fracture											

TABLE 12

Specimen			Instron			Deformation		Test No.	21
Diameter	Cross-section	Gauge length	Chart speed	Cross-head speed	Extension on chart	Extension	Strain amplitude	Precipitate	⊖
								Temperature	Room
mm	mm^2	mm	in/min	in/min	inch	inches	%	Strain Ampl.	±0.64
2.55	5.1	8	2.0	0.002 0.1	2.0	±0.002	±0.64		

Cycle No.	Load in lbs.			Stress in Kg/mm^2 factor: lbs. x 0.0875			A	H	W	A/W	H/A/W	$\frac{\Sigma H}{\Sigma A/W}$	Remarks
	Tens.	Comp.	Rev.	σ_F	σ_C	σ_R	mm^2	mm	mm				
1	95	109	<0	8.3	9.6	<0	827	48.2	23.4	35.4	1.36		
							853	55.2	17.8	47.9	1.15	1.242	
2	110	116		9.6	10.21								
5	132	137	25	11.55	12.0		775	67	12.45	62.3	1.075		
							604	69.3	10.3	58.6	1.18	1.15	
10	152	153	35	13.3	13.4								
15							358	81.1	4.44	80.6	1.005		
							249	81.1	2.8	65.6	1.23	1.11	
25	164	166	55	14.4	14.55		161.5	83.5	2.04	79.3	1.053		
							161.5	84.0	2.24	70.6	1.19	1.12	
120	165	169		14.5	14.7								
300	162	168		14.2	14.7								
500	162	162		14.2	14.2								
750	160	160		14.0	14.0								
1120	159	163		13.9	14.3								
1380	157	162		13.75	14.2								
1640	155	158		13.6	13.8								
2015	155	162		13.6	14.2								
2450	152	160		13.3	14.0								
3800	150	160		13.15	14.0								
9560	146	146		12.8	12.8								

TABLE 13

Specimen			Instron			Deformation		Test No.	15
Diameter	Cross-section	Gauge length	Chart Speed	Cross-head speed	Extension on chart	Extension	Strain amplitude	Precipitate	GP
								Temperature	Room
mm	mm^2	mm	in/min	in/min	inch	inches	%	Strain ampl.	±0.66
2.5	4.9	8.0	2.0	0.002 0.1	2.0	±0.002	±0.66		

Cycle No	Load in lbs			Stress in Kg/mm^2 factor: lbsx0.0025			A	H	W	A/W	H/A/W	$\frac{\Sigma H}{\Sigma A/W}$	Remarks
	Tens.	Comp.	Rev.	σ_F	σ_C	σ_R	mm^2	mm	mm				
1	140	141	110	13.0	13.05	10.4	394	71.0	7.62	51.6	1.373		
							410	71.6	7.36	55.8	1.28	1.325	
5	157	155		14.35	14.35								
26	160	160		14.8	14.8								
100	160	160		14.8	14.8								
230	158	161		14.6	14.9								
460	160	162		14.8	15.0								
780	155	160		14.4	14.8								
1380	153	163		14.7	15.1								
2000	157	159		14.5	14.75								
3650	155	158		14.4	14.6								
4830	155	159		14.4	14.75								
6050	153	159		14.2	14.75								
6440	155	160		14.6	14.6								
6910	155	162		14.7	14.7								
7060	153	160		14.5	14.5								
8610	152	159		14.4	14.4								
10600	153	160		14.4	14.4								
12040	151	160		14.4	14.4								
18880	145	155		13.9	13.9								
24640	115			10.7									

TABLE 14

Specimen			Instron			Deformation		Test No.	23
Diameter	Cross-section	Gauge length	Chart speed	Cross-head speed	Extension on chart	Extension	Strain amplitude	Precipitate	0"
								Temperature	Room
mm	mm^2	mm	in/min	in/min	inch	inches	%	Strain Ampl.	±0.64
2.37	4.4	8.0	2.0	0.002	2.0	±0.002	±0.64		

Cycle No.	Load in lbs.			Stress in Kg/mm^2 factor: lbs. x 0.1035			A	H	W	A/W	H/A/W	$\frac{\Sigma H}{\Sigma A/W}$	Remarks
	Tens.	Comp.	Rev.	σ_F	σ_C	σ_R	mm^2	mm	mm				
1	125	133	100	12.9	13.8	10.35							
5	137	145		14.2	15.0								
10	148	154		15.3	15.9								
20	156	155		16.2	16.0								
26	157	156		16.3	16.2								
Heat treat at 152°C for 12 hours													
1	162	156		16.8	16.2								
30	156	152.5		16.2	15.8								
Heat treat at 152°C for 12 hours													
1	162	156		16.8	16.2								
30	157	156		16.3	16.2								
Heat treat at 152°C for 1½ hours													
1	160	156		16.6	16.2								
5	158	150		16.4	15.5								
Heat treat at 152°C for 12 hours													
1	161	155		16.7	16.1								
30	157	151		16.3	15.6								

References

1. N. Thompson and N. Wadsworth: Advances in Physics, 7, 72 (1958).

2. N. Thompson: Z. für Metallk., 53, 71 (1962).

3. J. C. Grosskreutz and P. Waldow: Acta Met. 11, 717 (1963).

4. R. L. Segall: Electron Microscopy and Strength of Metals, Interscience Publishers, New York, 515 (1963).

5. R. L. Segall and J. M. Finney: Acta Met. 11, 685 (1963).

6. C. E. Feltner: A Debris Mechanism of Cyclic Strain Hardening for F.C.C. Metals, Scientific Laboratory, Ford Motor Company, (May 1, 1964).

7. C. E. Feltner: Phil. Mag. 8, 2121.

8. K. U. Snowden: Acta Met. 11, 675 (July 1963).

9. E. E. Laufer and W. N. Roberts: Phil. Mag. 10, No. 107, 883 (November 1964).

10. J. T. McGrath and G. W. J. Waldron: Phil. Mag. 9, No. 98, 249 (February 1964).

11. E. Orowan: PRS A 171, 79 (1939).

12. R. F. Hanstock: J. Inst. Met. 83, 11 (1954-55).

13. T. Broom, J. H. Molineaux and V. N. Whittaker: J. Inst. Met. 84, 357 (1955-56).

14. T. Broom, J. A. Mazza, V. N. Whittaker: J. Inst. Metl 86, 17 (1957-58).

15. D. Turnbull: Rep. Conf. on Defects in Cryst. Solids (Phys. Soc.), 203 (1955).

16. B. L. Averbach: Trans. Amer. Soc. Metals 41, 262 (1949).

17. H. K. Hardy: J. Inst. Met. 83, 529 (1954-55).

18. D. V. Wilson: Acta Met. 5, 293 (1957).

19. A. M. Freudenthal and J. H. Weiner: J. Appl. Phys. 27, 44 (1956).

20. J. D. Eshelby and P. L. Pratt: Acta Met. 4, 560 (1956).

21. P. J. E. Forsyth and C. A. Stubbington: J. Inst. Met. 83, 395.

22. P. J. E. Forsyth and C. A. Stubbington: J. Inst. Met. 85, 339.

23. P. J. E. Forsyth: Acta Met. 11, 703 (July 1963).

24. I. J. Polmear and I. F. Bainbridge: Phil. Mag. 4, No. 48, 1293 (1959).

25. A. Kelly and R. B. Nicholson: 1963 Prog. Mat. Sci. 10, 172.

26. W. DeSorbo, H. N. Treaftis and D. Turnbull: Acta Met. 6, 401 (1958).

27. A. Guinier: Acta Cryst. 5, 51 (1952).

28. Hardy and Heal: Prog. Met. Phys. 5, 143.

29. R. B. Nicholson and J. Nutting: Phil. Mag., Series 8, 3, 531 (1958).

30. R. B. Nicholson: Ph.D. Thesis, Cambridge (1959).

31. V. Gerold: Z. Metallk. 45, 593, 599 (1954).

32. A. Guinier: J. Phys. Radium 8, 122 (1954).

33. J. M. Silcock, T. J. Heal and H. K. Hardy: J. Inst. Met. 82, 239 (1954).

34. A. Guinier: Acta Cryst. 5, 121 (1952).

35. R. Graf: Ph.D. Thesis, Paris (1955).

36. R. B. Nicholson, G. Thomas and J. Nutting: J. Inst. Met. 87, 429 (1958-59).

37. G. Thomas and J. Nutting: Acta Met. 7, 515 (1959).

38. R. B. Nicholson: Proc. Eur. Reg. Conf. on Electron Microscopy, 375.

39. R. B. Nicholson: Electr. Micr. and the Strength of Metals, Interscience Publishers (1962).

40. G. Thomas and J. Nutting: The Mechanism of Phase Transformation in Metals, p. 280, Inst. Met. (1956).

41. H. Wilsdorf and D. Kuhlmann-Wilsdorf: Defects in Crystalline Solids, p. 175, Phys. Soc. (1955).

42. L. G. Bonar: Ph.D. Thesis, Cambridge (1962).

43. H. J. Axon, W. Hume-Rothery: Proc. Roy. Soc. A 193, 1 (1948).

44. C. Laird and H. I. Aaronson: Ford Motor Corporation, Dearborn, Michigan, Ford Report No. SL 65-13, 94th AIME Meeting, February 14th-18th, Chicago.

45. D. Vaughan and J. M. Silcock: Acta Met. 12, No. 12, 1463 (December 1964).

46. E. Orowan: Symposium on Internal Stresses in Metals and Alloys, Inst. of Metals (1948).

47. N. F. Mott, F. R. N. Nabarro: Report of a Conference on the Strength of Solids, Phys. Soc., 1 (1948).

48. A. H. Cottrell: Dislocation and Plastic Flow in Crystals, Oxford University Press (1953).

49. F. R. N. Nabarro: Proc. Phys. Soc. 58, 669 (1946).

50. F. R. N. Nabarro: Advances in Physics, 1, 270 (1952).

51. E. W. Hart: Relation of Properties to Microstructure, 95, Amer. Soc. for Metals (1953).

52. A. Kelly and M. E. Fine: Acta Met. 5, No. 7, 365 (July 1957).

53. T. Suzuki: Sci. Rep. Res. Inst. Tohaku Univ. A 1, 183 (1949).

54. H. K. Hardy: J. Inst. Met. 84, 429 (1956).

55. N. F. Mott and F. R. N. Nabarro: Pros. Phys. Soc. 52, 86 (1940).

56. H. Franz and E. Kröner: Z. Metallk. 46, 639 (1955).

57. G. Saada: Acta Met. 8, 200 (1960).

58. V. Gerold: Z. Metallk. 45, 593, 599 (1954).

59. A. A. Griffith: Phil. Trans. Roy. Soc. A 221, 163 (1920).

60. J. C. Fisher: Acta Met. 2, 9 (1954).

61. R. O. Williams: Acta Met. 5, 241 (1957).

62. A. Kelly: Phil. Mag. 8 3, 1472 (1958).

63. G. J. Byrne, M. E. Fine and A. Kelly: Phil. Mag. 8 6, 1119 (1961).

64. R. L. Fleischer: Acta Met. 8, 598 (1960).

65. A. Seeger: Second Int. Conf. on the Peaceful Uses of Atomic Energy A/CONF/15/P/989 (1958).

66. N. F. Mott: Phil. Mag. 8 1, 568 (1956).

67. A. Seeger: Phil. Mag. 7 45, 771 (1954).

68. R. I. Price and A. Kelly: Acta Met. 12, 159 (1964).

69. R. L. Fleischer: Electron Microscopy and Strength of Crystals, Thomas and Washburn, Interscience Publishers, p. 990 (1963).

70. A. Kelly: Ibid, p. 992.

71. G. S. Ansell, F. V. Lenel: Acta Met. 8, 612 (1960).

72. G. S. Ansell: Acta Met. 9, 518 (1961).

73. J. C. Fisher, E. W. Hart, and R. H. Pry: Acta Met. 1, 336 (1953).

74. D. Dew-Hughes and W. D. Robertson: Acta Met. 8, 147 (1960).

75. L. G. Bonar: referring to W. Tyson's work to be published.

76. C. S. Roberts, R. C. Carruthers and B. C. Averbach: Trans. Amer. Soc. Metals 44, 1150 (1952).

77. J. H. Van Der Merwe: Proc. Phys. Soc. 63A, 616 (1950).

78. G. Thomas and J. Nutting: Inst. Met. 86, 7 (1957-58).

78a. Ibid, 85, 1.

79. M. F. Ashby and G. C. Smith: Phil. Mag. 8 5, 299 (1960).

80. P. B. Hirsch: J. Inst. Met. 86, 13.

81. M. F. Ashby: Z. für Metallk., p. 5 (January 1964).

82. J. T. Barnby and E. Smith: Acta Met. 12, 1353 (December 1964).

83. D. P. Kedzie and R. A. Dodd: Trans. Met. Soc. AIME, 230, 758 (June 1964).

84. N. Gane and R. N. Parkins: J. Inst. Met. 88, 173 (1959-60).

85. C. A. Stubbington: J. Inst. Met. 88, 227 (1959-60).

86. A. J. McEvily, Jr., J. B. Clark, E. C. Utley and W. H. Herrnstein III: Trans. Met. Soc. AIME, 227, 1093 (October 1963).

87. P. J. E. Forsyth and R. N. Wilson: J. Inst. Met. 92, 82 (November 1963).

88. S. Koda and T. Takeyama: J. Inst. Met. 86, 277 (1957-58).

89. J. B. Clark and A. J. McEvily, Jr.; Acta Met. 12, No. 12, 1359 (December 1964).

90. S. Koda, K. Matsuura, S. Takahashi: J. Inst. Met. 91, 229 (March 1963).

91. V. G. Rakin and N. N. Buinov: The Physics of Metals and Metallography, 11, No. 1 (1961).

92. J. B. Mitchell, S. K. Mitra, J. E. Dorn: University of California Report, U.C.RL. 10469.

93. J. C. Grosskreutz and P. Waldow: Acta Met. 11, 717 (1963).

94. S. I. Liu and G. Sachs: AIME 180, 193 (1949).

95. N. J. Wadsworth: Acta Met. 11, 663 (July 1963).

96. R. W. K. Honeycombe: Met. Rev. 1958-59 (59 4 vol.).

97. B. Chalmers: Physical Metallurgy (Textbook 1959).

98. Carpenter and Elam: Proc. Roy. Soc. (A) 100, 329 (1921).

99. A. Kelly and Chiou: Acta Met. 6, 565 (1958).

100. E. N. da C. Andrade: Proc. Roy. Soc.(A) 163, 16 (1958).

101. T. Fujiwara: J. Sci. Hiroshima Univ. A9, 227 (1939).

102. G. Hägg and N. Karlsson: Acta Cryst. 5, 728 (1952).

103. T. J. Tiedema: Acta Cryst. 2, 261 (1949).

104. C. G. Dunn: Trans. Amer. Inst. Min. Met. Eng. 185, 72 (1949).

105. J. Talbot: I.R.S.I.D. Rep. Series A, No. 137 (1956).

106. C. J. Beevers: unpublished work.

107. J. Garstone, R. W. K. Honeycombe and G. Greetham: Acta Met. 4, 485 (1956).

108. Williamson and Smallman; Acta Met. 1, 487 (1953).

109. Beck and Sperry: J. Appl. Phys. 21, 150 (1950).

110. Beck et al: J. Appl. Phys. 21, 420 (1950).

111. E. T. Whittaker and G. N. Watson: A Course of Modern Analysis, London, Cambridge University Press, p. 159 (1950).

112. R. E. Smallman: Modern Physical Metallurgy (Second Edition).

113. DeSorbo, Treaftis and Turnbull: Acta Met. 6, 401, (1958).

114. Turnbull, Rosenbaum and Treaftis: Acta Met. 8, 277 (1960).

115. Z. Matyas: Phil. Mag. 7 40, 324 (1949).

116. J. M. Silcock: Acta Met. 8, 589 (September 1960).

117. R. W. Wooley: Phil. Mag. 44, 597 (1953).